UNIVERSITY OF CALIFORNIA

SANTA CRUZ

Molecular mechanisms governing the balance between alveolar proliferation and differentiation in the mammary gland.

A dissertation submitted in partial satisfaction

of the requirements for the degree of

DOCTOR OF PHILOSOPHY

in

MOLECULAR, CELL AND DEVELOPMENTAL BIOLOGY

by

Julien Menendez

September 2022

The Dissertation of Julien Menendez is approved:

_____

Professor Lindsay Hinck, chair

_____

Professor Bin Chen

_____

Professor Camilla Forsberg

_____

Professor Zhu Wang

_____

Peter Biehl
Vice Provost and Dean of Graduate Studies

Table of Contents

List of Figures

Abstract

Molecular mechanisms governing the balance between alveolar proliferation and differentiation in the mammary gland.

Julien Menendez

The goal of my thesis work was to resolve the molecular mechanisms governing mammary gland alveologenesis during pregnancy. Alveologenesis is the essential process by which alveolar progenitor cells undergo rapid expansion during early pregnancy and subsequent differentiation into mature milk-producing alveolar cells during late pregnancy, generating a functional mammary gland capable of providing nourishment for offspring. How the mammary gland maintains a balance between massive proliferation and functional differentiation, however, remains unclear. Here, we show that the mammary gland couples proliferation with differentiation by means of endoreplication, the cellular process of replicating DNA in the absence of cell division to generate a polyploid cell. Through pharmacological inhibition and transgenic loss-of-function studies, we show that the DNA damage response to replication stress is activated during the rapid proliferation of early pregnancy. This, in turn, results in early mitotic arrest through WEE1-mediated CDK1 inhibition and subsequent endoreplication during early lactation, generating a population of terminally differentiated polyploid alveolar cells that are essential for efficient milk production. Furthermore, Notch signaling has long been known to be essential for maintenance of the alveolar progenitor population, and it must be attenuated to achieve alveologenesis. Despite the importance of Notch signaling, however, the mechanisms that regulate Notch activity to ensure proper alveolar proliferation and

differentiation during pregnancy are not well understood. Through transgenic loss-of-function and 3D organoid studies, our preliminary data suggest ROBO2 functions from the luminal epithelial compartment to promote expression of the Notch ligand JAG1 in the basal epithelial compartment, potentially through the direct inhibition of ROBO1 in basal cells. This, in turn, induces the Notch activity of alveolar progenitor cells in a juxtacrine manner, maintaining them in the progenitor state to inhibit their differentiation. Moreover, our preliminary data also suggest NOTCH1 activation inhibits the DNA damage response to replication stress and alveolar endoreplication through the interaction of its intracellular domain with the DNA damage response kinase ATR. Taken together, the results of my thesis work elucidate multiple molecular mechanisms by which the mammary gland achieves a balance between the rapid proliferation of alveolar progenitor cells and their functional differentiation into mature milk-producing alveolar cells during late pregnancy and lactation.

Acknowledgements

First and foremost, I would like to thank my P.I. and mentor Dr. Lindsay Hinck. I have been in your lab since I was an undergraduate and have grown a lot since then, both as a person and as a scientist. You gave me the independence to ask my own questions, form my own hypotheses and, most importantly, make my own mistakes. You also showed me that striving for perfection often impedes progress in research, and thus taught me to be more focused. For these reasons, I have not only learned a lot from you, but a lot from myself in the process. You are always present for me when I seek guidance and advice, and I know that you always have my best interests in mind. Thank you.

Second, I would like to thank my best friend and labmate Dr. Rut Molinuevo Llaria. I do not mean to diminish my accomplishments when I say this, but none of this would have been possible without you. You breathed new life into our lab when you joined, and you brought us all in exciting new directions of study. At the time you arrived, I had encountered many obstacles in my research. You not only taught me to persevere, but rekindled my spark of interest for research. You have a natural aptitude and excitement for this work, and I believe that you bring it out in those around you. Beyond the lab though, you have been the best of friends. You have been kind and supportive of me throughout this journey, but, most importantly, you have been patient. More than anything, though, you have been a constant source of encouragement and motivation, helping me acknowledge the potential that I have as

well as the areas I can improve. I believe you bring out the best in me, and for that I want to say thank you.

Next, I would like to express my deepest gratitude to my family. My parents have always been a source of light on this journey. No matter where I am, I can feel their support, their pride in me, and the comfort of knowing I can that they are always there whenever I may need them. To my mom, you have always seemed impressed by what I have done, and that has helped me believe in myself. Thank you. To my dad, your constant energy and positivity has been an important source of encouragement for me when I am down and frustrated. Thank you. To my brother, you have been so much more than that. You have been a best friend since we were young, and you have been a constant reminder for me to have fun and find joy in all the little things. Thank you. To my sister, you have been my inspiration this entire time. I have always been motivated but your achievement, both as a biologist yourself and as someone who has made a fulfilling life for herself. I think it is obvious to say that I have been following in your footsteps, so I want to thank you for leading the way.

Last, but not least, I want to thank everybody else that has provided me with some kind of support, assistance or maybe even just a well-needed distraction along this journey. As Lindsay says, “It takes a village to do research”, so I would like to thank all other members of the Hinck lab that have helped move this work forward. I would also like to thank members of my graduate cohort and members of other labs that

have shared their knowledge, ideas and resources to help complete this project, as well as the faculty that have provided us with the tools to do so. Last of all, I would like to thank my friends in Santa Cruz that provided good company and lent me their ears when I was explaining my excitement or frustration with my research.

Chapter 1: Physiological DNA Damage Promotes Functional Polyploidization of Mammary Gland Alveolar Cells During Lactation.

Introduction

1. Homeostasis control in developing tissues.

Developing tissues undergo phases of rapid cell proliferation. In order to achieve proper tissue size, function and homeostasis, cell proliferation must be arrested at a certain point, as uncontrolled proliferation can lead to loss of tissue integrity or carcinogenesis. For this reason, there exist fundamental mechanisms of limiting cell proliferation: senescence, apoptosis and terminal differentiation. Senescence refers to an irreversible arrest of proliferation and the secretion of numerous biological factors, such as proinflammatory cytokines, growth factors and protease, which alter the tissue microenvironment. While senescence is implicated in promoting tissue remodeling during development (Muñoz-Espín et al., 2013; Storer et al., 2013), the accompanying alterations in microenvironment have also been associated with tumor progression, age-related degenerative pathologies, type 2 diabetes, and the induction of senescence in neighboring cells through paracrine signaling (Acosta et al., 2013; Baker et al., 2011; Coppé et al., 2008; Krtolica, Parrinello, Lockett, Desprez, & Campisi, 2001; Laberge, Awad, Campisi, & Desprez, 2012; D. Liu & Hornsby, 2007; Minamino et al., 2009; Sone & Kagawa, 2005). Apoptosis or programmed-cell death, on the other hand, is the selective and controlled physical elimination of unnecessary or undesirable cells, and it plays a vital role in shaping

overall tissue size and organization during embryogenesis, post-natal development and homeostasis (Glücksmann, 1951; Jacobsen, Weil, & Raff, 1996; Kerr, Wyllie, & Currie, 1972; D. Macias et al., 1997; Monier et al., 2015; Nakao, Shinoda, Nakai, Murase, & Uyemura, 2002; Pampfer & Donnay, 1999). By their very nature, senescence and apoptosis would be deleterious to tissues that must undergo rapid expansion to accomplish a specialized function, such as the prodigious proliferation that occurs in the mammary gland (MG) in response to pregnancy. To circumvent these adverse effects, cells have evolved a different mechanism; they undergo terminal differentiation, the process by which a stem or progenitor cell becomes more specialized, losing the capacity to proliferate in the process due to highly structured alterations in gene expression (Chen & Dent, 2014; De La Serna, Ohkawa, & Imbalzano, 2006). The molecular mechanisms that couple proliferation with terminal differentiation during development, however, remain largely unknown, yet they must depend on the strict regulation of the cell cycle (Buttitta & Edgar, 2007).

2. The mitotic cell cycle.

Proliferation occurs through the mitotic cell cycle. This cycle comprises a series of cellular processes contributing to the duplication of a cell's genomic DNA and its division, producing two identical daughter cells. It consists of four well defined phases: G1 (gap 1), S (DNA synthesis), G2 (gap 2) and M (mitosis). The G1 phase primarily entails cell growth, replication of organelles, and synthesis of RNA and proteins required by the DNA replication machinery in the subsequent phase. During the S phase, this machinery is put to use, faithfully duplicating genomic DNA to

generate an identical copy for each daughter cell. The G2 phase, much like G1, is a period of cell growth, replication of organelles, and synthesis of RNA and proteins required for mitosis, with the addition of the replenishment of energy stores and dismantling of the cytoskeleton in order to provide further resources for division. Together, the G1, S and G2 phases are known as interphase. The M phase can be subdivided into two major processes: karyokinesis and cytokinesis. During karyokinesis, the nuclear envelope breaks down and the duplicated genomic DNA is condensed into pairs of homologous chromatids, termed chromosomes, which are pulled apart toward opposite poles of the cell by the mitotic spindle assembly. At each pole, the nuclear envelope then reforms and the chromatids decondense, producing a single cell with two complete nuclei. During the final phases of karyokinesis, cytokinesis is concurrently performed, in which a contractile ring composed of actin and myosin forms perpendicular to the axis of the spindle and pinches the cell into two, dividing the cytoplasmic components. The end result of the mitotic cell cycle is the generation of two identical daughter cells, each with a complete set of chromosomes and organelles, and each capable of beginning the cycle again at G1. If further proliferation is unfavorable, a cell can alternatively adopt a quiescent state known as G0, in which it will reside until receiving the appropriate signals stimulating its re-entry into the cell cycle (Bruce et al., 2015). One-way passage through the cell cycle and timely progression from one phase to the next is ensured by a complex regulatory network that is conserved in most eukaryotes.

2.1 Cyclins and cyclin-dependent kinases (CDKs).

The colossal task of replicating billions of DNA base pairs with high fidelity and equally distributing them into two daughter cells requires a plethora of highly specialized proteins, the activity of which must be strictly regulated. Perhaps the most fundamental and well characterized of such proteins are cyclin-dependent kinases (CDKs), serine/threonine kinases that phosphorylate various substrates to induce changes in their enzymatic activity or interaction with other proteins. Of the twenty CDKs identified in humans, only four are considered to be directly involved in the cell cycle, CDKs 1, 2, 4 and 6, functioning as the core machinery by which cell cycle phase-specific gene expression and protein modifications are modulated (Cao et al., 2014; Wood & Endicott, 2018; Zabihi, Lotfi, Yousefi, & Bashash, 2022). CDKs were named for their functional dependence on cyclin proteins, which induce their enzymatic activity through direct interaction. Of the twenty-nine cyclins identified in humans, ten are known to regulate the cell cycle through CDKs 1, 2, 4 and 6. These cyclins are classified into four sub-groups: D-, E-, A and B-cyclins (Cao et al., 2014; Wood & Endicott, 2018; Zabihi et al., 2022). The amount of each CDK is relatively stable throughout the cell cycle, so proper progression through and transition between cell cycle phases relies on the precise coordination of these cyclins through well-timed synthesis and degradation.

2.2 Cyclin-CDK regulation of the cell cycle.

Off all cyclins, D-cyclins are unique in the sense that they serve as the link between the extracellular environment and the cell cycle apparatus. In response to

extracellular mitogenic stimuli, such as growth factors, cytokines and extracellular matrix components, cells in early G1 upregulate their expression of D-cyclins (Klein & Assoian, 2008). D-cyclins assemble into CDK4- and CDK6-containing complexes, which perform the initial phosphorylation of retinoblastoma-associated (RB) pocket proteins (Sanidas et al., 2019; Topacio et al., 2019). This causes conformational changes that partially disrupt the repressor complexes they form with E2F transcription factors, inducing modest expression of G1/S genes including E- and A-cyclins (Fischer & Müller, 2017; Sanidas et al., 2019; Schade, Oser, Nicholson, & Decaprio, 2019). Resulting E-cyclins associate with CDK2, and Cyclin D-CDK4/6 complexes sequester the CDK inhibitor (CKI) $p27^{Kip1}$ away from Cyclin E-CDK2 complexes, resulting in their activation (Abukhdeir & Park, 2008; Fischer & Müller, 2017; Planas-Silva & Weinberg, 1997). Cyclin E-CDK2 complexes then hyper-phosphorylates RBs, inducing the complete disassociation of their repressor complexes and a positive-feedback loop that triggers passage through the restriction point and commitment to the G1/S transition (Fischer & Müller, 2017; Sanidas et al., 2019). Through E2F activation and direct phosphorylation, Cyclin E-CDK2 activity contributes to numerous processes that are essential for S phase initiation and progression, such as assembly of the pre-initiation complex and histone biosynthesis (Fagundes & Teixeira, 2021; Tanaka & Araki, 2010; Woo & Poon, 2003). Cyclin E-CDK2 also promotes its own degradation by the SCF ubiquitin ligase complex through autophosphorylation, as well as expression of A-cyclins, which bind CDK2 in the absence of Cyclin E (Nakayama, Hatakeyama, & Nakayama, 2001; Schulze et al., 1995; Welcker et al., 2003; Zerfass-Thome et al., 1997). Eventually, a threshold

is reached, at which point Cyclin A replaces Cyclin E to form the Cyclin A-CDK2 complex, which is required for completion of the S phase and prevents re-replication through the inhibition of further replication complex assembly (Coverley, Pelizon, Trewick, & Laskey, 2000; Petersen, 1999). At the end of S phase, CDK1 displaces CDK2 to form the Cyclin A-CDK1 complex, marking entry into G2 (Limas & Cook, 2019). While the function of this complex during G2 is still not well understood, it has been implicated in the G2/M transition through promotion of Cyclin B-CDK1 complex activation (Gong & Ferrell, 2010; Hégarat et al., 2020; Vigneron et al., 2018). Cyclin B-CDK1 then orchestrates M phase progression through phosphorylation of substrates involved in processes such as mitotic spindle assembly, chromosome condensation and nuclear envelope breakdown (Ding et al., 2020). One of these substrates is the anaphase-promoting complex (APC/C), an E3 ubiquitin ligase that induces the degradation of Cyclins A and B and promotes the completion of mitosis and cytokinesis (Fujimitsu, Grimaldi, & Yamano, 2016; M. Li & Zhang, 2009).

2.3 CDK inhibitors (CKIs).

In addition to regulation by their cyclin partners, the activity of CDKs is also modulated by two families of CDK inhibitor proteins (CKIs). The INK4 family of CKIs includes $p16^{INK4A}$, $p15^{INK4B}$, $p18^{INK4C}$ and $p19^{INK4D}$. These proteins are potent inhibitors of CDK4 and CDK6, competing with Cyclin D for association with CDK4/6 to prevent progression of the cell cycle past the G1 restriction point (Cánepa et al., 2007; Jeffrey, Tong, & Pavletich, 2000; Sherr & Roberts, 1999). The Cip/Kip family of CKIs, including $p21^{Cip1}$, $p27^{Kip1}$ and $p57^{Kip2}$, has a broader range of control over the cell

cycle, interacting with all the involved cyclin-CDK complexes (Besson, Dowdy, & Roberts, 2008). $p21^{Cip1}$ is a major transcriptional target of p53 and induces cell cycle arrest at the G1/S and G2/M transitions in response to a myriad of stressors, such as DNA damage, membrane damage and oxidative stress (Amani et al., 2021; el-Deiry et al., 1993; Gartel & Tyner, 1999). $p27^{Kip1}$, on the other hand, is primarily active in G0 and G1, and is rapidly downregulated upon mitogenic stimulation and entry into the cell cycle (Amani et al., 2021; Besson et al., 2006). $p57^{Kip2}$ is the most recently identified and least characterized CIP/KIP inhibitor. It has been shown to play a unique role during embryogenesis and be the only CKI required for embryonic development (M. H. Lee, Reynisdóttir, & Massagué, 1995; Matsuoka et al., 1995; Yan, Frisén, Lee, Massagué, & Barbacid, 1997). Furthermore, the activity of CDK2 and CDK1 is also determined by the balance of WEE1, CDC25 and 14-3-3 proteins. WEE1 is a kinase that phosphorylates CDK2 and CDK1 to inhibit their activity, while CDC25 is a family of phosphatases that activate CDK2 and CDK1 through removal of these phosphate groups (H. L. Smith, Southgate, Tweddle, & Curtin, 2020). 14-3-3 proteins activate WEE1 and sequester CDC25 proteins through direct interaction, further inhibiting CDK2 and CDK1 activity (Gardino & Yaffe, 2011). When considering the massive proliferation during tissue development, it is evident that interplay between cyclins, CDKs and CKIs is essential to ensure proper progression of the cell cycle and maintain genome stability.

3. The DNA damage response (DDR).

DNA is continuously being damaged in a variety of ways, resulting in DNA lesions that interfere with DNA replication, transcription and genomic integrity. Sources of DNA damage can be exogenous, such as ultraviolet (UV) radiation, infrared (IR) radiation and genotoxic chemicals, or endogenous, such as reactive oxygen species or replication stress (RS). To ensure homeostasis and safeguard inheritance, cells possess an additional network of pathways integrated within the cell cycle to avoid the propagation of mutations, known as the DNA damage response (DDR). The DDR includes both cell cycle checkpoints, which recognize DNA lesions and activate a signaling cascade that arrests the cell cycle, and mechanisms of DNA repair. The DDR is mediated by three members of the PI3K-related serine/threonine kinase family: DNA-protein kinase complex (DNA-PK), Ataxia-Telangiectasia mutated (ATM), and ATM and Rad3-related (ATR). In response to DNA damage, ATM and ATR signal transduction activates the G1/S, intra-S or G2/M checkpoints, whereas DNA-PK is primarily involved in the nonhomologous end joining (NHEJ) DNA repair pathway (Marechal & Zou, 2013).

3.1 The ATR-mediated response to replication stress (RS).

Unlike ATM and DNA-PK, ATR is the only DDR kinase that is essential for the survival of proliferating cells, and its deletion results in early embryonic lethality in mice and cell death in human cells (Ronco, Martin, Demange, & Benhida, 2017). This is likely due to the fact that, while ATM and DNA-PK primarily respond to double-stranded breaks (DSBs), ATR responds to a broad spectrum of DNA damage

implicated in intrinsic RS, although there is much overlap and redundancy between these two pathways (Zeman & Cimprich, 2014). RS refers to the slowing or stalling of replication forks, and can arise due to a variety of obstacle, such as nucleotide depletion, DNA lesions, DNA secondary structures, ribonucleotide incorporation and collision of the replication and transcription machineries (Zeman & Cimprich, 2014). When slowing or stalling of the replication fork occurs, MCM helicase becomes uncoupled from the DNA polymerase and continues to unwind double-stranded DNA (dsDNA), generating a length of single-stranded DNA (ssDNA) that becomes coated by replication protein A (RPA) (Byun, Pacek, Yee, Walter, & Cimprich, 2005; Zeman & Cimprich, 2014). The presence of ssDNA-RPA at a junction with dsDNA results in the recruitment of numerous protein complexes, including Rad17-RFC2-5, 9-1-1 and ATR-interacting protein (ATRIP)-ATR, and the proximity of these complexes ultimately allows for the TOPBP1-mediated activation of ATR (Burrows & Elledge, 2008; Marechal & Zou, 2013; Parrilla-Castellar, Arlander, & Karnitz, 2004; Zou & Elledge, 2003). Active ATR, in turn, phosphorylates numerous proteins involved in the DDR, initiating a signal cascade. One such protein is the serine/threonine kinase CHK1, which phosphorylates WEE1 and CDC25 proteins to induce their activity or degradation, respectively, thereby promoting inhibition of CDK2 and CDK1 (Barnum & O'Connell, 2014; H. L. Smith et al., 2020). Furthermore, active ATR, through both direct phosphorylation and transactivation of CHK1, promotes the stabilization of p53 and expression of $p21^{Cip1}$, contributing an additional mechanism of CDK2 and CDK1 inhibition (Barnum & O'Connell, 2014; Joaquin & Fernandez-Capetillo, 2012).

Together, these actions result in the arrest of the cell cycle at the G1/S, intra-S or G2/M checkpoints, allowing time for DNA to be properly repaired.

In addition to inducing cell cycle arrest at checkpoints, ATR also functions to preserve genome integrity and stimulate DNA repair. Through direct phosphorylation and transactivation of CHK1, ATR prevents the firing of late replication origins and promotes the replenishment of nucleotide pools to limit further replication stress. In addition, it facilitates the stabilization, recovery and restart of replication forks (Saldivar, Cortez, & Cimprich, 2017; Zeman & Cimprich, 2014). Furthermore, ATR phosphorylates numerous substrates involved in the recruitment and activity of DNA repair machinery. One such substrate is the histone H2A.X, which is phosphorylated in a region up to 1-2 megabases around sites of DNA damage(Ciccia & Elledge, 2010; Ward & Chen, 2001). H2A.X can be phosphorylated by DNA-PK, ATM and ATR, exemplifying the overlap between DDR pathways (Clay & Fox, 2021). Phosphorylation of H2A.X recruits MDC1, which acts as a protein scaffold, recruiting chromatin modifiers that relax heterochromatin and expose the region of DNA damage. MDC1 also recruits the MRN complex, which binds and activates ATM to further amplify the signal. This results in the accumulation of repair factors to the vicinity of DNA damage, such as BRCA1 and 53BP1, which promote homologous repair and non-homologous end-joining repair pathways, respectively. While H2AX is not required for their localization, it plays a vital role in amplifying and maintaining the DDR signal to sufficiently recruit these factors (Ciccia & Elledge, 2010; H. L. Smith et al., 2020). Nevertheless, the ATR-mediated response to RS is not always effective at

repairing replication forks and DNA damage. If excessive replication fork stalling occurs, ssDNA can be subject to nuclease activity, resulting in further DNA lesions and RS (Saldivar et al., 2017; Técher, Koundrioukoff, Nicolas, & Debatisse, 2017; Zeman & Cimprich, 2014).

3.2 The DDR and cell fate.

The DNA damage response exists to recognize and repair DNA damage, in order to avoid the propagation of mutations that could lead to genomic instability, disruption of homeostasis and disease. In response to extensive or irreparable DNA damage, however, the DDR is known to promote senescence, apoptosis and differentiation to prevent the proliferation of damaged cells. DNA damage-induced senescence is mediated by p53 transactivation of $p21^{Cip1}$, which inhibits CDK activity to induce permanent G1 arrest and senescence (Mijit, Caracciolo, Melillo, Amicarelli, & Giordano, 2020; Speidel, 2015). $p16^{INK4A}$ is also implicated in maintaining senescence by preventing the phosphorylation of RBs by Cyclin D-CDK4/6 complexes, allowing RBs to recruit chromatin modifiers that silence expression of genes that drive cell cycle progression (Mijit et al., 2020; Narita et al., 2003). Differing levels of p53 appear to contribute to the decision between senescence or apoptosis, with increased p53 expression favoring apoptosis (Clay & Fox, 2021). DNA damage-induced apoptosis is largely mediated by p53 transactivation of pro-apoptotic factors, such as Puma, Noxa and Bax (Speidel, 2015). These factors promote the permeabilization of the mitochondrial membrane, allowing the release of proteins that activate the caspase signaling cascade into the cytosol (Nakano & Vousden, 2001;

Shibue et al., 2006). More recently, the DDR has been shown to elicit the differentiation programs of several cell types, including hematopoietic stem cells, B lymphocyte precursors, neuronal stem cells, melanocytes and keratinocytes (A. Freije et al., 2014; Inomata et al., 2009; T. Li, Zhou, Ju, & Wang, 2016; Santos et al., 2014; Schneider et al., 2013; Wang et al., 2014; Zanet et al., 2010). Despite the importance to genomic integrity and tissue homeostasis, the mechanisms driving DDR-induced differentiation remain unclear.

4. Endoreplication as a link between the cell cycle and differentiation.

Developmentally programmed endoreplication is the process by which a cell undergoes DNA replication in the absence of cell division, becoming polyploid, and is linked to terminal differentiation. The mechanisms by which endoreplication is achieved are diverse and vary between tissues. Endoreplication results in tetraploid cells (4C DNA content); however, cells can also undergo further endoreplication and become polyploid (>4C DNA content). This can be accomplished either by cytokinetic failure or early mitotic arrest (Z. Ullah, Lee, Lilly, & DePamphilis, 2009). During endoreplication by cytokinetic failure, a cell progresses through mitosis unperturbed, but fails to divide, resulting in a tetraploid binucleated cell. These binucleated cells can arise in several ways, such as failure to specify a cleavage plane due to insufficient RhoA activation or cleavage furrow ingression failure due to improper anchoring of the actomyosin ring (Leone, Musa, & Engel, 2018; Margall-Ducos, Celton-Morizur, Couton, BréGerie, & Desdouets, 2007). Alternatively, endoreplication induced by early mitotic arrest occurs when a cell undergoes DNA

replication without progressing through mitosis. This results in a tetraploid, with the number of nuclei depending on when mitotic arrest occurred. Endoreplication through early mitotic arrest requires inhibition of the Cyclin B/CDK1 complex that facilitates progression from the G2 phase to the M phase. This can occur through downregulation of Cyclin B, as well as through direct inhibition of CDK1 by CKIs (Tan et al., 2002; Zakir Ullah, Kohn, Yagi, Vassilev, & Depamphilis, 2008; Ying Zhang, Wang, & Ravid, 1996).

4.1 DDR-induced endoreplication.

In addition to developmentally programmed endoreplication, the DDR has been shown to trigger endoreplication and terminal differentiation in several mammalian tissues through DDR-mediated early-mitotic arrest. This has, for the most part, been observed in the epidermis, which undergoes developmentally programmed endoreplication and is frequently exposed to exogenous sources of DNA damage. It was found that, while UV irradiation induces apoptosis of epidermal keratinocytes, sub-lethal levels of UV irradiation induce endoreplication and terminal differentiation, suggesting there exists a physiological threshold for DNA damage in the epidermis (de Pedro, Alonso-Lecue, Sanz-Gómez, Freije, & Gandarillas, 2018). Moreover, induction of endoreplication was also observed with oncogenic insults and genotoxic drug treatments that induce DNA damage, such as the c-Myc overexpression, Cyclin E overexpression, loss of p53 and doxorubicin treatment (A Freije et al., 2012; A. Freije et al., 2014; Gandarillas, Davies, & Blanchard, 2000; Rut Molinuevo, Freije, Contreras, Sanz, & Gandarillas, 2020). This was confirmed to be driven by the DDR,

and the mitotic transcription factor FOXM1 rescued the effect of genotoxic insults on endoreplication, suggesting it occurs through early mitotic arrest (Rut Molinuevo et al., 2020; R. Molinuevo et al., 2017). Intriguingly, a similar phenomenon was observed in keratinocytes of the oral epithelium, suggesting this mechanism may be conserved in tissues that are susceptible to genotoxic insult (Sanz-Gómez et al., 2018). Furthermore, outside of the epidermis, it has also been observed that persistent inflammatory stimulus induces the DDR-mediated endoreplication and terminal differentiation of macrophage precursors (Herrtwich et al., 2016). While examples of DDR-mediated endoreplication and terminal differentiation are few, it is important to note that all are in the context of exogenous genotoxic insults, oncogenic transformation or chronic inflammatory conditions that promote hyperactivation of the cell cycle.

4.2 Endoreplication during pregnancy.

Beyond embryogenesis, the most dramatic period of development, in both rate and scale, within the lifetime of an organism occurs during pregnancy. In order to foster the development of offspring, a mother must undergo rapid expansion of numerous specialized tissues in a manner that limits disruption of homeostasis and promotion of disease. This requirement for rapid tissue growth necessitates a strict balance between proliferation and differentiation. Accordingly, developmentally programmed endoreplication occurs in several mammalian tissues during pregnancy. In the placenta, trophectoderm cells undergo endoreplication and differentiate into trophoblast giant cells, which penetrate the uterus and promote blastocyst

implantation (Gardner & Davies, 1993; Hemberger, Hanna, & Dean, 2020; MacAuley, Cross, & Werb, 1998). Subsequently, in the uterus, stromal cells of the endometrium endoreplicate and differentiate into decidual cells, which further facilitate blastocyst implantation and vascularization (Ansell, Barlow, & McLaren, 1974; Kirk & Clingan, 1980; SACHS & SHELESNYAK, 1955). Another example of pregnancy-induced endoreplication is liver growth that occurs through hepatocyte hypertrophy (Milona et al., 2010). Finally, in the mammary gland (MG), alveolar cells undergo endoreplication at the onset of lactation (Banerjee & Wagner, 1972; Banerjee, Wagner, & Kinder, 1971; Rios et al., 2016; G. H. Smith & Vonderhaar, 1981). While these phenomena have long been observed and considered necessary adaptations for pregnancy-induced tissue development, the molecular mechanisms driving these endoreplication events remain poorly understood. Given the rapid expansion that occurs in tissues during pregnancy, however, it is tempting to speculate that intrinsic replication stress may be a source of DNA damage driving these endoreplication events.

4.3 The mammary gland (MG): an endoreplicative tissue.

The MG plays an essential role in the survival of mammalian species by producing milk required for the nourishment of offspring. It comprises a branched tubuloalveolar epithelium, embedded within the stroma-rich fat pad of the breast, that is bi-layered in structure, consisting of an inner layer of luminal cells and an outer layer of myoepithelial or basal cells. The MG is a unique organ in the sense that the vast majority of its development occurs postnatally in response to hormonal cues. While a

rudimentary ductal tree, termed an anlage, is formed at the nipple during embryogenesis, it remains morphogenetically static until puberty. With the onset of puberty, the epithelium branches out into the fat-pad of the breast, generating an expansive ductal network through successive elongation and bifurcation events (Biswas, Banerjee, Baker, Kuo, & Chowdhury, 2022; H. Macias & Hinck, 2012). Additionally, with each estrous or menstrual cycle, the MG flows and ebbs, undergoing growth and differentiation of pseudo-alveoli in preparation for pregnancy, followed by the regression of these pseudo-alveoli and remodeling if pregnancy does not occur (Biswas et al., 2022). In the event of pregnancy, the mammary gland undergoes a profound transformation known as alveologenesis, in which luminal alveolar progenitors proliferate and subsequently differentiate into polyploid alveolar cells that completely occupy the fat-pad and secrete milk during lactation (Banerjee & Wagner, 1972; Banerjee et al., 1971; Ho, Guilbaud, Blow, Sale, & Watson, 2016; H. Macias & Hinck, 2012; Rios et al., 2016; G. H. Smith & Vonderhaar, 1981; Watson, 2022). This polyploidization of the MG is conserved across mammalian species, including mice and humans, and it is required for efficient milk production (Banerjee & Wagner, 1972; Banerjee et al., 1971; Rios et al., 2016; G. H. Smith & Vonderhaar, 1981). Once breastfeeding is complete, in a process known as involution, massive cell death clears these milk-producing polyploid cells and tissue remodeling brings the epithelium back to a pre-pregnancy-like state (Biswas et al., 2022; Kreuzaler et al., 2011; H. Macias & Hinck, 2012; Rios et al., 2016; Watson, 2022). Considering the potential for multiple pregnancies, endoreplication, by coupling proliferation with terminal differentiation, presents a developmental

advantage for cell survival and tissue function. MG alveolar endoreplication has been suggested to require Aurora A kinase upregulation and cytokinesis failure (Rios et al., 2016). Although the role of Aurora A during the G2/M transition and mitotic spindle assembly has been extensively studied, whether it is directly implicated in cytokinesis remains unclear (Reboutier, Benaud, & Prigent, 2015). Therefore, the mechanisms regulating the transition from a proliferative mitotic cell cycle to an endocycle in the MG have yet to be elucidated. For my thesis work, I investigated the role of the DDR in mammary alveolar endoreplication during lactation.

Objectives

- Characterize the alveolar polyploid population of the MG.
- Determine whether DNA damage plays a role in regulating mammary alveolar endoreplication.
- Determine whether RS is a source of DNA damage during alveologenesis.
- Determine the molecular mechanisms by which the cell cycle is arrested during alveolar endoreplication.

Results

Endoreplication results in a heterogeneous alveolar population during lactation.

Mammary alveolar cells have previously been shown to undergo endoreplication during lactation, a process essential for efficient milk production (Banerjee & Wagner, 1972; Banerjee et al., 1971; Rios et al., 2016; G. H. Smith & Vonderhaar, 1981). How these cells become committed to endoreplication and the outcome of this endoreplication (in terms of DNA content and number of nuclei) remains unclear. It has previously been shown that a significant percentage of alveolar cells become tetraploid (4C) and binucleated during lactation (Ho et al., 2016; Rios et al., 2016). Through IHC staining and *in situ* 3D DNA content analysis of tissue sections from lactation day (LD) 5 MGs, we further detect polyploid (> 4C) mononucleated alveolar cells and binucleated cells containing polyploid nuclei (Figure 1.1a). Additionally, we detect the rare occurrence of multinucleated cells (Figure 1.1b, arrows). To better understand the heterogeneity of the alveolar population, we performed FACS DNA content analysis of the Cytokeratin-8 positive ($CK8^+$) luminal cell population from MGs of nulliparous, pregnancy day (PD) 17.5, LD2 and LD5 mice (Figure 1.2a-e). As previously reported (Rios et al., 2016), we observe a substantial increase in the proportion of tetraploid cells during lactation (Figure 1.2d, e). In addition, we identify a novel polyploid subpopulation that arises at the end of pregnancy and expands during lactation (Figure 1.2c-e). Through visualization of the FACS-purified $CK8^+$ population from LD5 MGs, we find ~35% of tetraploid cells are mononucleate, with the remaining ~65% binucleate, whereas polyploid cells are observed to be both

mononucleate and binucleated in a ~ 50/50 ratio (Figure 1.2f, g). Together, these results demonstrate mammary alveolar cells are heterogeneous during lactation with respect to DNA content and nuclei number.

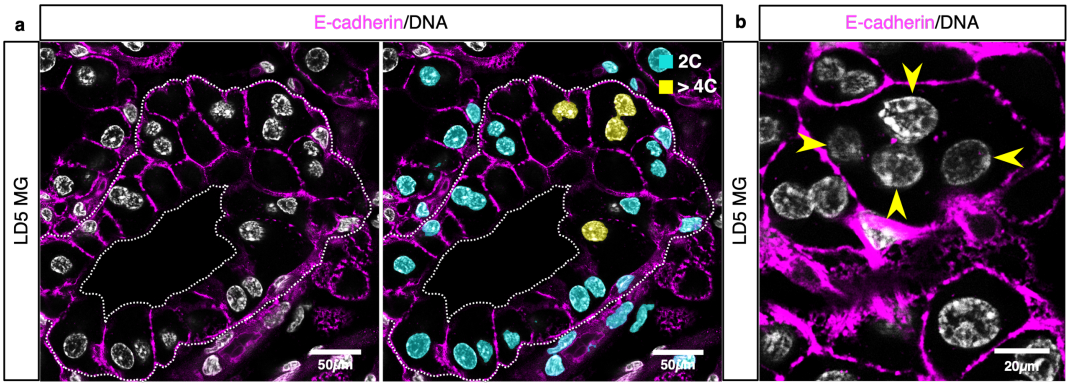

Figure 1.1: Alveolar luminal cells are heterogeneous in regard to ploidy and number of nuclei during lactation. a) Optical section from a 3D confocal image showing an alveolar unit from a MG at LD5 (left). Right image illustrates the heterogeneity of the MG by representing the DNA content of individual nuclei (2C in blue, > 4C in yellow) calculated by in situ 3D DNA content analysis. E-cadherin detected in magenta. White broken line represents the border of the alveolus. Nuclear DNA by Hoechst. **b)** Optical section from a 3D confocal image at LD5 focused on a polyploid multinucleated alveolar cell. Arrows point to each of the 4 nuclei. E-cadherin shown in magenta. Nuclear DNA by Hoechst.

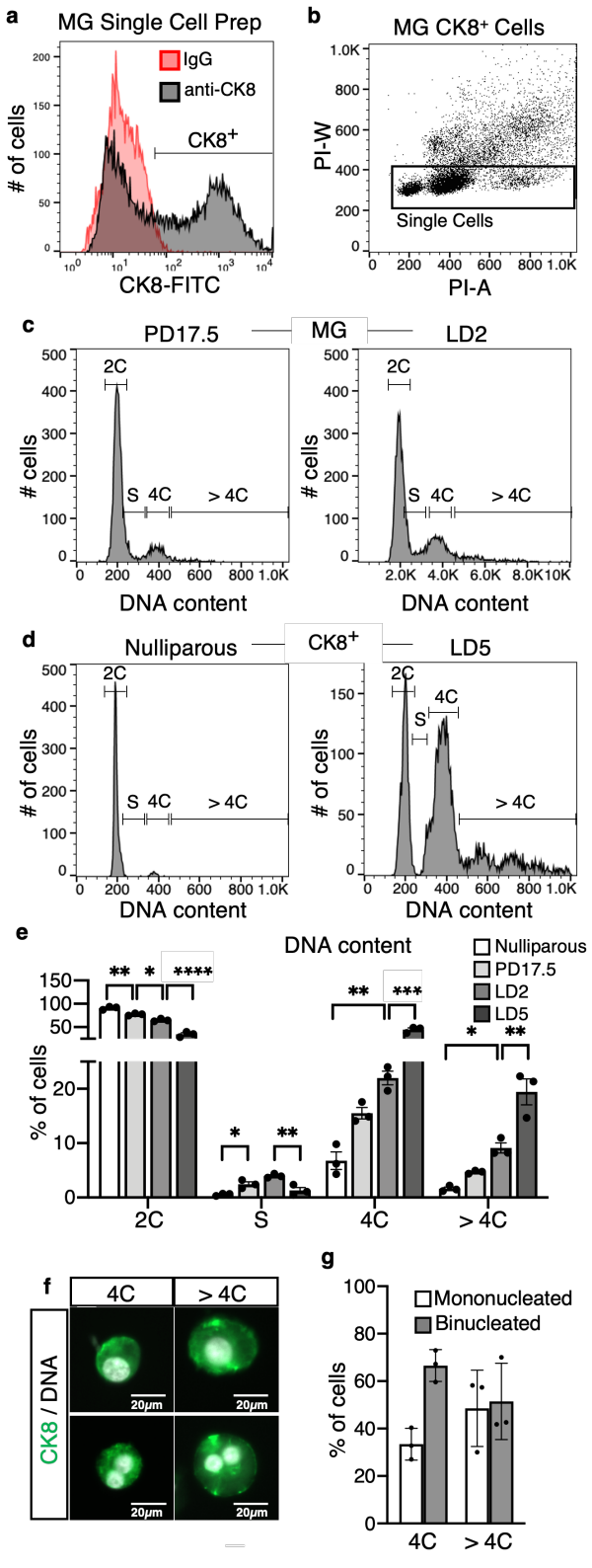

Figure 1.2: Endoreplication results in a heterogeneous alveolar population during lactation. a) FACS analysis of a representative MG single cell preparation used for the identification of the luminal CK8+ population. Red histogram represents the negative isotype control (IgG). Gate indicates the CK8+ population in relation to the negative isotype control. **b)** FACS analysis of the MG CK8+ cells for the identification of single cells, based on propidium iodide area (PI-A) versus width (PI-W). Black box shows the gating strategy for single cell identification. **c)** Representative FACS histograms for DNA content analysis of the CK8+ population in PD17.5 (left) and LD2 MGs (right). **d)** Representative FACS histograms for DNA content analysis of the CK8+ population in the nulliparous (left) and LD5 MGs (right). **e)** Quantification of FACS DNA content analysis showing the percentage of CK8+ cells with 2C, 4C or > 4C DNA content, or in the S phase, from nulliparous, PD17.5, LD2 and LD5 MGs. **f)** Representative images and **g)** quantification of mononucleated and binucleated CK8+ cells from LD5 MGs, sorted based on DNA content (4C or >4C). Nuclear DNA by propidium iodide. Data are shown as the mean ± SD; n=3 biological replicates. For **(f)** one-way ANOVA Tukey's test. p values: * < 0.05, **< 0.001, *** < 0.0005, **** < 0.0001.

To further investigate the role of endoreplication during alveologenesis, we took advantage of the HC11 murine mammary cell line as an *in vitro* lactation model. This cell line resembles the MG in that it undergoes differentiation into milk-producing secretory cells when cultured in the presence of the lactogenic hormones dexamethasone, insulin, and prolactin (DIP, Figure 1.3a). As previously published (Sornapudi et al., 2018), we find ~80% of differentiated HC11 cells undergo G0/G1 arrest, presenting 2C DNA content (Figure 1.3b, c). In addition, we identify a population of polyploid HC11 cells that increases during differentiation (Figure 1.3b, c). This observation suggests HC11 cells undergo endoreplication during differentiation, in accordance with the role of endoreplication in milk production. To further investigate this, we treated undifferentiated HC11 cells at 80% confluence with blebbistatin (Blebbi, 30uM), a myosin II inhibitor that prevents cytokinesis and induces endoreplication through cytokinesis failure (Straight et al., 2003). FACS DNA content analysis 6 hours post-treatment shows blebbistatin efficiently induces mitotic arrest in HC11 cells, increasing the proportion of tetraploid cells (Figure 1.4a). By differentiation day 3 (DIP3), cells escape the mitotic arrest imposed by blebbistatin and undergo further endoreplication, becoming polyploid (Figure 1.4b). Increased polyploidy is accompanied by an increase in the formation of milk-containing domes, and increased expression of the milk proteins β-Casein (*Csn2*) and Periplin-2 (PLIN2), detected by RT-qPCR and ICC respectively (Figure 1.4c-f). Together, these data demonstrate HC11 cells endoreplicate when cell division is blocked, resulting in increased milk production. They are, therefore, a suitable *in vitro* model to investigate endoreplication during alveolar differentiation.

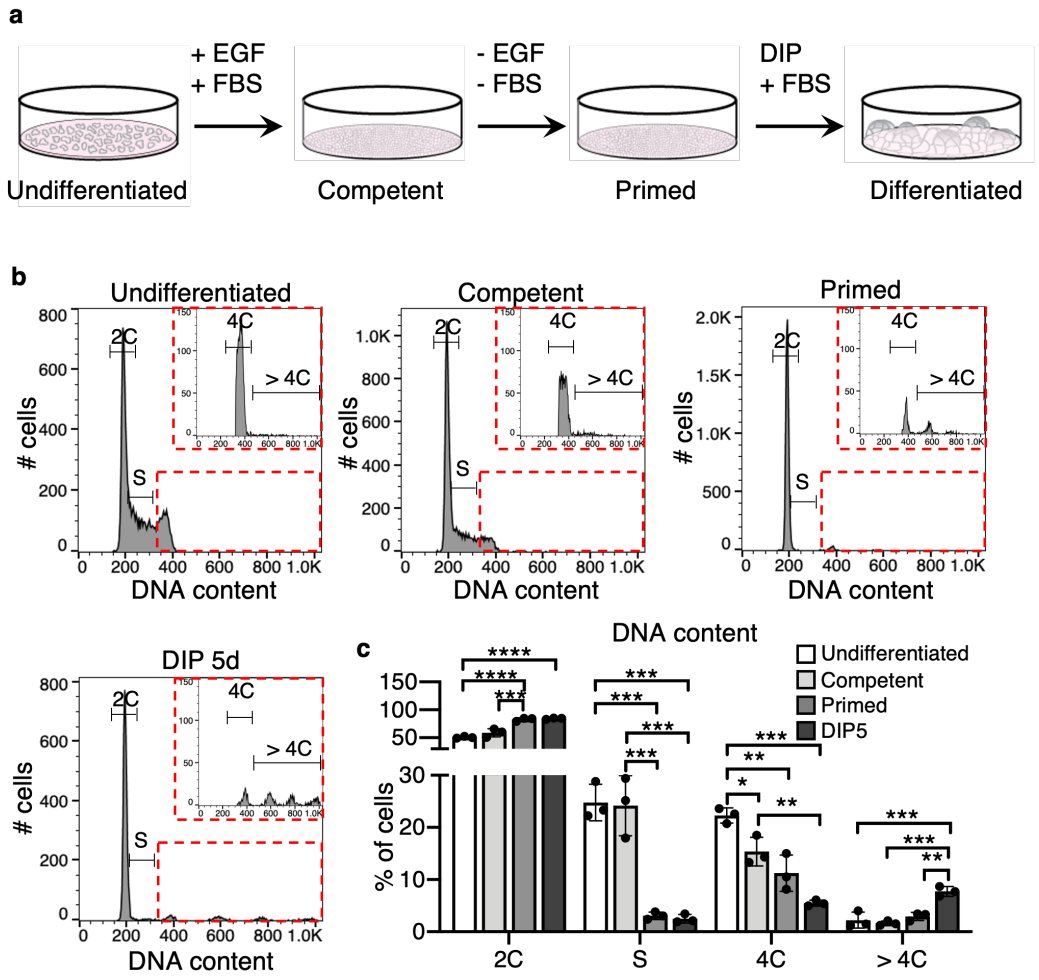

Figure 1.3: HC11 cells undergo endoreplication during *in vitro* lactogenic differentiation. a) Cartoon representing the differentiation process of HC11 cells. **b)** Representative FACS histograms for DNA content analysis of undifferentiated, competent, primed and differentiated (DIP5) HC11 cells. Red broken lines show a magnification of the histogram corresponding to the 4C and >4C populations. Histograms are representative of n=3 biological replicates. **c)** Quantification of FACS DNA content analysis showing the percentage of undifferentiated, competent, primed and differentiated (DIP5) HC11 cells with 2C, 4C or > 4C DNA content or in the S phase. Data shown as the mean ± SD; n=3 biological replicates; one-way ANOVA Tukey's test. p values: * < 0.05, **< 0.001, *** < 0.0005, **** < 0.0001.

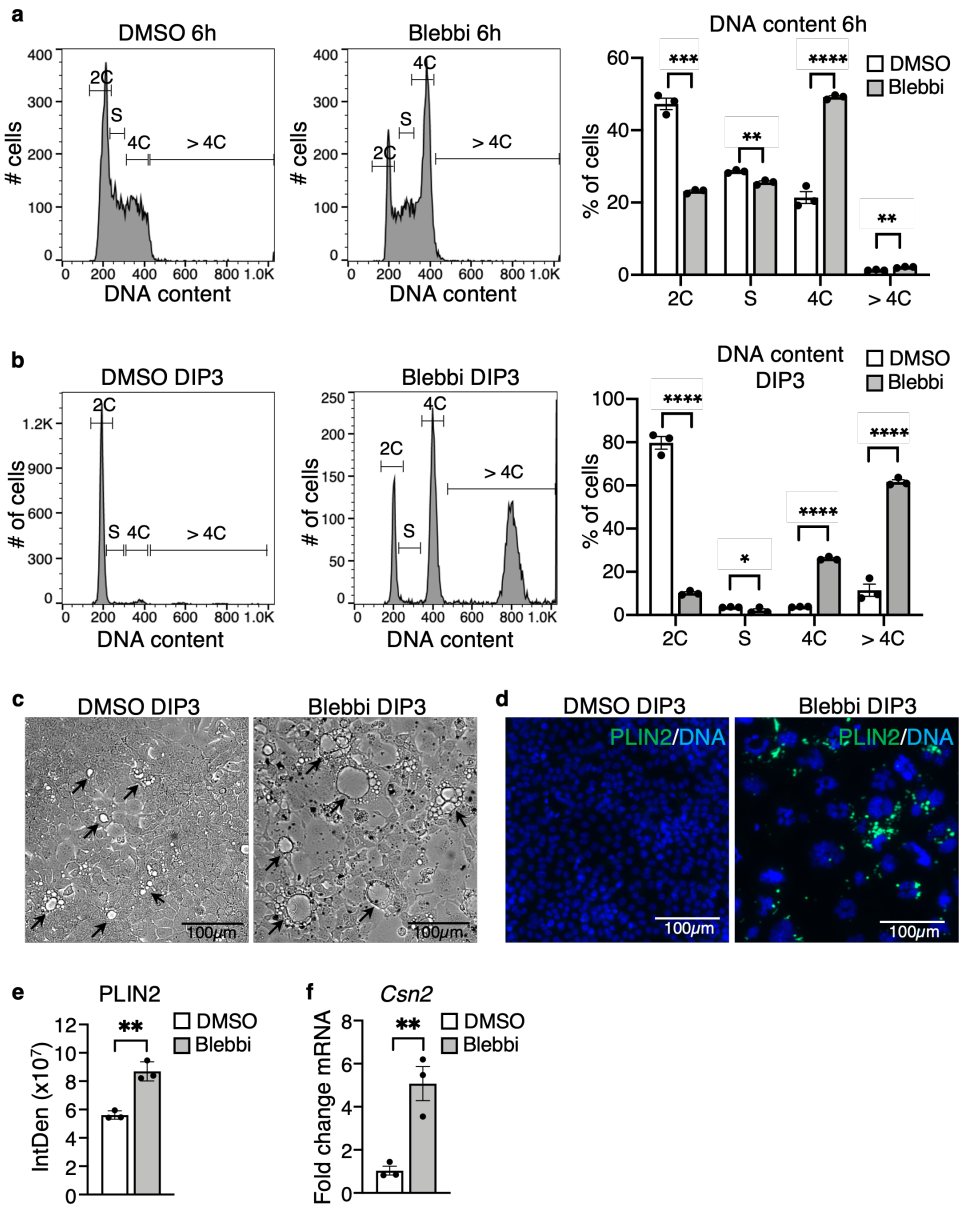

Figure 1.4: Cytokinesis failure results in increased HC11 endoreplication and milk production. a) Representative FACS histograms for DNA content analysis (left) and quantification (right) of undifferentiated HC11 treated with DMSO or blebbistatin (Blebbi) for 6 hours. **b)** Representative FACS histograms for DNA content analysis (left) and quantification (right) of differentiated HC11 (DIP3) treated with DMSO or Blebbi. **c)** Phase contrast images of showing milk domes in differentiated (DIP3) HC11, treated with DMSO or Blebbi. **d)** Detection of Perilipin2 (PLIN2, green) in differentiated (DIP3) HC11, treated with DMSO or Blebbi. Nuclear DNA by Hoechst. Images are representative of n=3 biological replicates. **e)** Quantification of PLIN2 expression in differentiated (DIP3) HC11, treated with DMSO or Blebbi. **f)** Quantification of *Csn2* expression in differentiated (DIP3) HC11, treated with DMSO or Blebbi, as detected by RT-qPCR. Data shown as the mean ± SD except for **(f)** data shown as mean ± S.E.M; n=3 biological replicates; two-tailed Student's t-test. p values: * < 0.05, **< 0.001, *** < 0.0005, **** < 0.0001.

CDK1 inhibition drives endoreplication of alveolar cells through an early mitotic arrest.

Through visualization of FACS-purified subpopulations, we observe that a large proportion of polyploid HC11 cells were mononucleate at DIP3 (Figure 1.5a). While cytokinetic failure has been suggested to generate binucleated alveolar cells *in vivo* (Rios et al., 2016), the presence of mononucleate polyploid cells both *in vitro* and *in vivo* indicates an early mitotic arrest at the G2/M transition is also a contributing factor. Endoreplication through early mitotic arrest requires the inactivation of the mitotic regulator CDK1 (Z. Ullah, Lee, & Depamphilis, 2009). In addition, there must be a transition in the activity of CDK/CYCLIN complexes. CYCLIN B must be downregulated to facilitate CDK1 inactivation and G2/M arrest, while the activity of the CDK2/CYCLIN E complex must persist to allow for DNA replication (Øvrebø & Edgar, 2018). Accordingly, we find, during lactogenic differentiation of HC11 cells, CYCLIN B expression is lost while CYCLIN E expression is maintained (Figure 1.5b). To investigate if CDK1 inactivation is sufficient to induce endoreplication during lactogenic differentiation, we treated undifferentiated HC11 at 80% confluence with the CDK1 inhibitor Ro-3306 (5uM). FACS DNA content analysis 6 hours after treatment with Ro-3306 shows CDK1 inhibition efficiently induces mitotic arrest, as detected by the accumulation of tetraploid cells (Figure 1.6a, b). By DIP3, cells escape the mitotic arrest imposed by Ro-3306 and undergo further endoreplication, becoming polyploid (Figure 1.6c, d). Accordingly, CSN2 expression increases, as detected by RT-qPCR and WB (Figure 1.6e, f). These results show CDK1 inhibition and early mitotic arrest are sufficient to drive endoreplication during lactogenic

differentiation in HC11 cells, resulting in increased milk production. Through visualization of FACS-purified subpopulations, we observe CDK1 inhibition generates mono-, bi- and multinucleated polyploid cells (Figure 1.6g). In contrast, treatment with blebbistatin predominantly generates bi- and multinucleated cells (Figure 1.6g). This shows that the heterogeneity of the MG observed *in vivo* is recapitulated by CDK1 inhibition, but not by the cytokinesis failure induced by blebbistatin. Altogether, these results suggest early mitotic arrest imposed by CDK1 inhibition is involved in alveolar endoreplication.

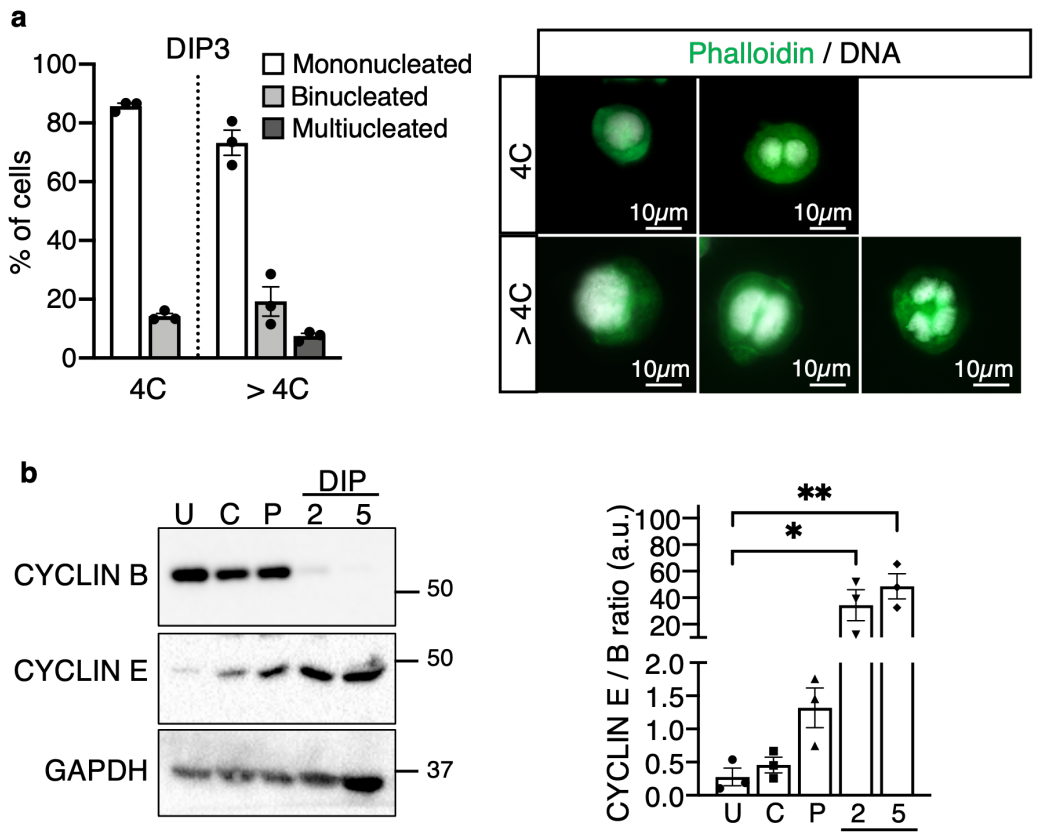

Figure 1.5: HC11 cells undergo endoreplication through an early mitotic arrest involving Cdk1 inactivation. a) Representative images (left) and quantification (right) of mono-, bi- and multinucleated (more than 2 nuclei) differentiated (DIP3) HC11, sorted based on DNA content (4C or >4C). Nuclear DNA by propidium iodide. Phalloidin shown in green. Data shown as the mean ± S.E.M; n=3 biological replicates. **b)** Representative western blot showing the expression of CYCLIN E and CYCLIN B in undifferentiated (U), competent (C), primed (P) and differentiated (DIP 2 and 5) HC11. Right histogram shows the quantification of the CYCLIN E: CYCLIN B ratio during HC11 differentiation. Data shown as the mean ± S.E.M; n=3 biological replicates; two-tailed unpaired Student's t-test. p values: * < 0.05, **< 0.001.

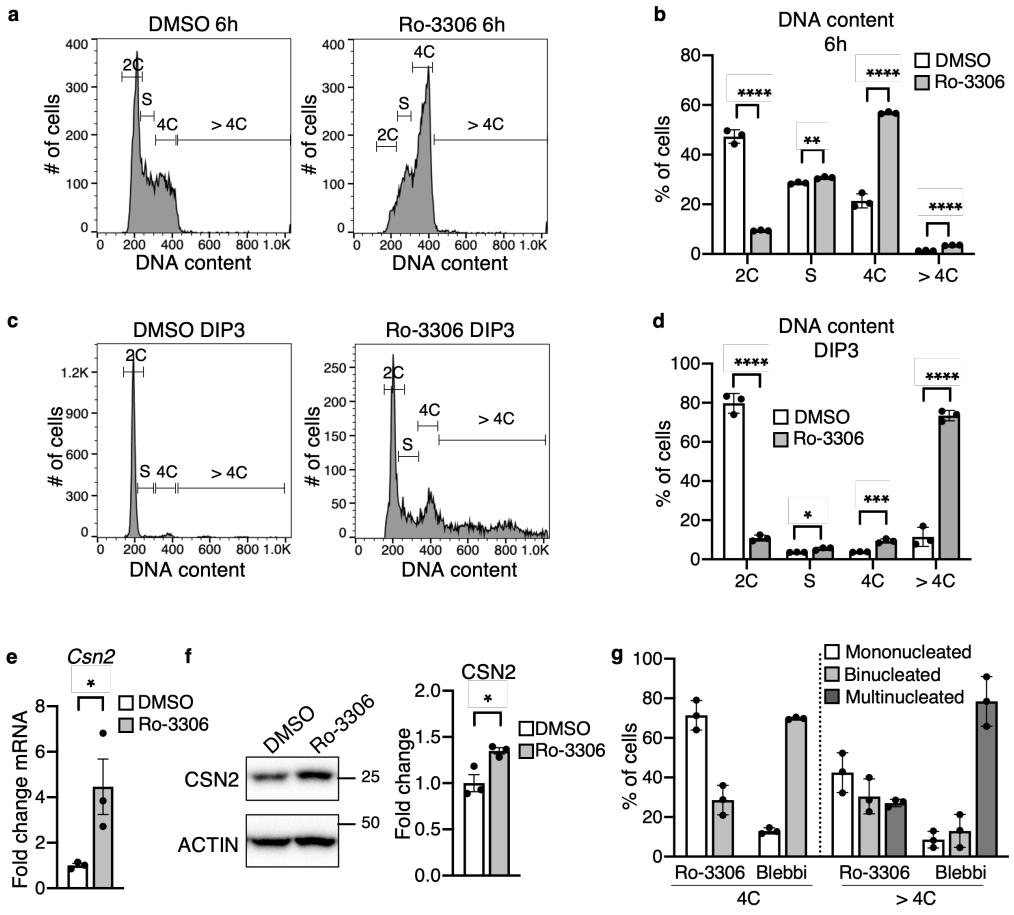

Figure 1.6: CDK1 inhibition increases HC11 endoreplication and milk production, and recapitulates the heterogeneity observed in the MG. a) Representative FACS histograms for DNA content analysis of undifferentiated HC11 treated with DMSO or Ro-3306 for 6 hours. **b)** Quantification of FACS DNA content analysis showing the percentage of HC11 cells with 2C, 4C or > 4C DNA content or in the S phase, 6 hours after treatment with DMSO or the Cdk1 inhibitor Ro-3306. **c)** Representative FACS histograms for DNA content analysis of differentiated HC11 (DIP3) treated with DMSO or Ro-3306. **d)** Quantification of FACS DNA content analysis showing the percentage of differentiated HC11 cells (DIP3) with 2C, 4C or > 4C DNA content or in the S phase, after treatment with DMSO or Ro-3306. **e)** Quantification of Csn2 expression in differentiated HC11 (DIP3) after DMSO or Ro-3306 treatment, as detected by RT- qPCR. **f)** Western Blot (left) and quantification (right) of CSN2 expression in differentiated HC11 (DIP3) after DMSO or Ro-3306 treatment. **g)** Quantification of percentage of mono-, bi- or multinucleated (more than 2 nuclei) differentiated HC11 (DIP3) treated with Ro-3306 or blebbistatin (blebbi) and sorted based on DNA content (4C or > 4C). Data shown as the mean ± SD except for (d) data shown as mean ± S.E.M; n=3 biological replicates; two-tailed Student's t- test. p values: * < 0.05, **< 0.001, *** < 0.0005, **** < 0.0001.

DNA damage during alveologenesis increases mammary alveolar endoreplication.

Developmentally programmed endoreplication occurs in different mammalian tissues not only during pregnancy (Ansell et al., 1974; Banerjee & Wagner, 1972; Banerjee et al., 1971; Gardner & Davies, 1993; Hemberger et al., 2020; Kirk & Clingan, 1980; MacAuley et al., 1998; Milona et al., 2010; Rios et al., 2016; SACHS & SHELESNYAK, 1955; G. H. Smith & Vonderhaar, 1981), but also during organogenesis and tissue regeneration in response to injury (de Pedro et al., 2018; Diril et al., 2012; Herrtwich et al., 2016; Lazzeri et al., 2018; Miyaoka et al., 2012; Sanz-Gómez et al., 2018; Senyo et al., 2013). In addition, DNA damage induced by genotoxic stress has been shown to induce endoreplication and terminal differentiation through the activation of the G2/M cell cycle checkpoint in various mammalian tissues (de Pedro et al., 2018; A. Freije et al., 2014; R. Molinuevo et al., 2017; Sanz-Gómez et al., 2018). In the MG, DNA damage occurs in alveolar cells during pregnancy (Xu et al., 2019), however, whether it plays a physiological role during alveologenesis remains unknown. To determine the extent of DNA damage during alveologenesis and lactation, we investigated the phosphorylation of histone H2A.X at Serine-139 (γH2AX), a site that is rapidly phosphorylated in the presence of DNA strand breaks (Fernandez-Capetillo, Lee, Nussenzweig, & Nussenzweig, 2004). We find γH2AX is present in CK8+ luminal cells throughout alveologenesis, with the peak occurring at PD10.5 (Figure 1.7a-c). In HC11 cells, γH2AX is highest in undifferentiated cells that are actively proliferating and lower in confluent cells during competency and priming (Figure 1.8a, b). However, we detect an increase in γH2AX

when HC11 cells underwent differentiation (Figure 1.8a, b), and phalloidin staining shows that γH2AX accumulates in cells forming milk domes (Figure 1.8c). These results suggest DNA damage plays a role in lactogenic differentiation and endoreplication. To investigate, HC11 cells were treated with doxorubicin (50nM), which induces DNA damage by inhibiting topoisomerase II during DNA replication. Accordingly, doxorubicin results in an increase of γH2AX 24h post-treatment (Figure 1.9a, b). FACS DNA content analysis shows the proportion of tetraploid cells increases after 24h of doxorubicin treatment, indicating the G2/M checkpoint was activated (Figure 1.9c, d). By DIP3, an increase in polyploidization is also detected (Figure 1.9e, f). Visualization of the FACS-purified population illustrates that DNA damage-induced endoreplication generated both mono- and binucleated polyploid cells, recapitulating the heterogeneity observed in the MG (Figure 1.9g). Polyploidization is accompanied by an increase of CSN2 detected by WB (Figure 1.9h).

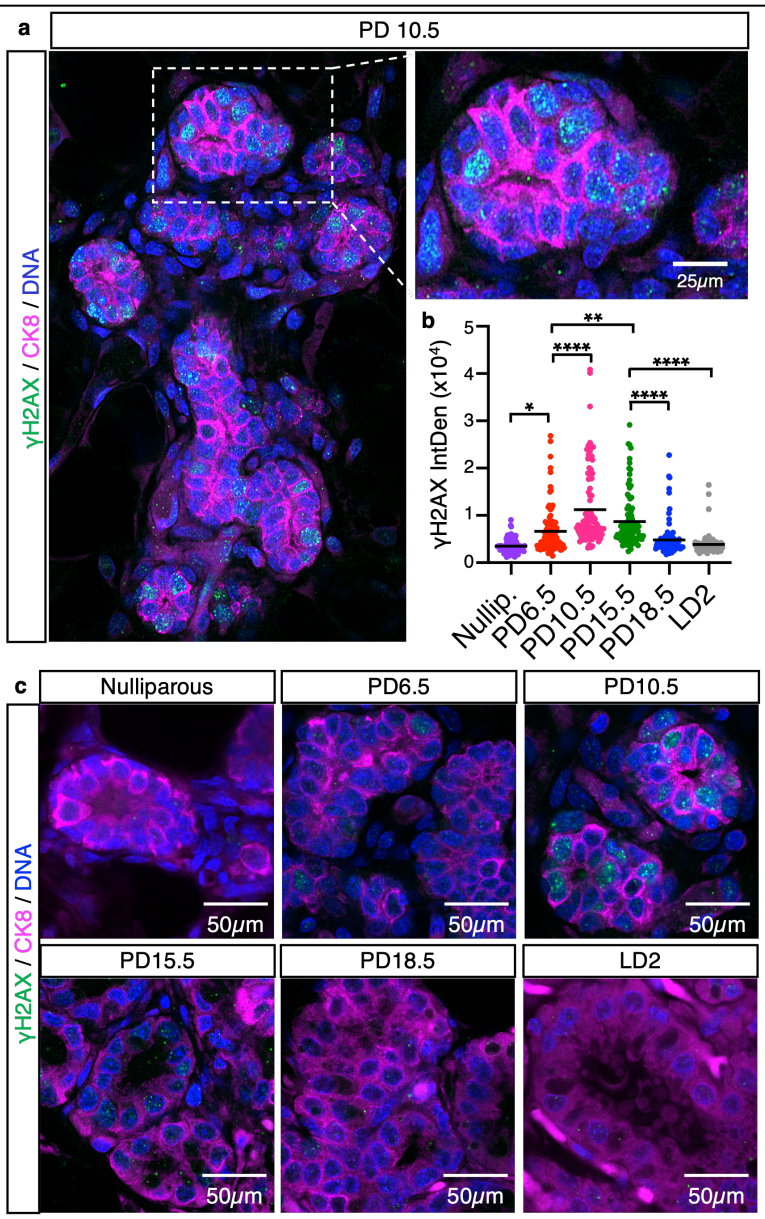

Figure 1.7: Physiological DNA damage occurs during alveologenesis. **a)** Detection of γH2AX (green) in optical-cleared MG sections at pregnancy day 10.5 (PD10.5). White broken lines indicate the single magnified alveolus that shows γH2AX in the luminal CK8+ cells (magenta). Nuclear DNA by propidium iodide. Images are representative of n=3 biological replicates. **b)** Quantification of γH2AX Integrated Density (IntDen) in the luminal CK8+ population from Nulliparous, PD6.5, PD10.5, PD15.5, PD18.5 and LD2 MGs. Data show values from 100 cells per time-point and are representative of n=3 biological replicates. Black horizontal bars represent the mean. Kruskal-Wallis with Dunn's multiple comparison test. **c)** Detection of γH2AX (green) in optical-cleared MG sections in nulliparous, PD6.5, PD10.5, PD15.5, PD18.5 and LD2. CDK8 shown in magenta. Nuclear DNA by propidium iodide. Images are representative of n=3 biological replicates. p values: * < 0.05, **< 0.001, **** < 0.0001.

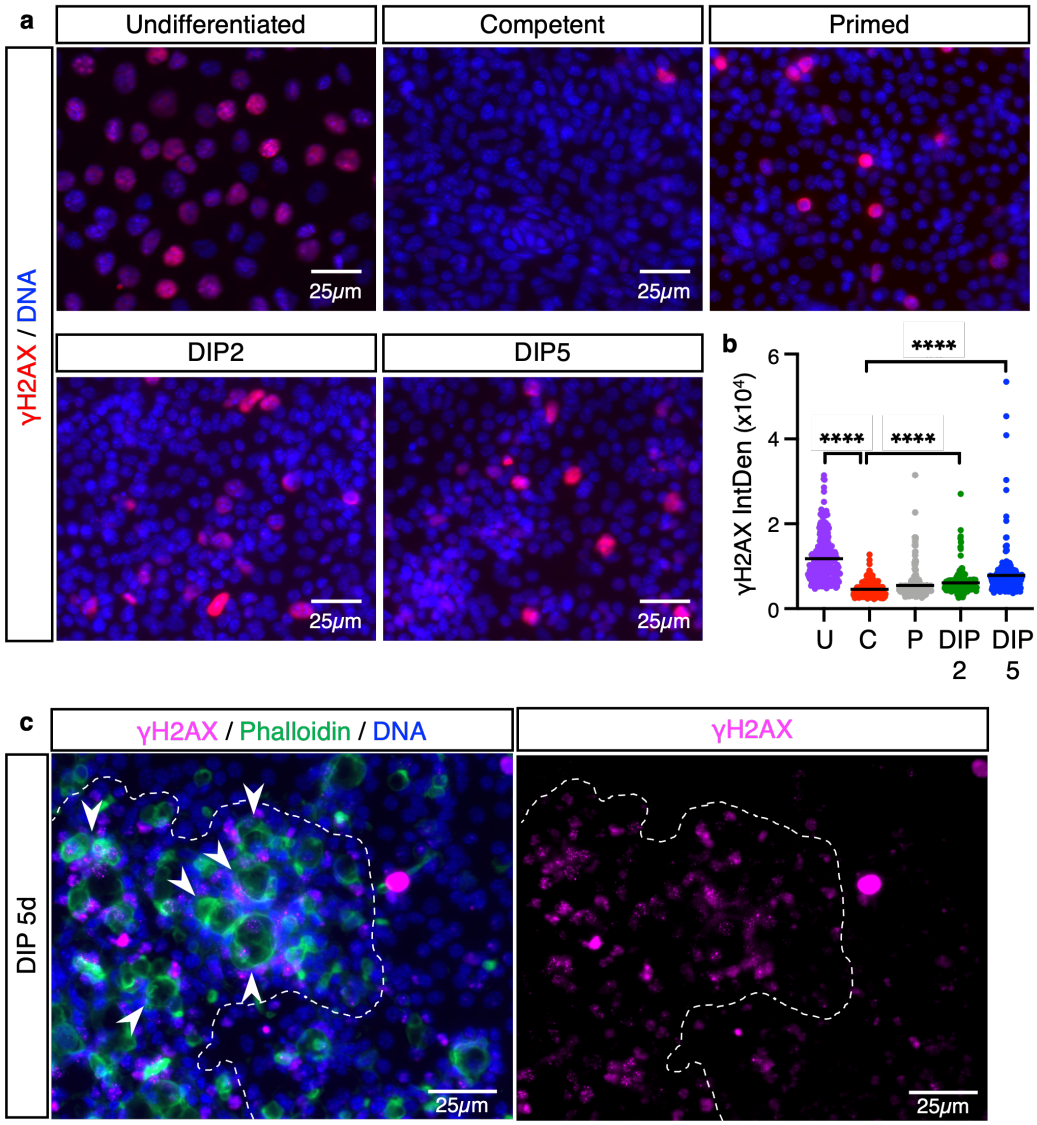

Figure 1.8: Physiological DNA damage occurs during HC11 lactogenic differentiation. a) Detection of γH2AX (red) in undifferentiated, competent, primed and differentiated (DIP 2 and 5) HC11. Nuclear DNA by Hoechst. Images are representative of n=3 biological replicates. **b)** Quantification of γH2AX Integrated Density (IntDen) detected in HC11 throughout differentiation. Data show values from 100 cells per time-point and are representative of n=3 biological replicates. Black horizontal bars represent the mean. Dunn's multiple comparison test. **c)** Representative images of differentiated HC11 (DIP5) showing that γH2AX (magenta) is high in areas with dome formation (white broken line, Phalloidin, green) Domes are indicated by arrows. Nuclear DNA by Hoechst. p values: **** < 0.0001.

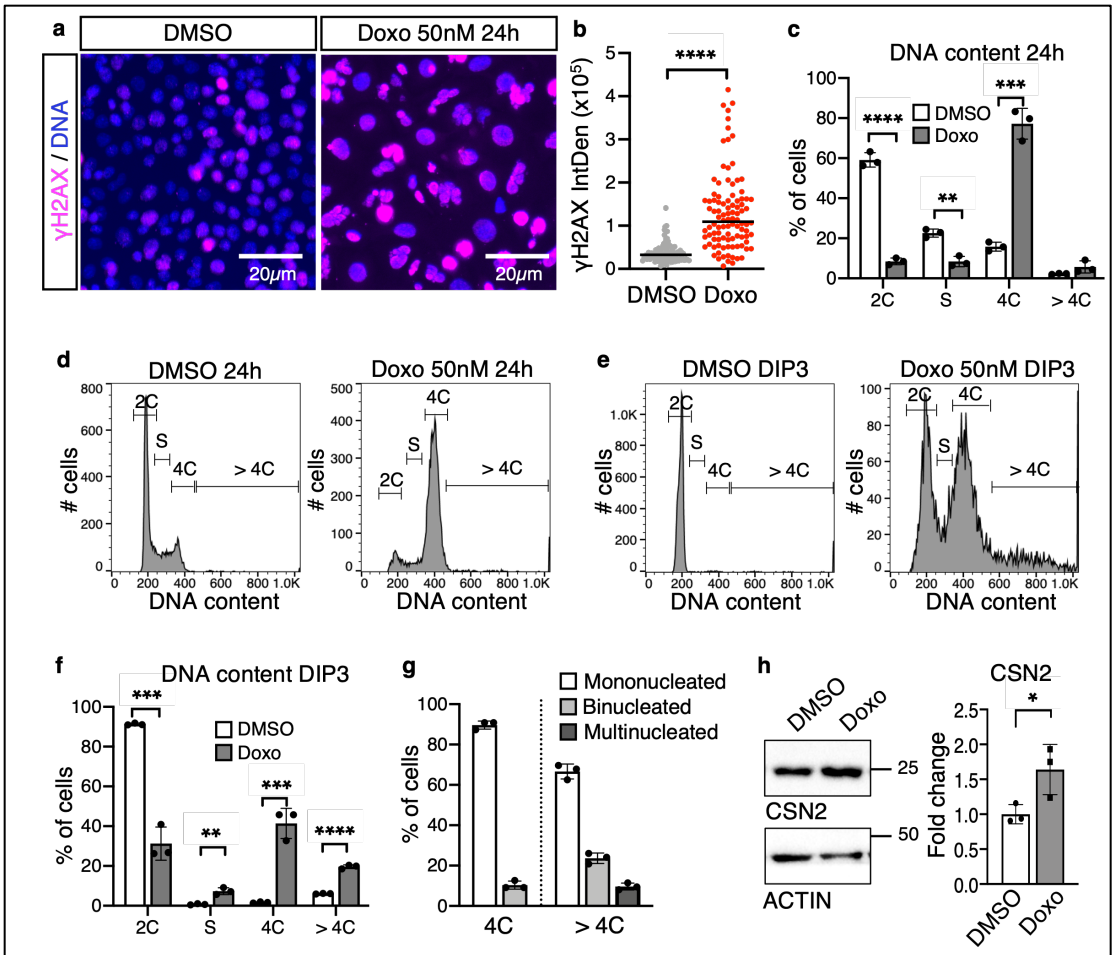

Figure 1.9: DNA damage increases HC11 endoreplication and milk production a) Detection of γH2AX (magenta) in undifferentiated HC11 treated with DMSO or Doxo for 24 hours. Nuclear DNA by Hoechst. Images are representative of n=3 biological replicates. **b)** Quantification of γH2AX Integrated Density (IntDen) 24 hours after treatment with DMSO or Doxo. Data show values from 100 cells per treatment and are representative of n=3 biological replicates. Black horizontal bars represent the mean. Mann-Whitney test. **c)** Percentage of undifferentiated HC11 with 2C, 4C or > 4C DNA content, or in the S phase, detected by FACS, 24 hours after treatment with DMSO or Doxo. Data shown as the mean ± SD; n=3 biological replicates; two-tailed unpaired Student's t-test. **d and e)** Representative FACS histograms for DNA content analysis of undifferentiated **(d)** and DIP3 **(e)** HC11 treated with DMSO or Doxo. **f)** Percentage of differentiated (DIP3) HC11 with 2C, 4C or > 4C DNA content, or in the S phase, detected by FACS, after treatment with DMSO or Doxo. Data shown as the mean ± SD; n=3 biological replicates; two-tailed unpaired Student's t-test. **g)** Quantification of differentiated HC11 (DIP3) treated with DMSO or Doxo, and sorted based on DNA content (4C or > 4C), that are mono-, bi- or multinucleated (more than 2 nuclei). Data shown as the mean ± S.E.M; n=3 biological replicates. **h)** Representative Western Blot (left) and quantification (right) of CSN2 expression in differentiated HC11 (DIP3) after DMSO or Doxo treatment. Data shown as the mean ± SD; n=3 biological replicates; two-tailed un-paired Student's t-test. p values: * < 0.05, **< 0.001, *** < 0.0005, **** < 0.0001.

To examine the *in vivo* consequences of damaging DNA during pregnancy, we performed contralateral intraductal injection (IDI) of doxorubicin or DMSO-containing vehicle into MGs at PD12.5 to extend the period of DNA damage that peaks at PD10 (Figure 1.7b and Figure 1.10a). We observe increased γH2AX in CK8+ luminal cells 24h post-injection with doxorubicin (Figure 1.10b, c), demonstrating doxorubicin was effectively delivered into the MG epithelium. FACS DNA content analysis of doxorubicin-injected MGs at PD17.5 shows an increase in the proportion of 4C and > 4C luminal populations (14.86% and 47.1% increase in the overall population, respectively), while the 2C population decreases (5.23% decrease in the overall population; Figure 1.10d-f). This increase in endoreplication is accompanied by an increase in milk production, as detected by RT-qPCR for the expression of *Csn2* (Figure 1.10g). Collectively, these results indicate DNA damage regulates alveolar endoreplication through the activation of the G2/M checkpoint and, consequently, milk production.

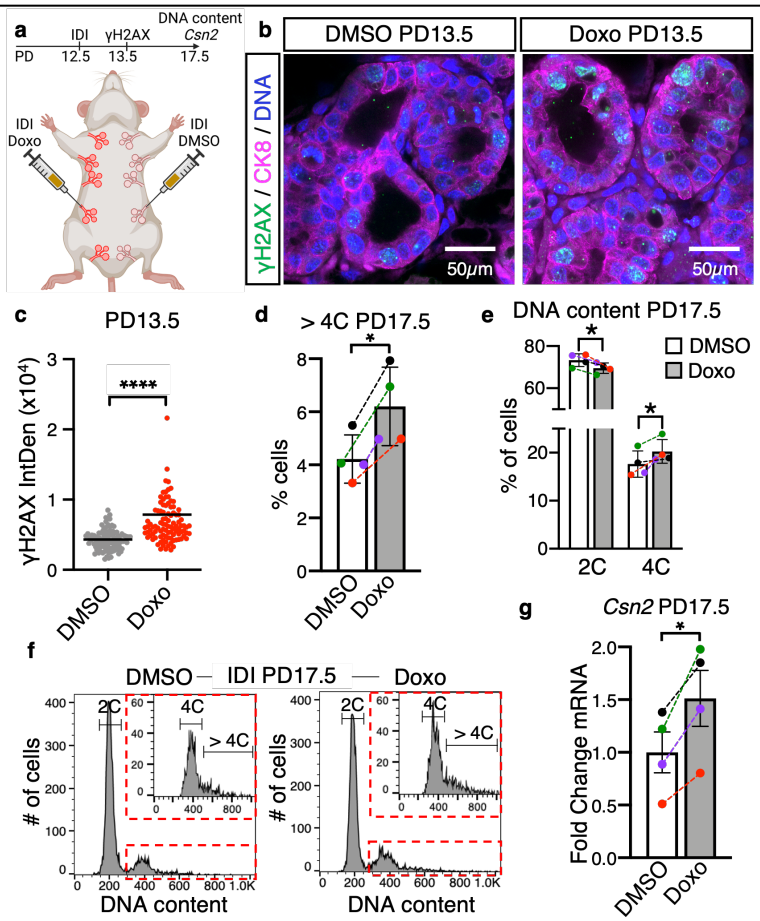

Figure 1.10: DNA damage increases alveolar endoreplication and milk production. a) Cartoon representing the contralateral intraductal injection (IDI) of MGs performed. Created with BioRender.com. **b)** Detection of γH2AX (green) at PD13.5, 24 hours after contralateral IDI with DMSO or doxorubicin (Doxo). CK8 shown in magenta. Nuclear DNA by propidium iodide. Images are representative of n=3 biological replicates. **c)** Quantification of γH2AX Integrated Density (IntDen) in the luminal CK8+ population after contralateral IDI with DMSO or Doxo. Data show values from 100 cells per treatment and are representative of n=3 biological replicates. Black horizontal bars represent the mean. Mann- Whitney test. **d)** Quantification of the percentage of CK8+ cells with > 4C DNA content, detected by FACS analysis, after contralateral IDI with DMSO or Doxo in PD17.5 MGs. Data shown as the mean ± SD; n=4 biological replicates; two-tailed paired Student's t-test. **e)** Percentage of CK8+ cells with 2C and 4C DNA content, detected by FACS, after contralateral IDI with DMSO or Doxo in PD17.5 MGs. Data shown as the mean ± SD; n=4 biological replicates; two-tailed paired Student's t-test. **f)** Representative FACS DNA content analysis histograms from CK8+ PD17.5 MGs after contralateral IDI with DMSO or Doxo. Red broken lines show a histogram magnification corresponding to the 4C and >4C populations. Data are representative of n=3 biological replicates. **g)** Quantification of Csn2 expression in PD17.5 MGs after contralateral IDI with DMSO or Doxo, as detected by RT- qPCR. Data shown as the mean ± S.E.M; n=4 biological replicates; two-tailed paired Student's t- test. p values: * < 0.05, **** < 0.0001.

Replication stress results in activation of the DNA damage response and endoreplication during alveologenesis.

To ensure genomic stability and safeguard inheritance, cells possess a DNA damage response (DDR) that monitors genomic integrity throughout the cell cycle. During normal development, cell proliferation frequently results in activation of the DDR due to replication stress (Miermont et al., 2019; Zeman & Cimprich, 2014). Given the tremendous amount of proliferation that occurs during early alveologenesis, we hypothesized that replication stress may be the source of DNA damage driving endoreplication of mammary alveolar cells. The response to DNA damage by replication stress is mediated by the kinase ATR, which is activated by phosphorylation at Threonine-1989 (pATR) (Nam et al., 2011). By IHC staining, we find, similarly to γH2AX (Figure 1.7a-c), that ATR is activated at PD10.5 when proliferation is at its peak (Richert, Schwertfeger, Ryder, & Anderson, 2000) (Figure 1.11a-c). However, while γH2AX decreases afterwards, pATR persists until the end of pregnancy, when polyploidization begins (Figure 1.11a-c). To investigate the role of replication stress in alveolar endoreplication, we induced it in HC11 cells through over-expression of CYCLIN E (*CCNE1*) prior to lactogenic differentiation (Figure 1.12a). CYCLIN E is an oncogene that accelerates DNA replication during the S phase of the cell cycle and results in DNA damage due to replication stress (Bester et al., 2011; Jones et al., 2013). FACS analysis shows *CCNE1* increases DNA replication, as measured by BrdU incorporation in HC11 cells (Figure 1.12b). In accordance with DNA damage accumulation due to replication stress, γH2AX and pATR also increase (Figure 1.12c-f). Additionally, FACS DNA content analysis

shows *CCNE1* increases endoreplication by DIP3, as well as CSN2 detected by WB (Figure 1.12g-i). To investigate the effect of inducing replication stress *in vivo* we performed contralateral IDI of Hydroxyurea (Hu) or PBS vehicle into MGs at PD8.5 and PD12.5 to encompass the peak of proliferation at PD10.5 (Richert et al., 2000) (Figure 1.13a), and detect increased γH2AX and pATR in the CK8+ population at PD13.5 by IHC staining (Figure 1.13b-d). FACS analysis of DNA content in $CK8^+$ cells reveals an increase in the 4C and > 4C populations by LD5 (2% and 48% increase in the overall population, respectively), while the 2C population decreases (5.5% decrease in the overall population; Figure 1.13e-g). This increase in endoreplication is accompanied by an increase in *Csn2* expression as detected by RT-qPCR (Figure 1.14a). Because we observe areas of high and low milk staining in a ~1cm^2 section of LD2 MG tissue, we imaged the entire section, quantified milk staining contained within each alveolus and calculated the average integrated density among alveoli in the whole section. We observe a ~15% increase in milk in HU-injected MGs (Figure 1.14b-d). These results suggest DNA damage produced by replication stress is sufficient to drive endoreplication during lactation.

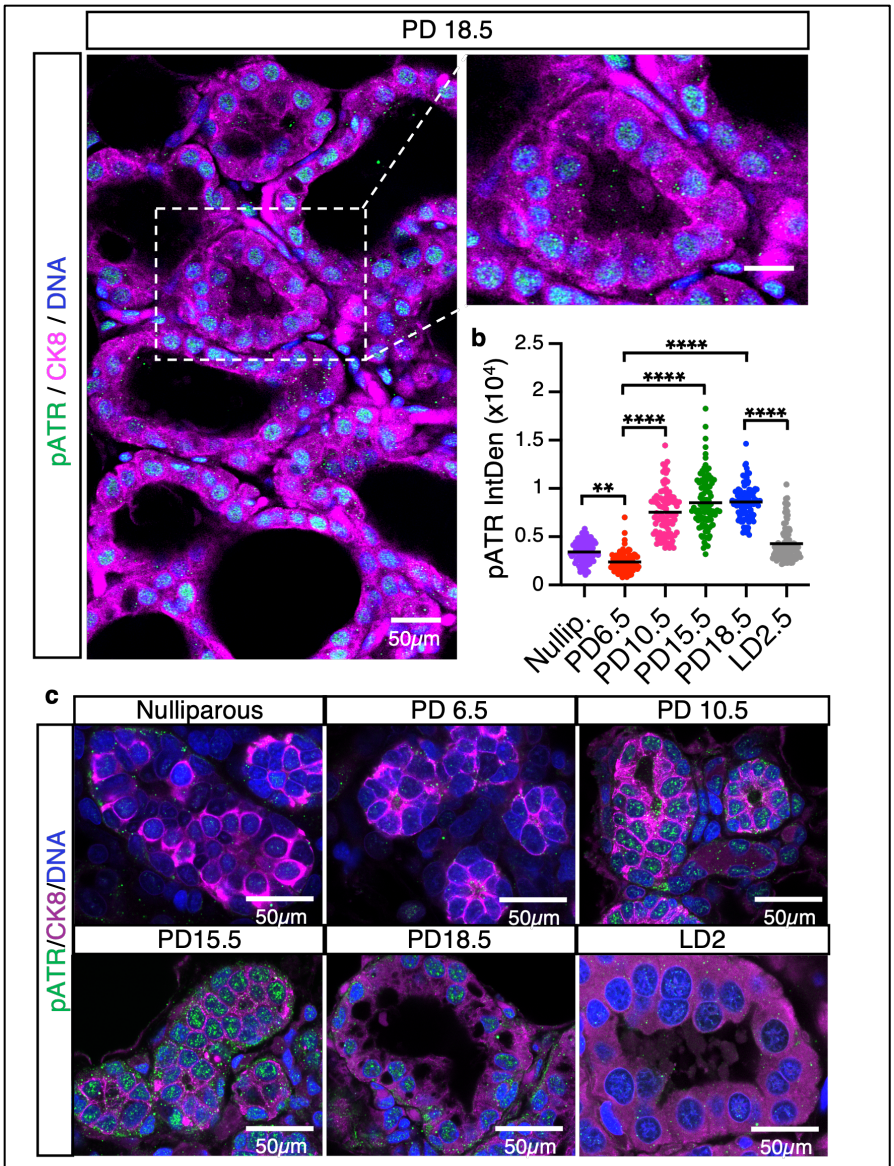

Figure 1.11: The DNA damage response is active during alveologenesis. a) Detection of pATR (green) in optical-cleared MG sections at PD18.5. White broken lines indicate the single magnified alveolus that shows pATR in the luminal CK8+ (magenta) cells. Nuclear DNA by propidium iodide. Images are representative of n=3 biological replicates. **b)** Quantification of pATR Integrated Density (IntDen) in the luminal CK8+ (magenta) population from nulliparous (Nullip.), PD6.5, PD10.5, PD15.5, PD18.5 and LD2 MGs. Data show values from 100 cells per time-point and are representative of n=3 biological replicates. Black horizontal bars represent the mean. Kruskal-Wallis with Dunn's multiple comparison test. **c)** Detection of pATR (green) in optical-cleared MG sections in nulliparous, PD6.5, PD10.5, PD15.5, PD18.5 and LD2. CK8 shown in magenta. Nuclear DNA by propidium iodide. Images are representative of n=3 biological replicates. p values: **< 0.001, **** < 0.0001.

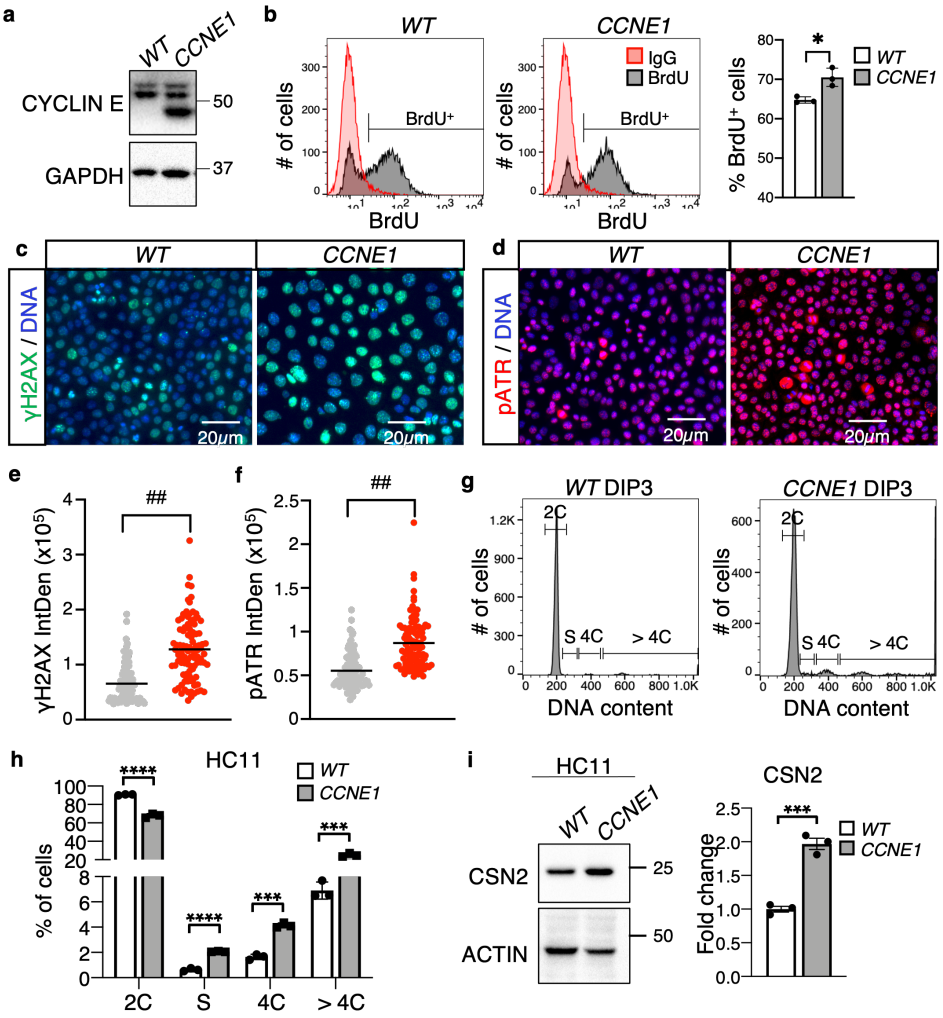

Figure 1.12: Replication stress activates the DNA damage response and results in increased alveolar endoreplication and milk production *in vitro*. **a)** Detection of CYCLIN E by Western Blot in wild-type (WT) or Cyclin E overexpressing (CCNE1) HC11. **b)** Representative FACS histograms showing BrdU incorporation in WT and CCNE1 undifferentiated HC11. Red histogram represents the negative isotype control (IgG). Black gate represents the identification of the BrdU+ cells according to negative isotype control. Right histogram shows the quantification of WT or CCNE1 HC11 that are BrdU+. Data shown as the mean ± SD; n=3 biological replicates; two-tailed un-paired Student's t-test. **c)** Detection of γH2AX (green) in undifferentiated WT or CCNE1 HC11. Nuclear DNA by Hoechst. Images are representative of n=3 biological replicates. **d)** Detection of pATR (red) in undifferentiated WT or CCNE1 HC11. Nuclear DNA by Hoechst. Images are representative of n=3 biological replicates. **e and f)** Quantification of γH2AX **(e)** or pATR **(f)** Integrated Density (IntDen) in undifferentiated wild-type (WT) or Cyclin E overexpressing (CCNE1) HC11. Data show values from 100 cells for WT or CCNE1 and are representative of n=3 biological replicates. Black horizontal bars represent the mean. Mann-Whitney test. **g)** Representative FACS histograms for DNA content analysis of WT or CCNE1 differentiated (DIP3) HC11. **h)** Quantification of FACS DNA content analysis showing the percentage of differentiated (DIP3) WT or CCNE1 HC11 with 2C, 4C or > 4C DNA content, or in the S phase. Data shown as the mean ± SD; n=3 biological replicates; two-tailed unpaired Student's t-test. **i)** Western Blot (left) and quantification (right) of CSN2 expression in differentiated (DIP3) WT or CCNE1 HC11. Data shown as the mean ± SD; n=3 biological replicates; two-tailed unpaired t-test. p values: * < 0.05, *** < 0.0005, **** < 0.0001.

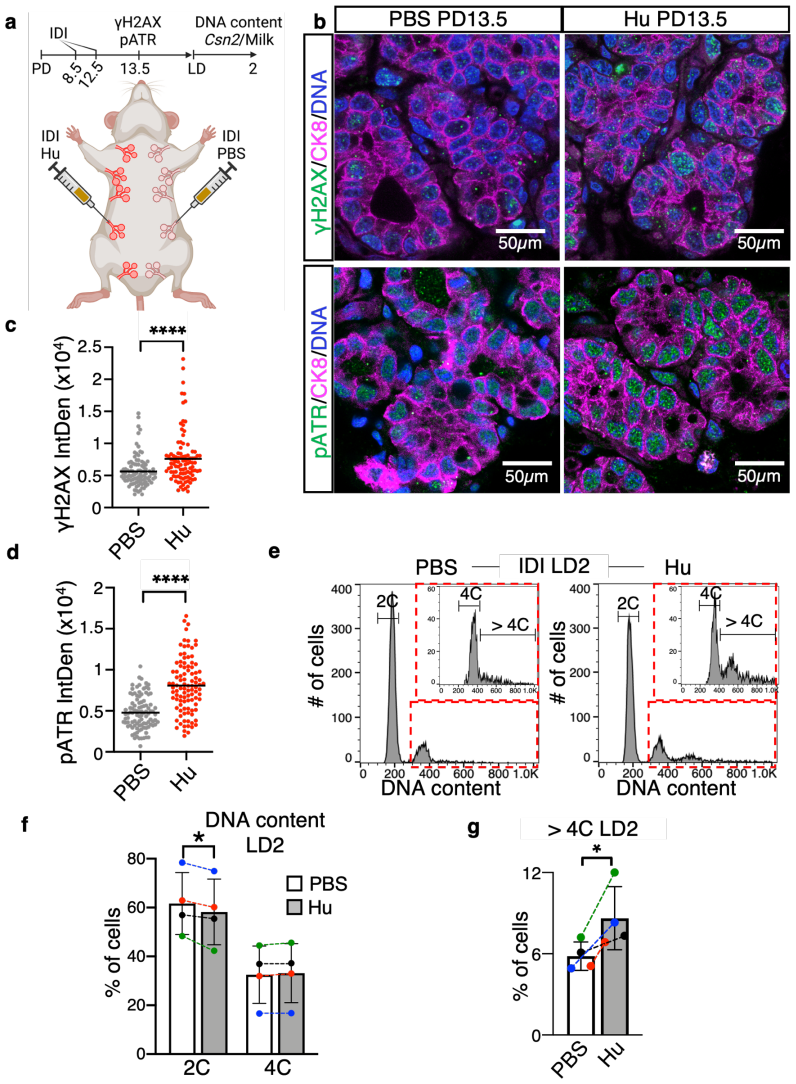

Figure 1.13: Replication stress activates the DNA damage response and results in increased alveolar endoreplication. a) Cartoon representing the contralateral intraductal injection (IDI) of MGs performed. Created with BioRender.com. **b)** Detection of γH2AX (green, top) or pATR (green, bottom) in optical-cleared MG sections after contralateral IDI with PBS or hydroxyurea (Hu). CK8 shown in magenta. Nuclear DNA by propidium iodide. Images are representative of n=2 biological replicates. **c and d)** Quantification of γ H2AX **(c)** or pATR **(d)** Integrated Density (IntDen) in the luminal CK8+ population after contralateral IDI with DMSO or Hu. Data show values from 100 cells per treatment and are representative of n=2 biological replicates. Black horizontal bars represent the mean. Mann-Whitney test. **e)** Representative FACS DNA content analysis histograms from CK8+ LD2 MGs after contralateral IDI with PBS or hydroxyurea (Hu). Red broken lines show a magnification of the histogram corresponding to the 4C and >4C populations. Histograms are representative of n=3 biological replicates. **f)** Quantification of the percentage of CK8+ cells with 2C or 4C DNA content, detected by FACS analysis, after contralateral IDI with PBS or Hu in LD2 MGs. Data shown as the mean ± SD; n=4 biological replicates; two-tailed paired Student's t-test. **g)** Quantification of the percentage of CK8+ cells with > 4C DNA content, detected by FACS analysis, after contralateral IDI with PBS or Hu in LD2 MGs. Data shown as the mean ± SD; n=4 biological replicates; two-tailed paired Student's t-test. p values: * < 0.05, **** < 0.0001.

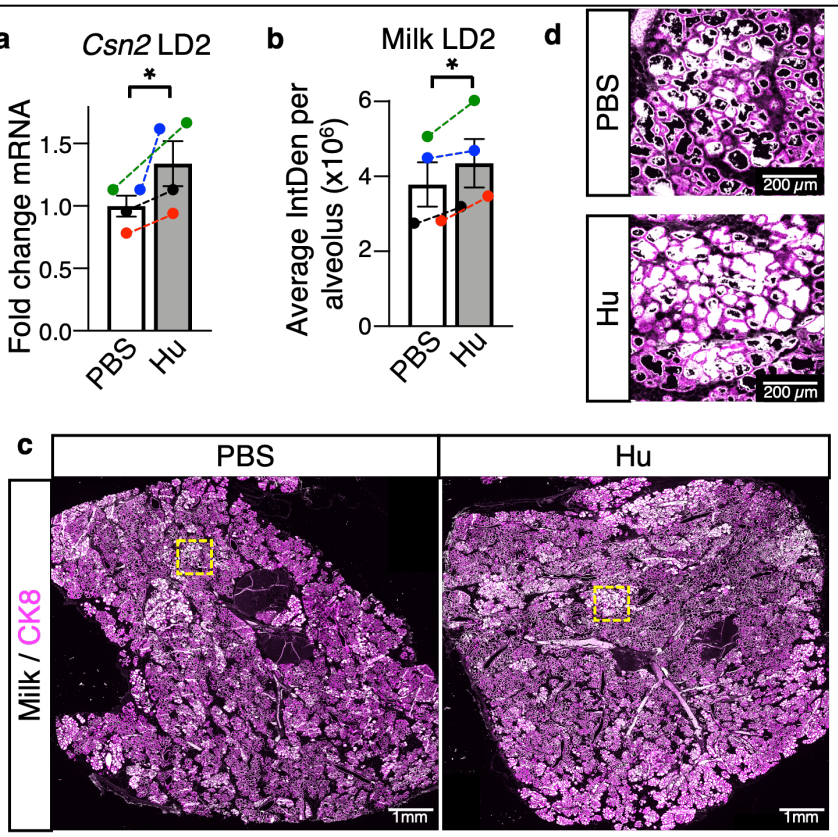

Figure 1.14: Replication stress results in increased milk production during lactation. a) Quantification of Csn2 expression in LD2 MGs after contralateral IDI with PBS or Hu, as detected by RT-qPCR. Data shown as the mean ± S.E.M; n=4 biological replicates; two-tailed paired Student's t-test. **b)** Quantification of milk average Integrated Density (IntDen) per alveolus detected in LD2 MG alveoli after contralateral IDI with PBS or Hu. Data shown as the mean ± S.E.M; n=4 for biological replicates; two-tailed Student's paired t-test. **c and d)** Detection of milk (white) in LD2 MGs after contralateral IDI with PBS or Hu. CK8 shown in magenta. Yellow squares indicate the magnified area shown in **(d)**, illustrating the milk contained within the alveoli. Images are representative of n=4 independent experiments. p values: * < 0.05.

Previous studies have shown supplementation of nucleosides (Nucs) can relieve replication stress in cultured cells (Bester et al., 2011; Halliwell et al., 2020). To investigate if nucleosides reduce replication stress *in vivo*, we performed contralateral IDI of nucleosides or PBS vehicle into MGs at PD8.5 and PD12.5 again to encompass the peak of proliferation (Figure 1.15a), and observe decreased γH2AX and pATR in the CK8+ population at PD13.5 by IHC staining (Figure 1.15b-d). FACS analysis of DNA content in CK8+ luminal cells also reveals a decrease in the 4C population at LD2 (22.15% decrease in the overall population), and both the 4C and > 4C populations by LD5 (6.05% and 14.79% decrease in the overall population, respectively; Figure 1.15e-j). Accordingly, the 2C population increases at both LD2 and LD5 (9% and 49% increase in the overall population, respectively; Figure 1.15e-j). These results suggest nucleoside IDI relieves replication stress during pregnancy and inhibits the activation of G2/M checkpoint at LD2, resulting in decreased endoreplication by LD5. This decrease in endoreplication is accompanied by a decrease in *Csn2* expression and a 21% decrease in milk production, detected by RT-qPCR and IHC, respectively (Figure 1.16a-d). Altogether, these findings strongly suggest replication stress during early alveologenesis causes DNA damage and leads to prolonged DDR. This, in turn, triggers the activation of the G2/M checkpoint and endoreplication of alveolar cells at the onset of lactation.

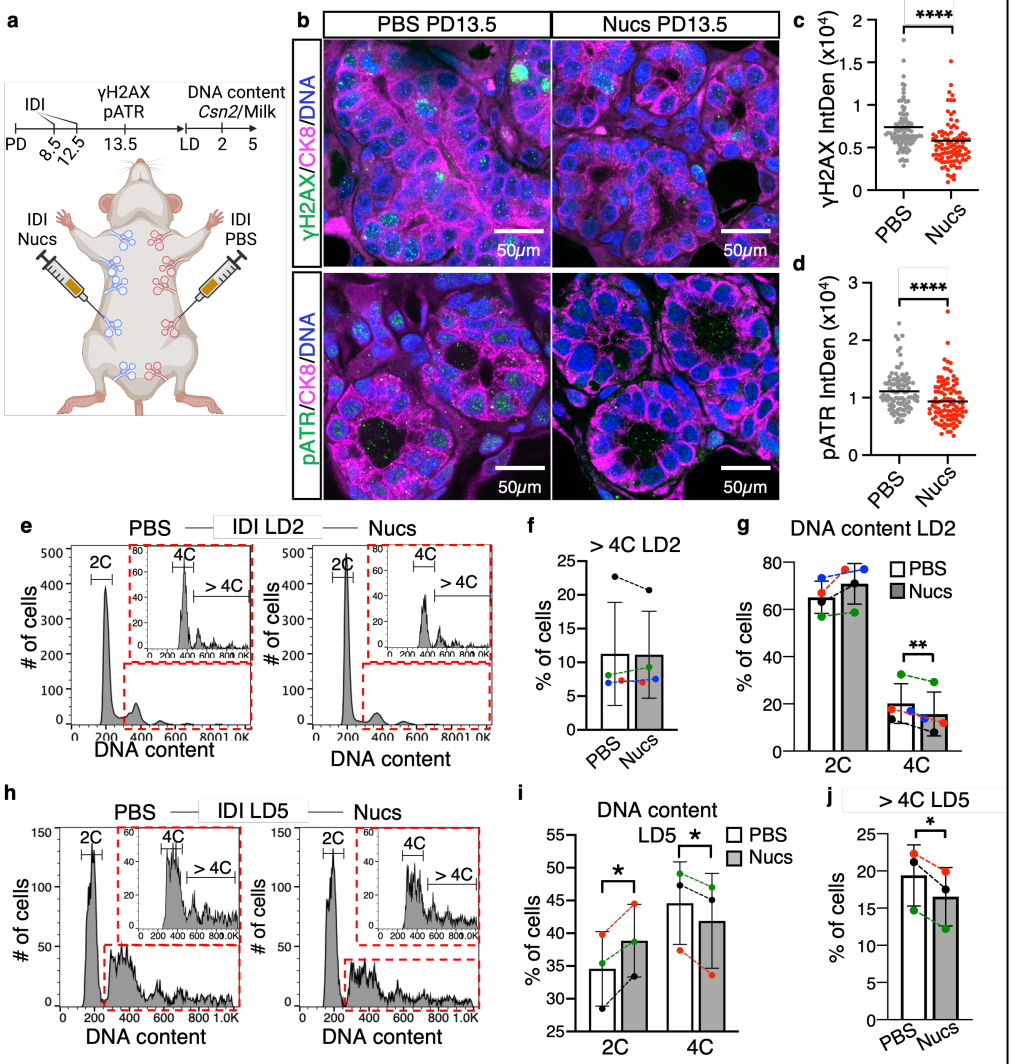

Figure 1.15: Relieving replication stress inhibits the DNA damage response and results in decreased alveolar endoreplication. a) Cartoon representing the contralateral intraductal injection (IDI) of MGs performed. Created with BioRender.com. **b**) Detection of γH2AX (green, top) or pATR (green, bottom) in optical-cleared MG sections after contralateral IDI with PBS or nucleosides (Nucs). CK8 shown in magenta. Nuclear DNA by propidium iodide. Images are representative of n=3 biological replicates. **c and d)** Quantification of γH2AX **(c)** or pATR **(d)** Integrated Density (IntDen) in the luminal CK8+ population after contralateral IDI with DMSO or Nucs. Data show values from 100 cells per treatment and are representative of n=3 biological replicates. Black horizontal bars represent the mean. Mann-Whitney test. **e)** Representative FACS DNA content analysis histograms from CK8+ LD2 MGs after contralateral IDI with PBS or nucleosides (Nucs). Red broken lines show a magnification of the histogram corresponding to the 4C and >4C populations. Histograms are representative of n=4 biological replicates. **f and g)** Quantification of the percentage of CK8+ cells with > 4C **(f)**, 4C and 2C **(g)** DNA content, detected by FACS analysis, after contralateral IDI with PBS or Nucs in LD2 MGs. Data shown as the mean ± SD; n=4 biological replicates; two-tailed paired Student's t-test. **h)** Representative FACS DNA content analysis histograms from CK8+ LD5 MGs after contralateral IDI with PBS or nucleosides (Nucs). Red broken lines show a magnification of the histogram corresponding to the 4C and >4C populations. Histograms are representative of n=3 biological replicates. **i and j)** Quantification of the percentage of CK8+ cells with 2C, 4C **(i)** and >4C **(j)** DNA content, detected by FACS analysis, after contralateral IDI with PBS or Nucs in LD5 MGs. Data shown as the mean ± SD; n=3 biological replicates; two-tailed paired Student's t-test. p values: * < 0.05, **< 0.001, **** < 0.0001.

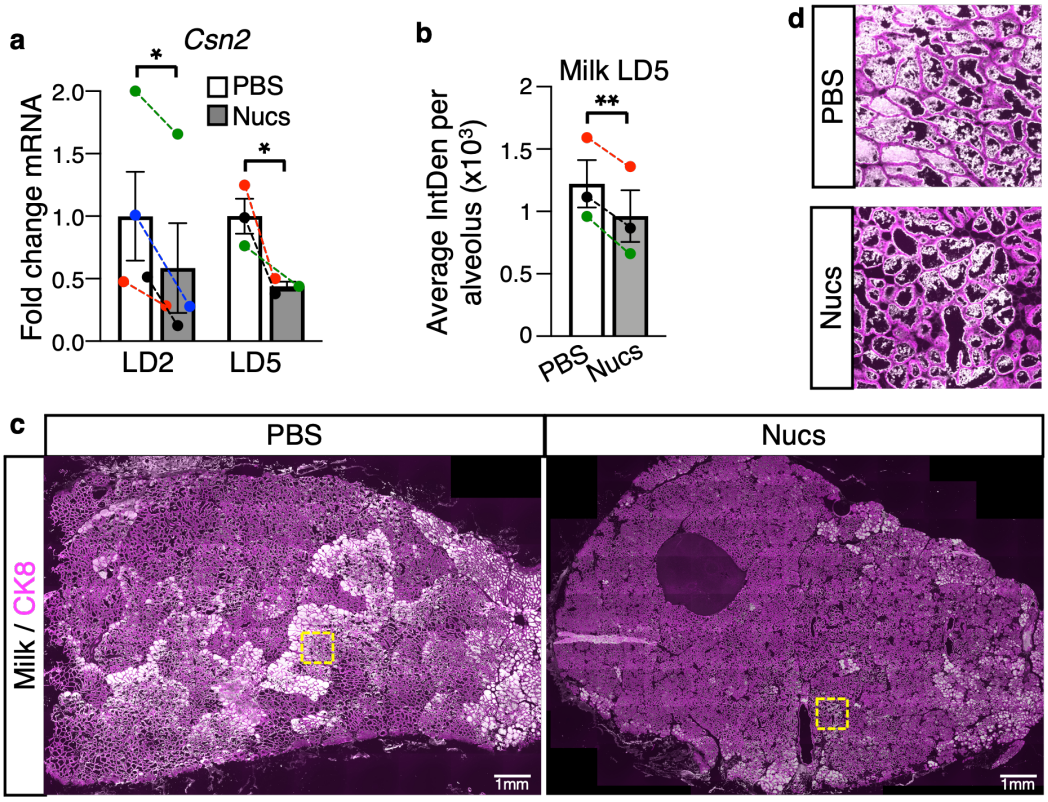

Figure 1.16: Relieving replication stress results in decreased milk production during lactation. a) Quantification of Csn2 expression in LD2 or LD5 MGs after contralateral IDI with PBS or Nucs, as detected by RT-qPCR. Data shown as the mean ± S.E.M; n=4 for LD2 and n=3 for LD5 biological replicates; two-tailed Student's paired t-test. **b)** Quantification of milk average Integrated Density (IntDen) per alveolus detected in LD5 MG alveoli after contralateral IDI with PBS or Nucs. Data shown as the mean ± S.E.M; n=3 for biological replicates; two-tailed Student's paired t-test**. c and d)** Detection of milk (white) in LD5 MGs after contralateral IDI with PBS or Nucs. CK8 shown in magenta. Yellow squares indicate the magnified area shown in **(d)**, illustrating the milk contained within the alveoli. Images are representative of n=3 independent experiments. p values: * < 0.05, **< 0.001

The DNA Damage Response regulates endoreplication via WEE1.

CDK1 inactivation during G2/M arrest can occur through several different inhibitors. The Cip and Kip family of CDK inhibitors, composed of $P21^{Cip1}$, $P27^{Kip1}$ and $P57^{Kip2}$, is involved in the regulation of endoreplication (Z. Ullah, Lee, & Depamphilis, 2009). In addition, the CDK1 inhibitor WEE1 is required for proper DNA replication and for the activation of the G2/M checkpoint in response to replication stress (Elbæk, Petrosius, & Sørensen, 2020; H. L. Smith et al., 2020). WEE1 also regulates endoreplication in plants (Chevalier et al., 2011; Gonzalez, Gevaudant, Hernould, Chevalier, & Mouras, 2007; Sun et al., 1999). To determine which of these inhibitors may be regulating CDK1 activity during alveologenesis, we analyzed their expression during pregnancy and lactation by RT-qPCR. We find expression of *Cdkn1a* and *Cdkn1b*, which encode for $P21^{Cip1}$ and $P27^{Kip1}$, respectively, remain unchanged in comparison to their expression in the nulliparous MG (Figure 1.17a). Conversely, *Wee1* is upregulated during the cell proliferation occurring in early pregnancy, and again at LD2, during endoreplication (Figure 1.17b). RT-qPCR of FACS-purified MG populations demonstrates *Wee1* upregulation during lactation occurs specifically in the luminal population (Figure 1.17c). Furthermore, we find *Wee1* is upregulated in response to IDI of doxorubicin and hydroxyurea into the pregnant MG and downregulated in response to IDI of nucleosides (Figure 1.17d), demonstrating a direct correlation between *Wee1* expression and the extent of endoreplication during alveologenesis. Consequently, we investigated the role of WEE1 during alveolar endoreplication *in vivo* by performing contralateral IDI of the WEE1 inhibitor Mk-1775 or DMSO-containing vehicle into MGs at PD16.5, to capture the beginning of

endoreplication occurring by PD17.5 (Figure 1.2e and Figure 1.18a). FACS analysis of DNA content in CK8+ luminal cells reveals that injection of Mk-1775 decreases the 4C population at LD2 (19.4% decrease in the overall population), and both the 4C and > 4C populations by LD5 (3.2% and 16.31% decrease in the overall population, respectively; Figure 1.18b-g). Accordingly, the 2C population increases at both LD2 and LD5 (7.7% and 12.4% increase in the overall population, respectively; Figure 1.18b-g). This decrease in endoreplication is accompanied by a decrease of *Csn2* expression and a 21% decrease in milk production, detected by RT-qPCR and IHC, respectively (Figure 1.19a-d).

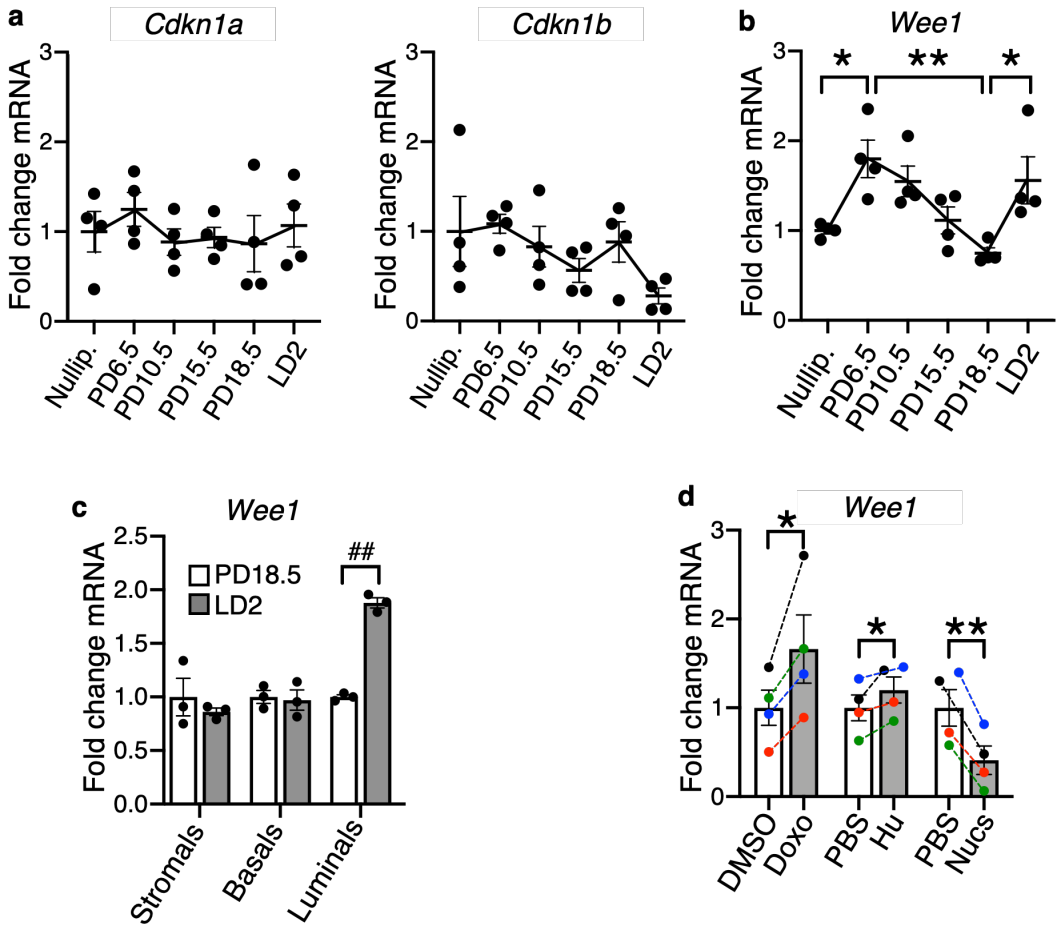

Figure 1.17: The DNA damage response to replication stress regulates expression of *Wee1* in alveolar luminal cells. a) Quantification of Cdkn1a (left) and Cdkn1b (right) expression in whole tissue from nulliparous, PD6.5, PD10.5, PD15.5, PD18.5 and LD2 MGs, as detected by RT-qPCR. Data shown as the mean ± S.E.M; n=4 for biological replicates. one-way ANOVA Tukey's test. **b)** Quantification of Wee1 expression in whole MG tissue from nulliparous, PD6.5, PD10.5, PD15.5, PD18.5 and LD2 MGs, as detected by RT-qPCR. Data shown as the mean ± S.E.M; n=4 biological replicates. one-way ANOVA Tukey's test. **c)** Quantification of Wee1 expression in sorted luminal, basal and stromal populations from PD18.5 and LD2 MGs, as detected by RT-qPCR. Populations were FACS-sorted based on expression of CD24 and CD29. Data shown as the mean ± S.E.M; n=3 biological replicates. two-tailed paired Student's t-test. **d)** Quantification of Wee1 expression in whole MG tissue after contralateral IDI with DMSO/Doxo, PBS/Hu or PBS/Nucs. Data shown as the mean ± S.E.M; n=4 biological replicates. two-tailed paired Student's t-test. p values: * < 0.05, **< 0.001

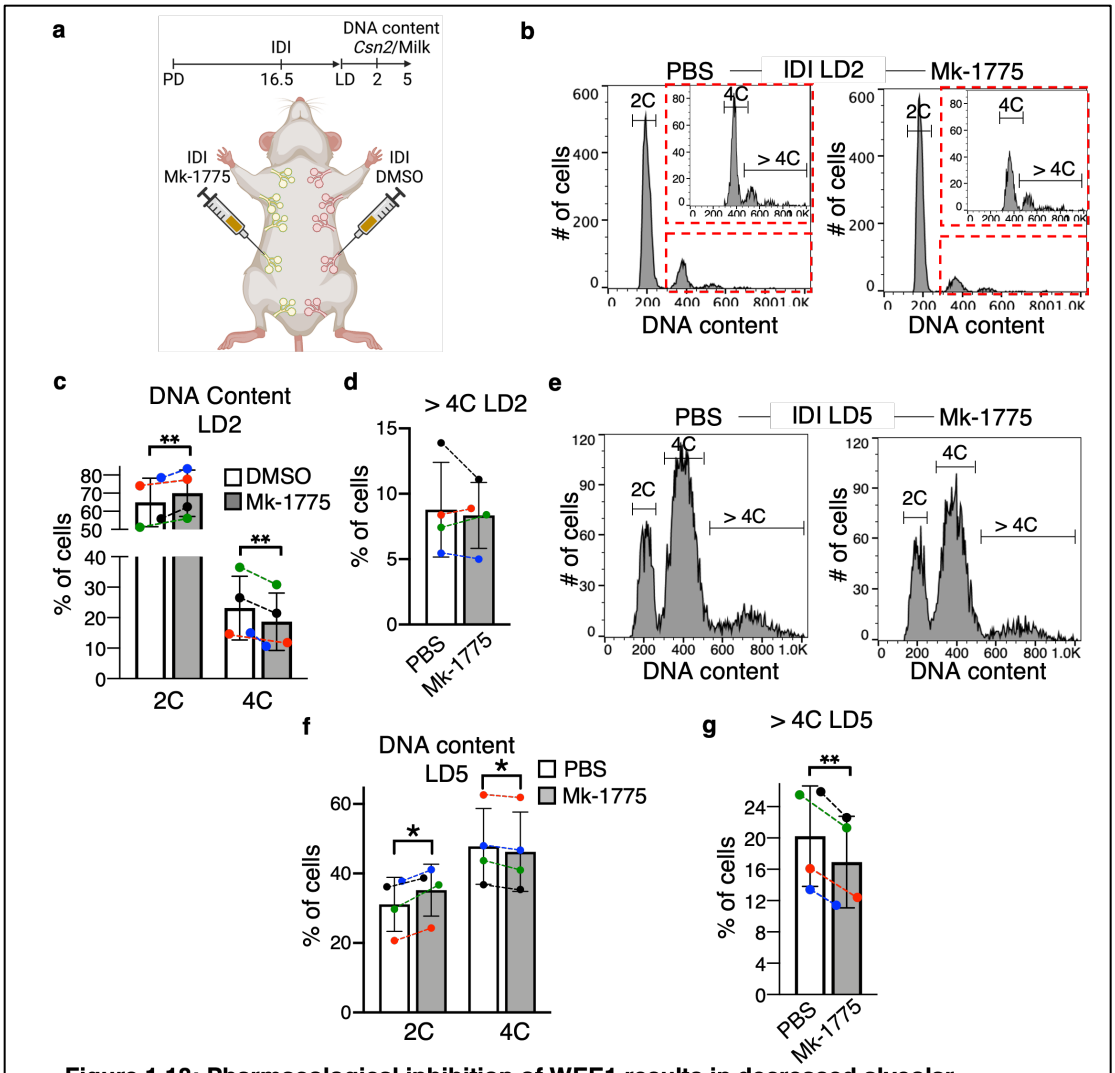

Figure 1.18: Pharmacological inhibition of WEE1 results in decreased alveolar endoreplication. a) Cartoon representing the contralateral intraductal injection (IDI) of MGs performed. Created with BioRender.com. **b)** Representative FACS DNA content analysis histograms from CK8+ LD2 MGs after contralateral IDI with DMSO or Mk-1775. Red broken lines show a magnification of the histogram corresponding to the 4C and >4C populations. Histograms are representative of n=4 biological replicates. **c and d)** Quantification of the percentage of CK8+ cells with 2C, 4C **(c)** and >4C **(d)** DNA content, detected by FACS analysis, after contralateral IDI with DMSO or Mk-1775 in LD2 MGs. Data shown as the mean ± SD; n=4 biological replicates; two-tailed paired Student's t-test. **e)** Representative FACS DNA content analysis histograms from CK8+ LD5 MGs after contralateral IDI with DMSO or nucleosides Mk-1775. Red broken lines show a magnification of the histogram corresponding to the 4C and >4C populations. Histograms are representative of n=3 biological replicates. **f and g)** Quantification of the percentage of CK8+ cells with 2C, 4C **(f)** or >4C **(g)** DNA content, detected by FACS analysis, after contralateral IDI with DMSO or Mk-1775 in LD5 MGs. Data shown as the mean ± SD; n=4 biological replicates; two-tailed paired Student's t-test. p values: * < 0.05, **< 0.001.

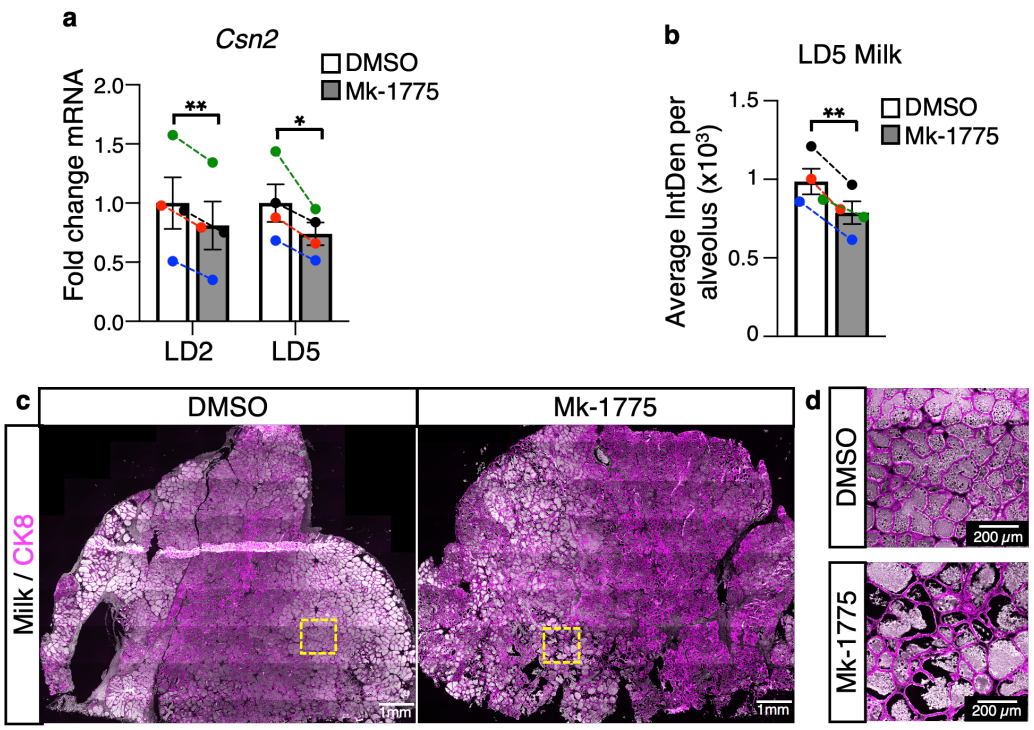

Figure 1.19: Pharmacological inhibition of WEE1 results in decreased milk production during lactation. a) Quantification of Csn2 expression in LD2 or LD5 MGs after contralateral IDI with DMSO or Mk-1775, as detected by RT-qPCR. Data shown as the mean ± S.E.M; n=4 biological replicates; two-tailed paired Student's t-test. **b)** Quantification of milk average Integrated Density (IntDen) per alveolus, detected by IHC, after contralateral IDI with DMSO or Mk-1775. Data shown as the mean ± S.E.M; n=4 biological replicates; two-tailed paired Student's t-test. **c and d)** Detection of milk (white) in LD5 MGs after contralateral IDI with DMSO or Mk-1775. CK8 shown in magenta. Yellow squares indicate the magnified area shown in **(d)**, illustrating the milk contained within the alveoli. Images are representative of n=4 independent experiments. p values: * < 0.05, **< 0.001

Next, we generated a *Wee1* conditional knock-out mouse line and deleted the gene specifically in luminal cells. We conditionally deleted this gene utilizing a tamoxifen-inducible *CreER* system under the control of the *Ck8* promoter, which also carries a *mTmG* reporter. Tamoxifen injections were performed at PD17.5 and LD2 to prevent potential deleterious effects caused by *Wee1* loss during early alveologenesis. FACS analysis of GFP expression from *Ck8-CreER/mTmG/Wee1*$^{fl/+}$ MGs at LD5 shows that recombination occurs specifically in the CK8^{+} population (Figure 1.20a, b). As expected, we detect decreased *Wee1* expression by RT-qPCR (Figure 1.20c). FACS analysis of DNA content in CK8+ luminal cells at LD5 reveals a decrease in the 4C and >4C populations in the *Ck8-CreER/mTmG/Wee1*$^{fl/+}$ MGs, while the 2C population increases (Figure 1.20d, e), showing that heterozygous loss of *Wee1* is sufficient to prevent endoreplication. Accordingly, we detect decreased *Csn2* expression and a 52% decrease in milk production by RT-qPCR and IHC, respectively (Figure 1.21a-d). Together, these results demonstrate that WEE1 mediates the DDR response to replication stress by activating the G2/M checkpoint and regulating alveolar endoreplication and milk production (Figure 1.22).

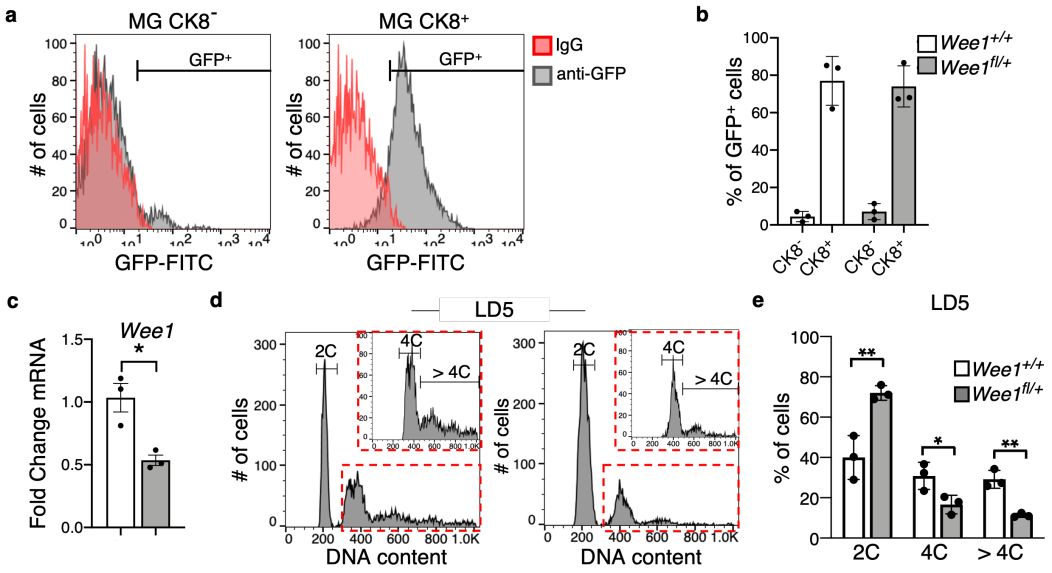

Figure 1.20: Heterozygous loss of *Wee1* results in decreased alveolar endoreplication. a) FACS analysis of mammary gland (MG) single cell preparation for the identification of GFP+ cells in the CK8- (left) and CK8+ (right) populations. Red histogram represents the negative isotype control (IgG). Gate indicates GFP+ cells based on negative isotype control. **b)** Quantification of the % of GFP+ cells in the CK8- and CK8+ populations from LD5 MGs from Ck8-CreER/mTmG/Wee1+/+ (Wee1+/+) or Ck8-CreER/mTmG/Wee1fl/+ (Wee1fl/+) mice. Data shown as the mean ± SD; n=3 biological replicates; two-tailed unpaired Student's t-test. **c)** Quantification of Wee1 expression in whole tissue from LD5 MGs from Wee1+/+ or Wee1fl/+ mice, as detected by RT-qPCR. Data shown as the mean ± S.E.M; n=3 biological replicates. two-tailed unpaired Student's t-test. **d)** Representative FACS DNA content analysis histograms from CK8+ LD5 MGs from Wee1+/+ or Wee1fl/+ mice. Red broken lines show a magnification of the histogram corresponding to the 4C and >4C populations. Histograms are representative from n=3 biological replicates. **e)** Quantification of FACS DNA content analysis showing the percentage of CK8+ cells with 2C, 4C or > 4C DNA content in LD5 MGs from Ck8-CreER/mTmG/Wee1+/+ (Wee1+/+) or Ck8-CreER/mTmG/Wee1fl/+ (Wee1fl/+) mice. Data shown as the mean ± SD; n=3 biological replicates; two-tailed unpaired Student's t-test. p values: * < 0.05, **< 0.001.

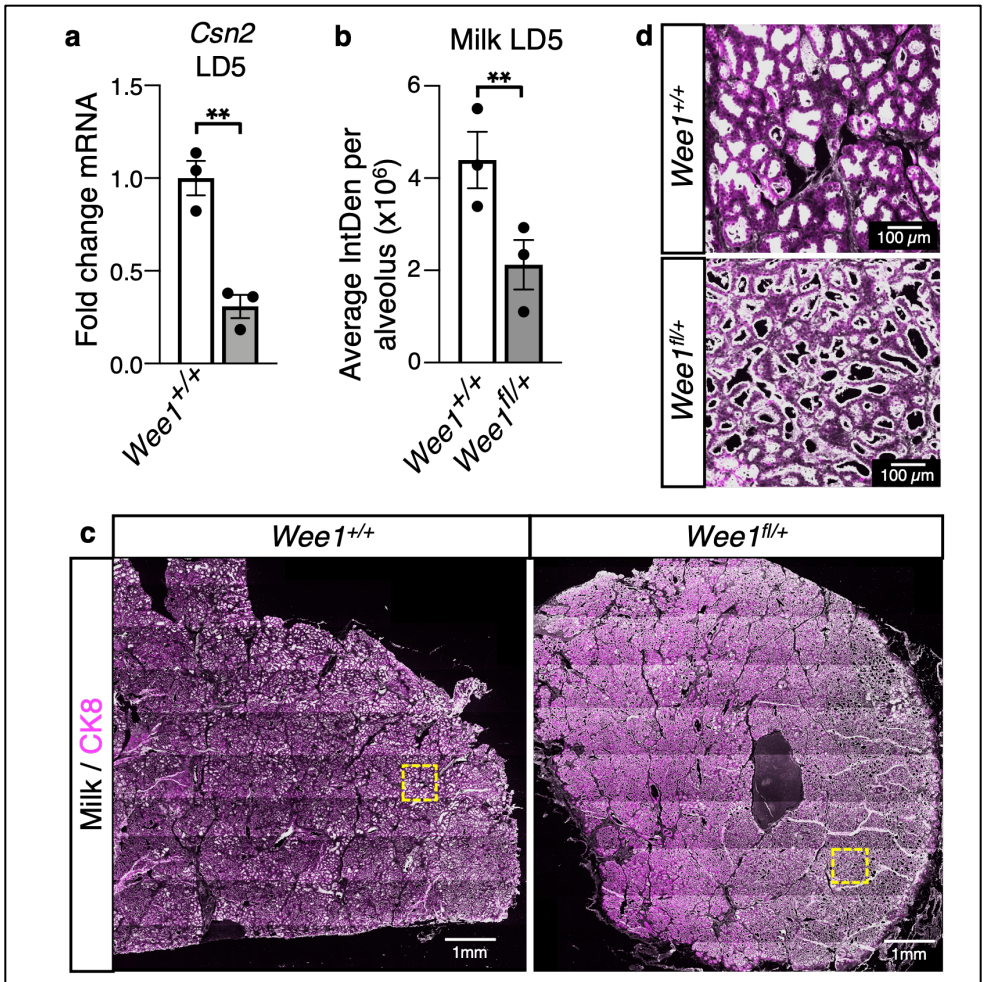

Figure 1.21: Heterozygous loss of *Wee1* results in decreased milk production during lactation. a) Quantification of Csn2 expression in LD5 MGs from Wee1+/+ or Wee1f/+ mice, as detected by RT-qPCR. Data shown as the mean ± S.E.M; n=3 biological replicates; two-tailed unpaired Student's t-test. **b)** Quantification of milk average Integrated Density (IntDen) per alveolus detected by IHC in Wee1+/+ or Wee1fl/+ mice at LD5. Data shown as the mean ± S.E.M; n=3 for biological replicates; two-tailed paired Student's t-test. **c and d)** Detection of milk (white) in LD5 MGs from Wee1+/+ or Wee1fl/+ mice. CK8 shown in magenta. Yellow squares indicate the magnified area shown in **(d)**, illustrating the milk contained within the alveoli. Images are representative of n=3 independent experiments. p values: **< 0.001.

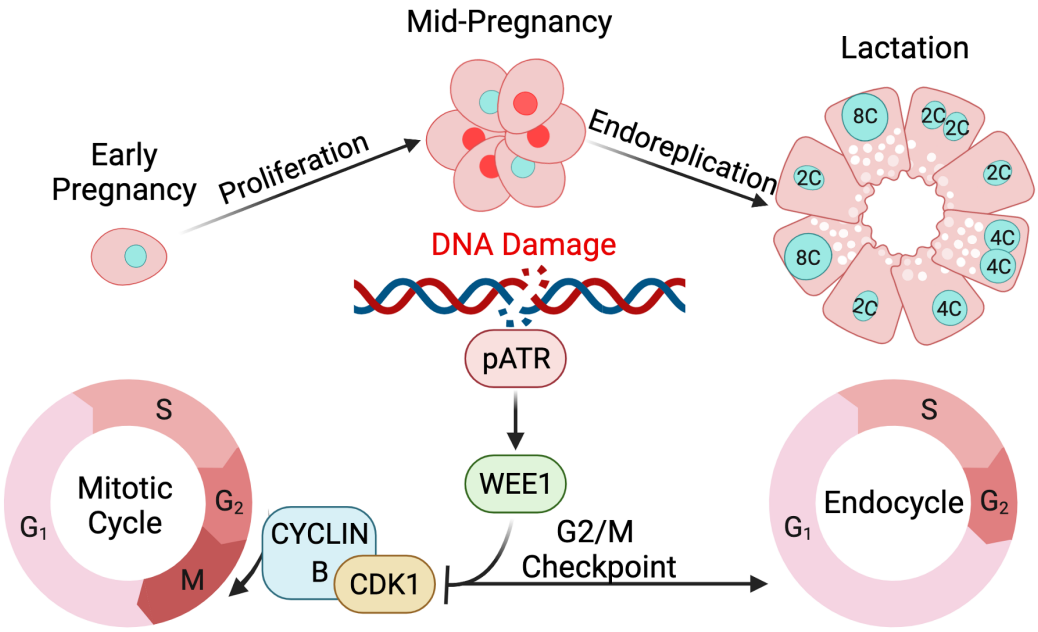

Figure 1.22: The DNA damage response regulates alveolar endoreplication and milk production via WEE1. Cartoon representing the regulation of alveolar endoreplication by the ATR-DNA damage response pathway. Proliferation of alveolar cells results in accumulation of DNA damage during pregnancy and activation of the ATR pathway. As a result, ATR mediates the transition from a mitotic cell cycle into an endocycle through the activation of the CDK1 inhibitor WEE1, which activates the G2/M checkpoint and regulates alveolar endoreplication during lactation.

Discussion

The MG alveolar population is heterogenous in regard to ploidy and nuclei number.

Functional differentiation of MG alveolar cells is linked to polyploidization (Banerjee & Wagner, 1972; Banerjee et al., 1971; Rios et al., 2016; G. H. Smith & Vonderhaar, 1981). Polyploidization is thought to benefit tissues by (1) amplifying copy number for the more efficient production of RNA and proteins and (2) creating large cells that improve resistance to mechanical tension (Zanet et al., 2010): both important in the MG, which serves to produce milk and contracts in response of oxytocin. In addition, it has also been suggested that polyploid cells may be more susceptible for removal during involution, once breastfeeding is complete (Kreuzaler et al., 2011; Rios et al., 2016; Watson, 2022). Previously, the spotlight has primarily been placed on alveolar cells that are tetraploid (4C) and binucleated during lactation (Ho et al., 2016; Rios et al., 2016). Here, however, we show that MG alveolar cells are heterogenous in regard to ploidy and nuclei number (Figure 1.1 and Figure 1.2). This alludes to the benefits of polyploidization lying primarily in increased DNA content, regardless nuclear morphology. Furthermore, we also show that endoreplication occurs in HC11 cells in response to lactogenic differentiation and regulates milk production, thus identifying a suitable *in vitro* model that will be of use for further investigation into MG alveolar polyploidization.

The DDR to intrinsic RS drives MG alveolar endoreplication.

In this study, we show the pathway to polyploidization in the MG via induction of differentiation through the DDR is also a response that limits proliferation of damaged cells in a context where senescence or apoptosis would be deleterious to tissue integrity and function. Our results demonstrate polyploidization in the MG is achieved through an early mitotic arrest imposed by activation of the DDR-mediated G2/M checkpoint. Although this type of functional endoreplication resulting in cell differentiation has been shown to occur in the context of exogenous genotoxic insults, oncogenic transformation or chronic inflammatory conditions (de Pedro et al., 2018; González-Rosa et al., 2018; Herrtwich et al., 2016; Sanz-Gómez et al., 2018), we identify an unconventional trigger, in which intrinsic DNA damage, accumulated due to RS during the massive proliferation of early pregnancy, drives alveolar functional polyploidization at the onset of lactation (Figure 1.22). This suggests DNA damage is not only an insult to genomic integrity and a potential source for carcinogenesis, but also an inevitable consequence of cell proliferation that can determine cell fate. Therefore, by coupling proliferation with terminal differentiation, endoreplication through the activation of the G2/M checkpoint presents a developmental advantage for cell survival and tissue function.

WEE1 regulates DDR-mediated MG alveolar endoreplication.

CDK1 inhibition is one of the key drivers of endoreplication, and various CDK1 inhibitors have been shown to regulate polyploidization in mammalian tissues (Z. Ullah, Lee, & Depamphilis, 2009). Our study demonstrates CDK1 activity in the MG during alveologenesis is inhibited by WEE1, leading to activation of the G2/M

checkpoint in response to DNA damage. Although WEE1 has been shown to regulate endoreplication in some plants (Chevalier et al., 2011; Gonzalez et al., 2007; Sun et al., 1999) and prevents apoptosis during keratinocyte endoreplication (de Pedro et al., 2018), here we identify a novel role for it in MG alveolar polyploidization. Why tissues achieve polyploidization through different CDK1 inhibitors, however, remains unclear. In the case of the MG, the role of WEE1 may be explained by its dual activities of maintaining genome stability and inhibiting CDK1 (Elbæk et al., 2020; H. L. Smith et al., 2020). On one hand, WEE1 safeguards DNA replication during proliferation by limiting replication initiation and exhaustion of nucleotide pools due to excessive origin firing. On the other hand, WEE1 inhibits proliferation by activating the G2/M checkpoint through the inhibitory phosphorylation of CDK1. Accordingly, we observed two waves of WEE1 upregulation in the MG: the first occurring during early pregnancy and the second at the onset of lactation. This suggests WEE1 ensures proper DNA replication during proliferation and induces endoreplication of damaged cells during functional differentiation. In agreement with the role of WEE1 in ensuring proper DNA replication, it has been shown that loss of the KRAB Zinc Finger protein, Roma/Zfp157, results in increased replication stress due to WEE1 downregulation (Ho et al., 2016). Increased replication stress in the *Roma* knock-out resulted in increased binucleation, presumably through cytokinesis failure (Ho et al., 2016; Rios et al., 2016). This suggests that in the presence of genomic instability triggered by the loss of *Roma* and downregulation of WEE1, alveolar cells may undergo endoreplication through a WEE1-independent

mechanism, such as cytokinesis failure, to limit uncontrolled proliferation of damaged cells.

Endoreplication and lactation insufficiency.

The molecular pathways that regulate alveolar cell differentiation and efficient milk production during lactation, although critical for the survival of mammals, remain unresolved. Breastfeeding provides a myriad of long-term advantages to both a mother and child (Chowdhury et al., 2015; Victora et al., 2016). Yet lactation insufficiency, defined as the inability of a nursing mother to produce the milk necessary for an infant's daily nutritional needs, is a global public health concern. Past endeavors to address this issue have primarily focused on manipulation of the prolactin pathway to enhance milk production. While some therapeutics have been approved, albeit not in the U.S.A., such as the dopamine antagonist domperidone, negative side effects prevent their widespread adoption (Sewell, Chang, Chehab, & Nguyen, 2017). Our model offers an explanation as to why MGs have a differential ability to build a milk supply during pregnancy. Our studies provide mechanistic insights into how DNA damage accumulation during massive proliferation couples cell generation and organ growth to efficient milk production. We further demonstrate that controlling CDK1 activity has the potential to mitigate lactation insufficiency by providing a non-hormonal means of targeting milk production.

Future directions.

While endoreplication has been suggested to provide several physiological benefits, including susceptibility to apoptosis during involution, there is little evidence to support this (Kreuzaler et al., 2011; Rios et al., 2016; Watson, 2022; Zanet et al., 2010). Therefore, the extent to which polyploidy, in comparison to a normal diploid state, enhances the efficiency of RNA and protein production, the resistance to mechanical tension, and the efficacy of involution in the MG remains unclear. Bioinformatic analyses of the transcriptome, proteome and metabolome of the alveolar polyploid population will undoubtedly provide valuable insights into these potential benefits, and the difficult task of isolating live alveolar cells by their DNA content will provide our first step in this direction. Nevertheless, there is a clear disadvantage in retaining polypoid cells, as increased ploidy is known to enhance the frequency of chromosomal aberrations and promote tumorigenesis (Fujiwara et al., 2005; Zack et al., 2013). Intriguingly, while *Wee1* can be oncogenic in several types of cancer, likely due to its role in preventing DNA damage during replication and thus reducing the potential for DDR-induced senescence or apoptosis, it acts as a tumor suppressor in the mouse MG and its expression is decreased in human tumor samples compared to normal breast tissue (Do, Doroshow, & Kummar, 2013; H. L. Smith et al., 2020; Vassilopoulos et al., 2015). It is, therefore, tempting to speculate that the role of WEE1 in coupling proliferation and terminal differentiation identified in this study may confer additional protection against breast cancer, however, further long-term investigation into the effect of *Wee1* loss on tumorigenesis is needed. Moreover, in the broader scope of women's health, the results of this study beg the

question as to whether other tissues that undergo pregnancy-induced endoreplication do so in response to the intrinsic RS involved in rapid expansion.

Chapter 2: ROBO2 inhibits the differentiation and endoreplication of mammary gland alveolar cells.

Introduction

1. SLIT/ROBO signaling.

Roundabout (Robo) receptors are highly conserved single-pass type-1 membrane proteins that belong to the immunoglobulin (Ig) superfamily. Four *Robo* paralogs have been identified in mammals: *Robo1*, *Robo2*, *Robo3* and *Robo4* (Dickson & Gilestro, 2006). ROBO1, ROBO2 and ROBO3 receptors share a common structure: an extracellular domain (ECD) containing five Ig domains and three fibronectin (FN) type-3 domains, a transmembrane helix, and an unstructured intracellular domain (ICD) containing two to four proline-rich conserved cytoplasmic (CC) motifs. The structure of ROBO4 is slightly different, containing only two extracellular Ig domains. Despite their common structure, *Robo* transcripts can undergo alternative splicing to produce different protein isoforms (Bisiak & Mccarthy, 2019; Blockus & Chédotal, 2016; Tong, Jun, Nie, Hao, & Fan, 2019). The resulting proteins can also be post-translationally modified or proteolytically cleaved, allowing their ICDs to translocate to the nucleus (Barak et al., 2014; Coleman, Labrador, Chance, & Bashaw, 2010; Seki et al., 2010). Furthermore, ROBO receptors have been shown to form homophilic interactions that regulate their activity (Timothy A Evans, Santiago, Arbeille, & Bashaw, 2015; Hivert, Liu, Chuang, Doherty, & Sundaresan, 2002; Ordan & Volk, 2015; Zakrys et al., 2014). The *Robo* family can thus generate a wide array

of proteins with diverse functions. SLITs are highly conserved secreted glycoproteins and the main ligands for ROBO receptors, although it is contended that they may not interact with ROBO3 and ROBO4 directly (Chédotal; Morlot et al., 2007; Sheldon et al., 2009; Zelina et al., 2014). There are three *Slit* paralogs identified in vertebrates: *Slit1*, *Slit2* and *Slit3*. SLIT proteins also share a common structure, containing four N-terminal leucine-rich repeat (LRR) domains, six epidermal growth factor-like (EGF-like) repeats, a laminin G-like domain, followed by three more EGF-like repeats and a C-terminal cysteine-rich knot. Like their receptors, SLIT ligands have also been shown to form homophilic interactions (Howitt, Clout, & Hohenester, 2004; Seiradake et al., 2009). Additionally, SLIT proteins can be proteolytically cleaved between the fifth and sixth EGF-like domains to generate a long N-terminal fragment (SLIT-N) and a short C-terminal fragment (SLIT-C), each with different properties (Bisiak & Mccarthy, 2019; Tong et al., 2019). Only full-length SLITs or Slit-Ns are capable of binding ROBO receptors, while SLIT-Cs have been shown to have functional interactions with other proteins PlexinA1 and Dystroglycan (Ba-Charvet et al., 2001; Delloye-Bourgeois et al., 2015; Wright et al., 2012).

1.1 SLIT/ROBO interaction.

ROBO receptors possess no autocatalytic or enzymatic activity; rather, their activation results in the recruitment of adapter proteins and signaling effectors to the CC motifs, which act as scaffolding elements (Tong et al., 2019). Over time, structural mechanisms contributing to this process have been gleaned from studies of ROBO1 and ROBO2 receptors, which share the highest degree of homology

amongst the ROBO family. Initial experiments demonstrated that ROBO activation is induced through the binding of SLITs, via their second LRR (LRR2) domain, with the first Ig (IG1) domain of ROBO receptors (Howard, Reichert, & Evans, 2021; Howitt et al., 2004; Z. Liu et al., 2004; Morlot et al., 2007). Heparan sulfate proteoglycans (HSPGs) were also observed to bind both ROBO receptors and SLIT ligands and shown to enhance the affinity and stability of their interaction (Fukuhara, Howitt, Hussain, & Hohenester, 2008; Hussain et al., 2006). Genetic studies employing chimeric ROBO receptors demonstrated that the functional diversity between receptors is imparted by modest structural differences in their ECDs, rather than different affinities for SLIT ligands, and suggested ROBO activity and function may be largely determined by multimerization (Timothy A. Evans & Bashaw, 2010). It was subsequently shown that that induced dimerization of their ICDs can stimulate their activity (Zakrys et al., 2014). Recent X-ray crystallography studies have provided new insights into how the interaction of ROBO receptors with each other and SLIT ligands may regulate their activation. Structures of both ROBO1 and ROBO2 extracellular components suggest that the Ig4 domain serves as a conserved module for dimerization and is required for activity (Aleksandrova et al., 2018; Barak et al., 2019; Yom-Tov et al., 2017). Moreover, it has been suggested that the Ig4 domain confers a means of auto-inhibition, as the dimerization interface appears hidden in the compact monomeric state of ROBO receptors, and that homophilic *trans* interactions mediated by the Ig5 domain may serve to further confine Ig4 and enhance this inhibition. It has also been proposed that binding of SLITs to the Ig1 domains of ROBO receptors would disrupt the *trans* interaction mediated by Ig5, thus

relieving them of their imposed confinement and allowing for dimerization in *cis* and subsequent activation. Alternatively, if there is no *trans* inhibition, SLIT dimers may also serve to bring ROBO receptors in close enough proximity that they overcome their auto-inhibition, dimerize and become activated (Barak et al., 2019). While X-ray crystallography has provided valuable insights into the structure of SLIT/ROBO extracellular interactions, it nevertheless remains unclear how this modulates the recruitment of downstream effectors to ROBO ICDs.

1.2 SLIT/ROBO signaling during development.

SLIT/ROBO signaling was first discovered for its role in neuronal axon guidance through genetic screens of commissural midline crossing defects in *Drosophila* (Brose et al., 1999; T. Kidd, Bland, & Goodman, 1999; Thomas Kidd et al., 1998; Simpson, Kidd, Bland, & Goodman, 2000; Tear, Seeger, & Goodman, 1993). Since its discovery, SLIT/ROBO signaling has been shown to be involved in the development of numerous other tissues. During organogenesis, SLIT/ROBO signaling has been observed to be critical for the proper development of the kidneys, lungs and heart (Domyan et al., 2013; Grieshammer et al., 2004; Mommersteeg et al., 2013). Moreover, SLIT/ROBO signaling has been shown to regulate stem and progenitor cell dynamics. In the nervous system, SLIT/ROBO signaling regulates the balance between self-renewal of ventricular zone progenitors and the generation of intermediate progenitors and neurons (Borrell et al., 2012). A similar role for SLIT/ROBO signaling in cell fate specification was identified in the intestine, in which ROBO2 regulates the generation of enteroendocrine cells by intestinal stem cells

(Biteau & Jasper, 2014). In the hematopoietic system, on the other hand, SLIT/ROBO signaling assists the localization and engraftment of stem cells to their niches in the bone marrow (Smith-Berdan et al., 2011). Furthermore, SLIT/ROBO signaling also has contrasting functions in vasculature, having been observed to both promote angiogenesis through chemotaxis, cell motility and proliferation, as well as inhibit angiogenesis through modulation of growth factor signaling (S. Li et al., 2015; Marlow et al., 2010; Nieminen et al., 2015; Rama et al., 2015; Sheldon et al., 2009; B. Zhang et al., 2009). It has been suggested that these contrasting functions are determined by the ratio of ROBO1 and ROBO4 in endothelial cells, as well as the cooperation between SLIT2 and Ephrin-A1 (Dunaway et al., 2011; Enomoto et al., 2016). As a likely consequence of its roles in stem/progenitor dynamics, chemotaxis, cell motility, and angiogenesis, SLIT/ROBO signaling has also been implicated in the tumorigenesis, metastasis and vascularization of several types of cancers (M. S. Ballard & Hinck, 2012; Gara et al., 2015; Jiang et al., 2019).

1.3 SLIT/ROBO signaling in the MG.

SLIT/ROBO signaling has been demonstrated to play a variety of roles during the development of the MG. The first was identified in branching morphogenesis during pubertal development. SLIT2/ROBO1 signaling, in cooperation with NTN1, was shown to mediate adhesive contacts between basal and luminal epithelial layers, maintaining the tubular bi-layered structure while allowing cell movement and reorganization (Strickland, Shin, Plump, Tessier-Lavigne, & Hinck, 2006). Subsequently, it was shown that SLIT2/ROBO1 signaling also inhibits lateral branch

formation by controlling the proliferation of the basal compartment through the inhibition of β-catenin nuclear translocation and transcription of Wnt signaling effector genes (H. Macias et al., 2011). SLIT/ROBO signaling was also found to regulate stem and progenitor cell dynamics in the MG. Similar to ROBO1, ROBO2 inhibits the nuclear translocation of β-catenin in basal progenitor cells in response to SLITs, albeit with a different outcome. In contrast to promoting proliferation through Wnt effectors, signaling through ROBO2 promotes senescence of basal progenitors by inhibiting β-catenin-mediated repression of $p16^{INK4A}$ expression (Harburg et al., 2014). Furthermore, SLIT2/ROBO1 signaling governs the self-renewal of basal progenitor cells by limiting the expression of INSC, a key member of the spindle orientation machinery, thus promoting asymmetric cell divisions and maintaining a homeostatic amount of progenitor cells (S. Ballard, Mimmi et al., 2015). Recently, a novel role for SLIT/ROBO signaling during pregnancy was identified. It was demonstrated that the ROBO1-mediated inhibition of β-catenin nuclear localization limits the expression of the NOTCH ligand Jagged1 (JAG1) in basal cells. In the absence of ROBO1, however, increased JAG1 signals in a juxtacrine manner to induce NOTCH activity in neighboring alveolar progenitor cells, promoting their self-renewal while inhibiting their differentiation into milk-producing alveolar cells (Cazares et al., 2021). Intriguingly, while loss of *Robo1* promotes the NOTCH activity of alveolar progenitors in MG, loss of both *Robo1* and *Robo2* in ventricular zone progenitors of the brain was observed to inhibit NOTCH activity, suggesting a potential interplay between the two receptors may govern this pathway (Borrell et al., 2012).

2. NOTCH signaling.

The NOTCH signaling pathway is a highly conserved hallmark pathway deeply involved in the embryonic and post-natal development of many tissues, as well as their homeostasis. Signaling through this pathway typically occurs in a juxtacrine manner, initiated by the close spatial association of a signal-receiving cell with a NOTCH receptor expressed on its surface and a signal-sending cell with a ligand expressed on its surface (Zhou et al., 2022). There are four *Notch* paralogs identified in mammals: *Notch1*, *Notch2*, *Notch3* and *Notch4*. *Notch* genes are peculiar in that they are transcribed and translated to produce NOTCH precursor proteins. These proteins are then glycosylated and proteolytically cleaved at a conserved site to produce heterodimers, which serve as the functional receptors. NOTCH receptors are single-pass type-1 transmembrane proteins and share a common structure: an ECD containing 29 to 36 tandem EGF-like repeats and a negative regulatory region (NRR), a transmembrane helix, and an ICD containing an RBPJ-association module (RAM) domain, seven ankyrin (ANK) repeats flanked by nuclear localization signal (NLS) domains and a C-terminal PEST domain. There are five canonical NOTCH ligands identified in mammals: Delta-like Ligand 1 (DLL1), DLL3, DLL4, JAG1 and JAG2, which present both redundant and unique functions (Gordon, Arnett, & Blacklow, 2008; Zhou et al., 2022). Like ROBO receptors, NOTCH receptors do not possess any auto-catalytic or enzymatic activity. Upon ligand binding, NOTCH receptors undergo proteolytic cleavage by ADAM proteases at the dimerization interface, releasing their ECD. Subsequently, the ICD is cleaved by γ-Secretase,

releasing from the transmembrane helix (Gordon et al., 2008; Kopan, 2012; Zhou et al., 2022). Once released, NOTCH ICDs can remain in the cytoplasm and engage in crosstalk with a variety of other signaling pathways or they can translocate to the nucleus, where they associate with various transcription factors, such as RBPJ, to regulate the expression of downstream signaling effectors. Through its downstream effectors, NOTCH activity regulates an abundance of biological processes, many of which in a tissue-specific or cell-specific manner (Zhou et al., 2022).

2.1 NOTCH signaling in the MG.

NOTCH signaling is critical to MG development, particularly due to its roles in regulating progenitor cell dynamics. In fact, NOTCH4, originally called Int3, was discovered in the MG as a proto-oncogene frequently activated through insertional mutagenesis of the mouse mammary tumor virus upstream of the DNA sequence encoding the ICD (D Gallahan & Callahan, 1987). This constitutively active mutant form impairs the functional development and differentiation of the MG and promotes tumorigenesis, an effect shown to be mediated by the ICD (Daniel Gallahan & Callahan, 1997; D. Gallahan et al., 1996; Jhappan et al., 1992; G. H. Smith et al., 1995; Uyttendaele, Soriano, Montesano, & Kitajewski, 1998). NOTCH4 was thus proposed to play an important role in regulating the self-renewal and proliferation of mammary stem cells. Later characterization of *Notch4 KO* mice, however, revealed no MG phenotype, and *Notch4* expression was hardly detected throughout MG development, suggesting the proto-oncogenic form does not have a significant role (Krebs et al., 2000; Raafat et al., 2011).

Nevertheless, similar roles in regulating stem and progenitor cell dynamics have been observed for the other NOTCH receptors since then. In recent years, it has been demonstrated that, while the MG possesses bipotent stem cells during embryonic development, the vast majority of post-natal development is facilitated by long-lived, lineage-restricted progenitor populations (Van Keymeulen et al., 2017; Van Keymeulen et al., 2011; Wuidart et al., 2016). *Notch1-3* have been shown to drive of the specification of lineage-restricted luminal progenitors. Indeed, *Notch1-3* are highly expressed in the luminal compartment and reach their peak expression during pregnancy, while notch inhibitors, such as *Numb*, are expressed in the myoepithelial compartment (Bouras et al., 2008; Raafat et al., 2011; Raouf et al., 2008; Y. Zhang et al., 2016). Functional studies employing loss- or gain-of-Notch receptors and Notch signaling components in mice confirmed the role of Notch signaling in maintaining the balance between myoepithelial and luminal populations, with the absence of Notch signaling leading to accumulation of the myoepithelial lineage and increased Notch signaling leading to expansion of the luminal lineage (Bouras et al., 2008; Buono et al., 2006; Hu et al., 2006; Raouf et al., 2008; Santoro, Vlachou, Carminati, Pelicci, & Mapelli, 2016; Yalcin-Ozuysal et al., 2010; Y. Zhang et al., 2016). Furthermore, lineage-tracing studies have confirmed the contribution of *Notch1-3* expressing cells to luminal lineages and have shown that Notch activity drives bipotent stem cells towards the luminal progenitor fate by late embryogenesis (Lafkas et al., 2013; Lilja et al., 2018; Rodilla et al., 2015; Šale, Lafkas, & Artavanis-Tsakonas, 2013). Interestingly, Notch signaling not only drives bipotent stem cells

toward a luminal progenitor fate, but maintains this fate through the inhibition of terminal differentiation, which may serve to explain the effect of increased Notch signaling on tumorigenesis (Bouras et al., 2008; Buono et al., 2006; Dontu et al., 2004; Hu et al., 2006; Kiaris et al., 2004; Raouf et al., 2008; Y. Zhang et al., 2016). It has been further shown that the prolactin-induced expression of the transcription factor ELF5 during mid-pregnancy drives the differentiation of these progenitors into mature alveolar cells through the inhibition of Notch signaling (Chakrabarti et al., 2012; Cordero et al., 2016; Harris et al., 2006; H. J. Lee et al., 2013; Oakes et al., 2008). Recently, it was also demonstrated that, upon ablation of luminal cells, Notch signaling is reactivated in myoepithelial progenitors to repopulate the luminal lineage, providing further confirmation of its role in the context of injury and regeneration (Centonze et al., 2020). Despite the importance of Notch signaling in specifying and maintaining the luminal-restricted progenitor population, the mechanisms that regulate Notch activity to ensure proper MG development during puberty and pregnancy are not well understood. ROBO1, through restricting the expression of JAG1 in basal cells, was identified as one such mechanism by which Notch signaling is curtailed to allow for proper alveolar differentiation (Cazares et al., 2021). Here, I propose an opposing role for ROBO2, in which it inhibits alveolar differentiation and endoreplication through the promotion of Notch signaling.

Objectives

- Characterize the expression of *Robo2* during alveologenesis.

- Determine whether ROBO2 plays a role in regulating alveolar differentiation, and the molecular mechanism that may be involved.

Results

Robo2 is dynamically expressed during pregnancy and early lactation.

While our lab has previously characterized the expression of *Robo2* in the nulliparous MG, the expression of *Robo2* during pregnancy and lactation has nevertheless remained unclear (Harburg et al., 2014; Strickland et al., 2006). In fact, multiple single-cell RNA sequencing (scRNA-seq) datasets from embryonic development through menopause suggest there is little to no expression of *Robo2* throughout the lineage trajectories of the MG, with 99.2% of cells having no *Robo2* reads, let alone a specific subpopulation in which it is enriched (Figure 2.1a, b)(Saeki et al., 2021; Speir et al., 2021). To further investigate *Robo2* expression in the context of pregnancy and early lactation, we isolated stromal, basal and luminal subpopulations by FACS and analyzed its expression in each subpopulation by RT-qPCR, normalizing to expression at PD6. In the stromal subpopulation, we find *Robo2* expression is highest during early pregnancy, maintained at a lower level during the remainder of pregnancy, then decreases further as lactation begins (Figure 2.1c). In the basal epithelial subpopulation, *Robo2* expression follows a similar pattern, peaking at PD6 and gradually decreasing with the progression of pregnancy and lactation (Figure 2.1d). Of note, in the luminal epithelial subpopulation, *Robo2* expression follows a unique pattern with two peaks. The first occurs during early pregnancy, when *Robo2* is upregulated considerably by PD10. Expression is then maintained at a lower level for the remainder of pregnancy, only to be upregulated again with the onset of lactation (Figure 2.1e). Having observed

the pattern of expression within each subpopulation, we next normalized *Robo2* expression in the epithelial subpopulations to that of the stromal cells at each timepoint, in order to compare expression between populations. We find that *Robo2* expression is lower in both epithelial subpopulations throughout pregnancy, compared to the normalized stromal expression. Intriguingly, with lactation, Robo2 expression in luminal, but not basal, epithelial cells surpasses that of stromal cells substantially (Figure 2.1f). Together, these results show that *Robo2* is dynamically expressed in all subpopulations during pregnancy and early lactation, and hint at a potential function for the protein in the processes of alveologenesis.

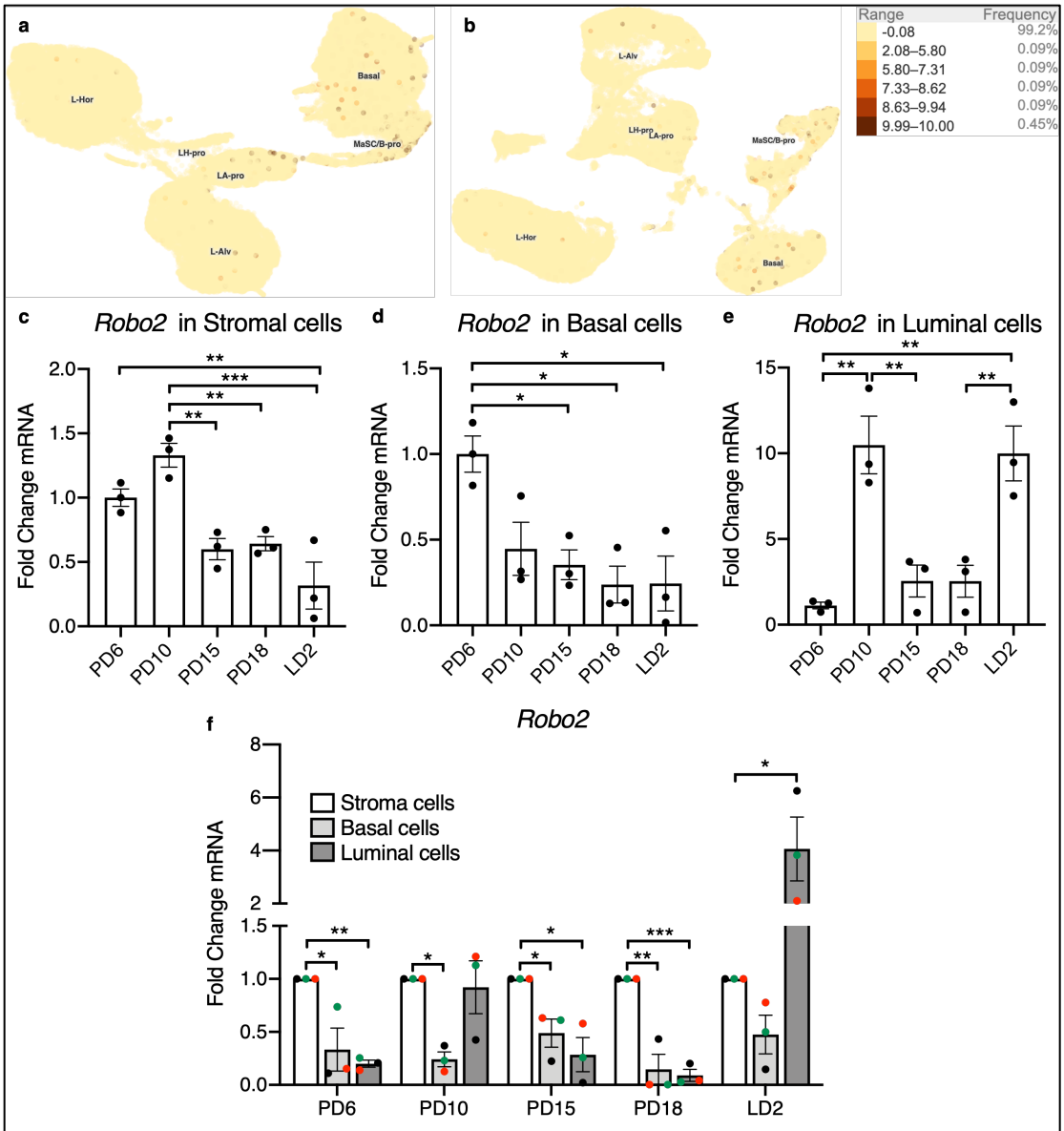

Figure 2.1: *Robo2* is dynamically expressed in MG subpopulations during pregnancy and early lactation. a,b) scRNA-seq datasets integrated with **(a)** Harmony and **(b)** Liger showing *Robo2* expression across MG subpopulations from embryonic, neonatal, pubertal, virgin adult, pregnant, lactating, involuted and menopause stage mice. Legend shows scale of high to low expression shown as red to beige, respectively, with % of cells in each range. Subpopulations: mammary stem cell/basal progenitor (MaSC/B-pro), basal (Basal), luminal hormone receptor-positive progenitor (LH-pro), luminal hormone receptor-positive (L-Hor), luminal alveolar progenitor (LA-pro) and luminal alveolar (L-Alv) [232,233]. **c-e)** Quantification of *Robo2* expression in FACS-isolated **(c)** stromal, **(d)** basal and **(e)** luminal subpopulations from PD6, PD10, PD15, PD18 and LD2 MGs, as detected by RT-qPCR. Data shown as the mean ± S.E.M, normalized to PD6 of each subpopulation; n=3 biological replicates; two-tailed unpaired Student's t-test. **f)** Quantification of *Robo2* expression in FACS-isolated stromal, basal and luminal subpopulations from PD6, PD10, PD15, PD18 and LD2 MGs, as detected by RT-qPCR. Data shown as the mean ± S.E.M, normalized to the stromal population at each timepoint; n=3 biological replicates; two-tailed unpaired Student's t-test. p values: *<0.05, **<0.01, ***<0.001

ROBO2 inhibits alveologenesis and milk production during pregnancy.

Our lab possesses a *Robo2* null mouse line that is a full knockout, thereby deleting *Robo2* in all tissues. To investigate the role of ROBO2 in the MG epithelium during alveologenesis, we contralaterally transplanted fragments of epithelium from *WT* and *Robo2 KO* MGs into the fat-pads of immunocompromised pre-pubertal mice whose endogenous epithelium had been removed. As the mice progressed through pubertal development, the fragments underwent branching morphogenesis to produce fully formed epithelia. We then performed timed-breeding of the adult mice and harvested the MGs at PD15 for subsequent analysis. By whole-mount carmine staining, we observe a phenotype in that *Robo2 KO* outgrowths form a denser network of alveolar structures, compared to the contralateral *WT* control (Figure 2.2a). This was confirmed by H&E staining, where we see that *Robo2 KO* outgrowths occupy a ~10% larger area of the host fat-pad (Figure 2.2b,c). Furthermore, by IHC staining, we find that the number of alveoli and size of *Robo2 KO* lumens were increased by ~70% and ~25%, respectively (Figure 2.2d-f). This was accompanied by a ~45% increase in milk production (Figure 2.2g). Together, these findings demonstrate that *Robo2* inhibits alveologenesis and milk production, and that this role is intrinsic to the epithelium.

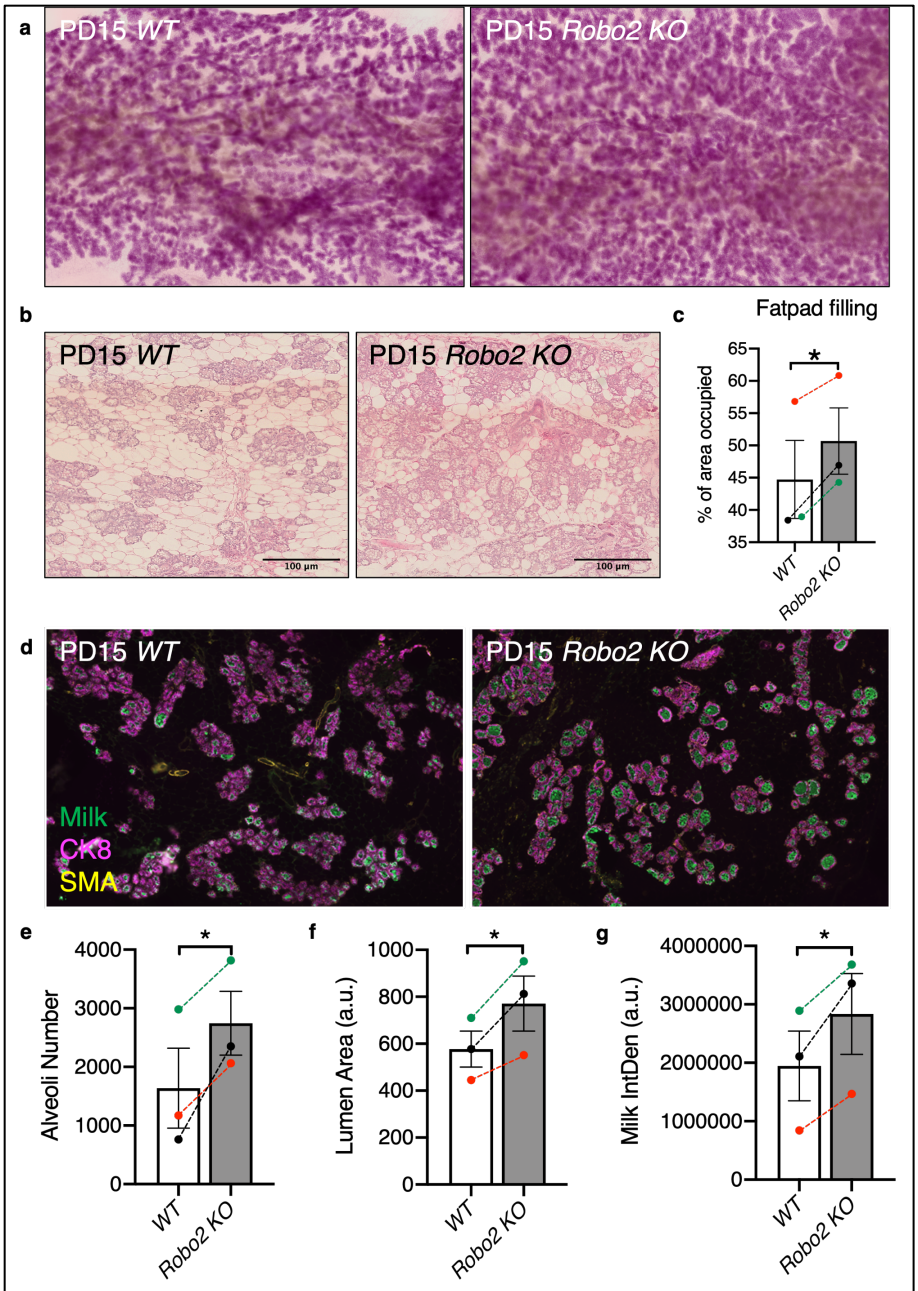

Figure 2.2: ROBO2 inhibits alveologenesis and milk production during pregnancy. a) Carmine staining of contralateral *WT* (left) and *Robo2 KO* (right) whole-mount PD15 MG epithelium outgrowths. Images are representative of n=3 independent experiments. **b)** H&E staining of contralateral *WT* (left) and *Robo2 KO* (right) PD15 MG epithelium outgrowth sections. Images are representative of n=3 independent experiments. **c)** Quantification of percentage of host fat-pad occupied by MG epithelium outgrowths, as detected by H&E. Data shown as the mean ± S.E.M; n=3 biological replicates; two-tailed paired Student's t-test. **d)** IHC staining of milk (green), CK8 (magenta) and SMA (yellow) in contralateral *WT* (left) and *Robo2 KO* (right) PD15 MG epithelium outgrowth sections. Images are representative of n=3 independent experiments. **e-g)** Quantification of **(e)** alveoli number, **(f)** lumen area and **(g)** milk integrated-density per alveoli in contralateral *WT* (left) and *Robo2 KO* (right) PD15 MG epithelium outgrowth sections, as detected by IHC. Data shown as the mean ± S.E.M; n=3 biological replicates; two-tailed paired Student's t-test. p values: *<0.05

ROBO2 functions to inhibit alveolar differentiation from the luminal compartment.

Having determined the role of ROBO2 to be intrinsic to the epithelium, we next sought to distinguish whether ROBO2 functions to inhibit alveologenesis from the basal compartment, luminal compartment or both compartments. To do so, we enriched basal and luminal subpopulations from *ActB-eGFP and Robo2 KO* MGs through enzymatic digestion, 2D culture and subsequent differential trypsinization. Enriched populations were then combined and cultured in a 3D extracellular matrix to form mosaic organoids in which *Robo2* was lost in the basal compartment only, in the luminal compartment only, in both compartments and in neither compartment (Figure 2.3a). After inducing the organoids to differentiate for 5 days (DIP5) through treatment with lactogenic hormones, we find that only loss of *Robo2* in the luminal compartment resulted in increased organoid size (Figure 2.3b-d). Moreover, by brightfield microscopy, we observe many organoids with what appear to be milk-filled lumens when *Robo2* is lost in both compartments and in the luminal compartment alone, whereas we only observe a discreet few in the other two conditions (Figure 2.3d). It was subsequently confirmed, by RT-qPCR, that loss of *Robo2* in both compartments and in the luminal compartment alone results in an increase in expression of the milk gene *Csn2*, as well as an increase in expression of the pro-alveolar differentiation transcription factor *Elf5* (Figure 2.3e,f). Curiously, loss of *Robo2* in both compartments did not yield an increase in organoid size (Figure 2.3d), and loss of *Robo2* in the basal compartment alone resulted in lesser increases in *Csn2* and *Elf5* expression (Figure 2.3e,f). It is important to note, however, that the

process of differential trypsinization only serves to enrich for basal and luminal subpopulations, rather than actually purifying them, and the mosaic conditions may include some organoids of a different genotypic combination. Nevertheless, the trend of these results suggests that ROBO2 may be acting from the luminal compartment to inhibit the differentiation of alveolar progenitor cells.

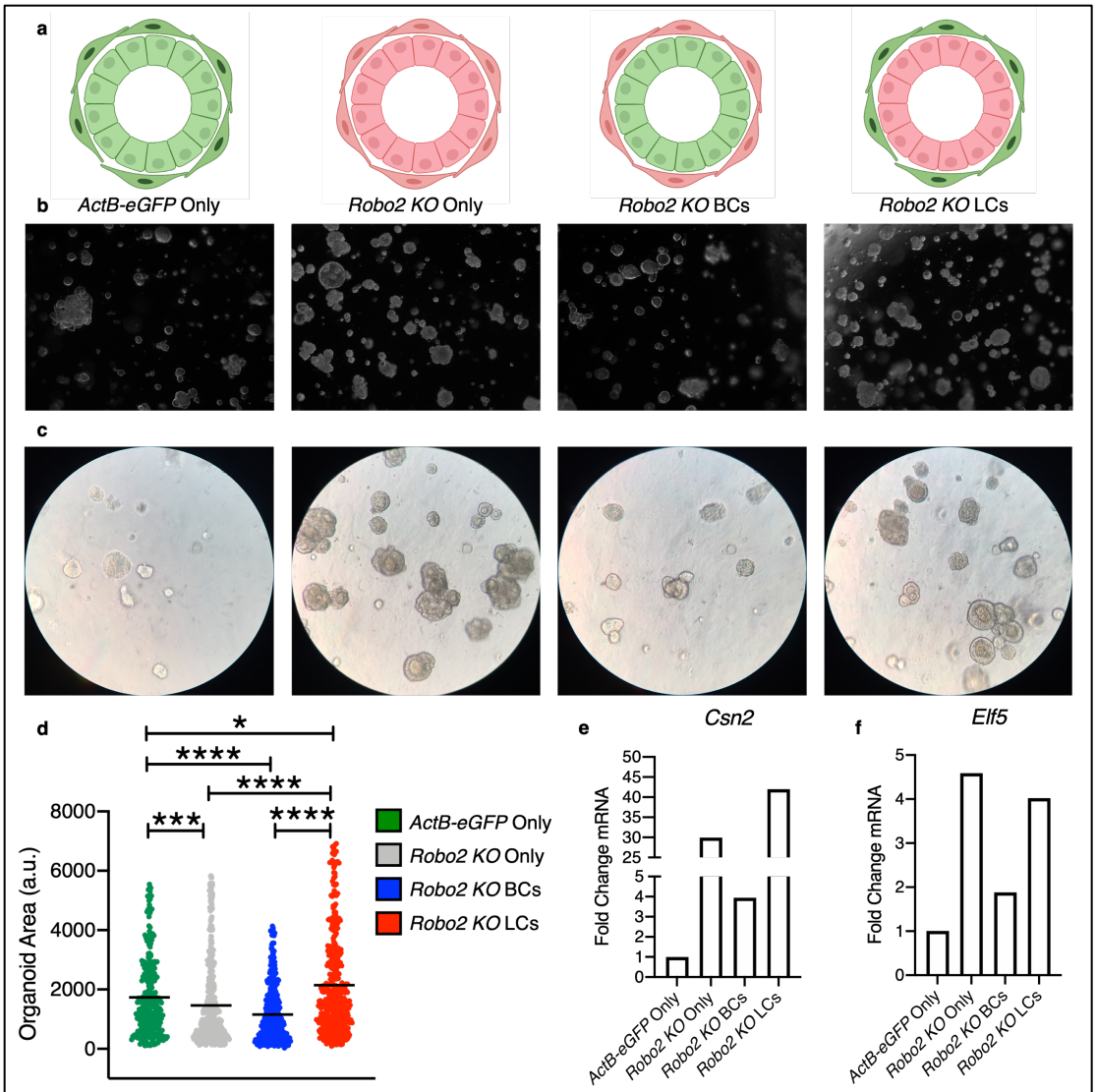

Figure 2.3: ROBO2 functions to inhibit alveolar differentiation from the luminal compartment. a) Cartoon representing mosaic organoid genotypic combinations of *ActB-eGFP* (green) and *Robo2 KO* (red) basal (outer) or luminal (inner) cells. **b, c) (b)** Darkfield and **(c)** brightfield images of DIP5 mosaic organoids. Genotypic combinations from left to right: *ActB-eGFP* Only, *Robo2 KO* Only, *Robo2 KO* BCs and *Robo2 KO* LCs. Images representative of n=1 biological replicates. **d)** Quantification of mosaic organoid area, as detected by darkfield microscopy. Black horizontal bars represent the mean. Kruskal-Wallis with Dunn's multiple comparison test. **e,f)** Quantification of **(e)** *Csn2* and **(f)** *Elf5* expression in mosaic organoids, as detected by RT-qPCR. p values: *<0.05, ***<0.001, ****<0.0001

ROBO2 inhibits alveolar endoreplication.

Alveolar cells undergo endoreplication at the onset of lactation, a process usually linked with terminal differentiation (refer to Chapter 1). To evaluate the effect of ROBO2 on alveolar endoreplication, we knocked down (KD) *Robo2* in HC11 cells, a murine mammary epithelial cell line that can be induced to differentiate and endoreplicate through treatment with lactogenic hormones, using a lentiviral construct. We then performed FACS DNA content analysis of HC11 cells at timepoints throughout lactogenic differentiation (Figure 2.4a-f). We observe that KD of *Robo2* results in an increase of the polyploid population in undifferentiated HC11 cells (Figure 2.4a,b). By the priming phase, *Robo2 KD* results in an increase in the proportions of both the tetraploid and polyploid populations (Figure 2.4c,d), and increased polyploidy is maintained into differentiation (Figure 2.4e,f). These results suggest that ROBO2 inhibits alveolar endoreplication *in vitro*. To determine if this effect occurs *in vivo*, we performed FACS DNA content analysis of the CK8+ luminal cell population from MGs of a *WT* and a *Robo2 KO* mouse at PD18 LD5. Accordingly, we observe increased proportions of tetraploid and polyploid cells in the *Robo2 KO* mouse at both timepoints (Figure 2.5a-d). While further biological replicates are needed to confirm its function *in vivo*, these results suggest ROBO2 inhibits alveolar endoreplication.

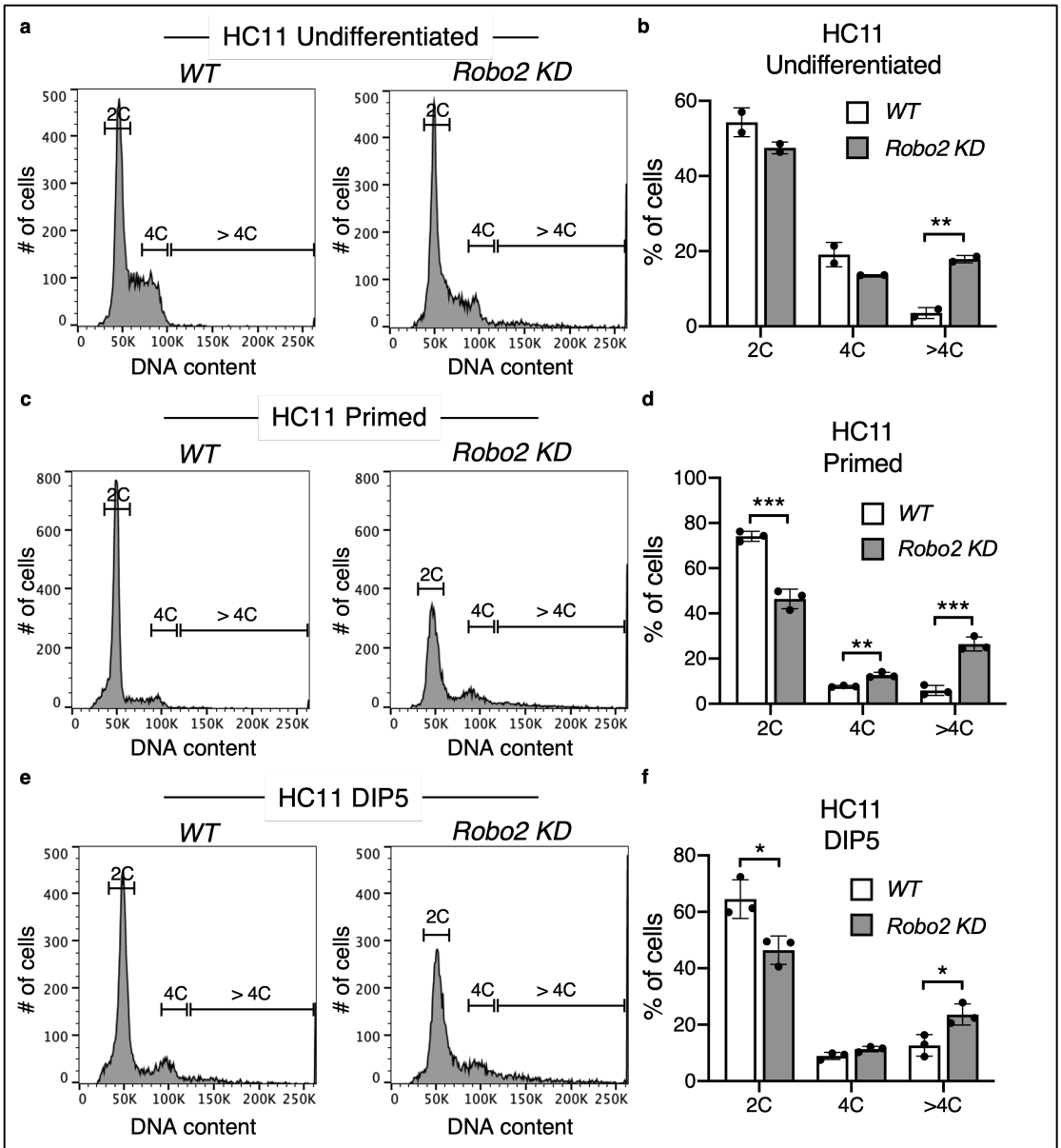

Figure 2.4: ROBO2 inhibits endoreplication in HC11 cells. a,c,e) Representative FACS histograms for DNA content analysis of **(a)** undifferentiated, **(c)** primed and **(e)** DIP5 *WT* and *Robo2 KD* HC11 cells. **b,d,f)** Percentage of **(b)** undifferentiated, **(d)** primed and **(f)** DIP5 *WT* and *Robo2 KD* HC11 cells with 2C, 4C or > 4C DNA content, detected by FACS. Data shown as the mean ± SD; n=2 biological replicates for undifferentiated, n=3 biological replicates for primed and DIP5; two-tailed unpaired Student's t-test. p values: *<0.05, **<0.01, ***<0.001

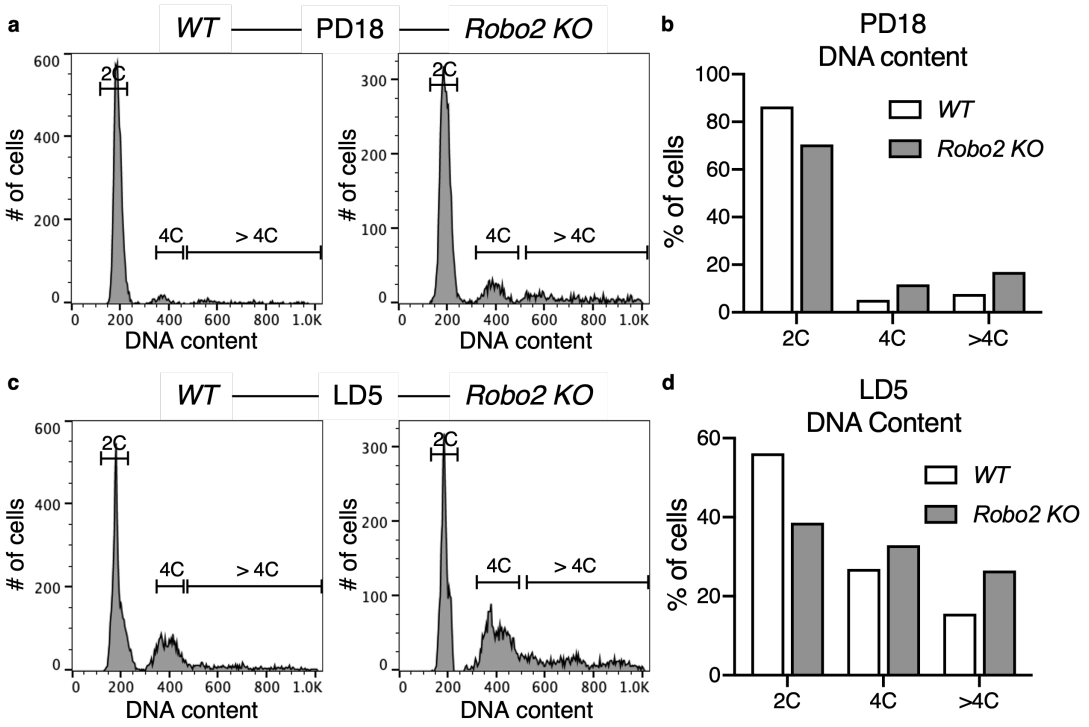

Figure 2.5: ROBO2 inhibits endoreplication in the MG. a,c) Representative FACS histograms for DNA content analysis of CK8+ cells from **(a)** PD18 and **(c)** LD5 *WT* and *Robo2 KO* MGs. **b,d)** Percentage of CK8+ cells from **(b)** PD18 and **(d)** LD5 *WT* and *Robo2 KO* MGs with 2C, 4C or > 4C DNA content, detected by FACS. Data shown as the mean ± SD; n=1 biological replicates. two-tailed unpaired Student's t-test.

ROBO2 inhibits the DDR.

Alveolar endoreplication is driven by the DDR to replication stress that occurs during the hyperproliferation of early pregnancy (refer to Chapter 1). To evaluate the relationship between ROBO2 and the DDR, we first examined the localization of ROBO2 and γH2AX in DIP5 HC11 cells by IHC staining. We observe that the presence of milk domes occurs in areas containing cells with higher levels of γH2AX and lower levels of ROBO2, suggesting a potential negative relationship between the two (Figure 2.6a). To further investigate the effect of ROBO2 on the activation of the DDR, we analyzed the presence of pATR, which mediates the DDR to replication

stress, in the nuclei of CK8+ alveolar luminal cells in PD10 MGs from *WT* and *Robo2 KO* mice, by IHC staining (Figure 2.6b). We find that loss of *Robo2* results in the increased presence of pATR, suggesting ROBO2 inhibits alveolar endoreplication and differentiation through the suppression of the DDR to replication stress during pregnancy (Figure 2.6c).

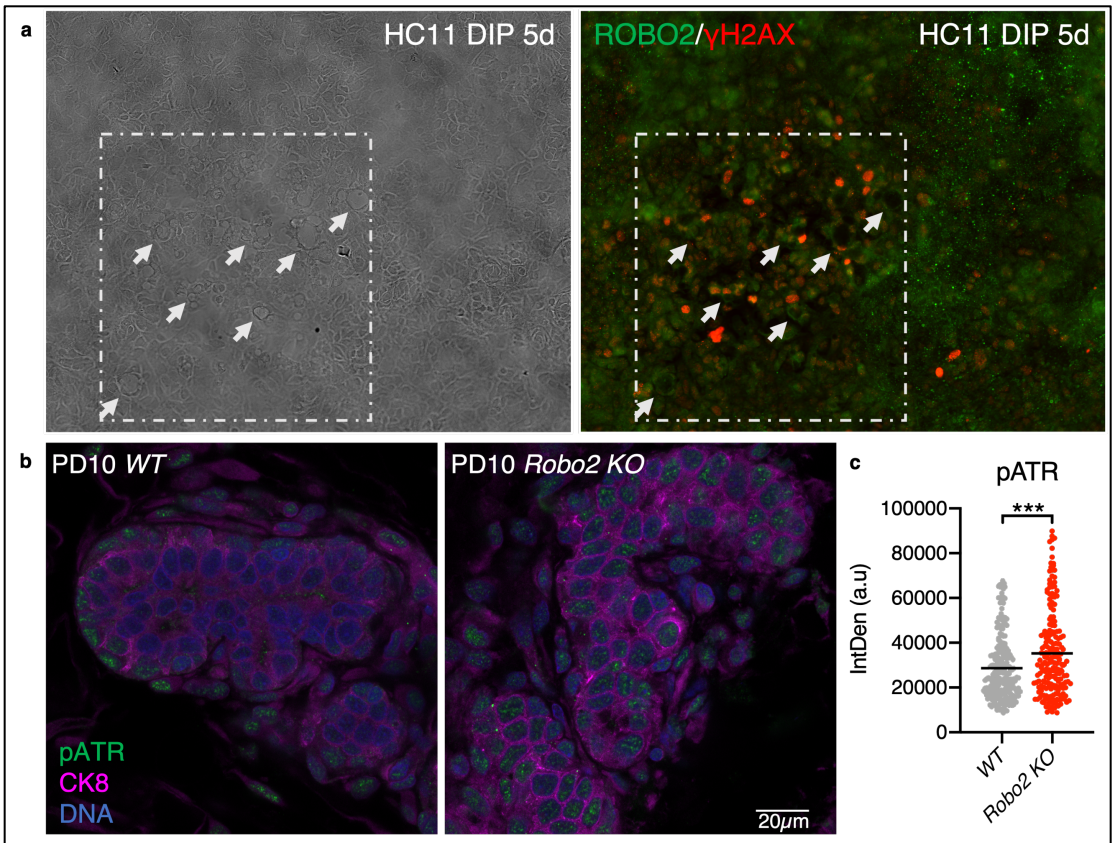

Figure 2.6: ROBO2 inhibits the DNA damage response. a) Phase-contrast image (left) and IHC staining of ROBO2 (green) and (γH2AX) in DIP5 HC11 cells. Arrows point to location of milk domes. Images representative of n=1 biological replicates. **b)** IHC staining of pATR (green), CK8 (magenta) and DNA (blue) in PD10 *WT* (left) and *Robo2 KO* (right) MG sections. Images representative of n=1 biological replicates. **c)** Quantification of pATR integrated-density per nuclei in PD10 *WT* and *Robo2 KO* MG sections, as detected by IHC. Data shown as the mean ± S.E.M; n=1 biological replicates; two-tailed unpaired Student's t-test. p values: ***<0.001

ROBO2 regulates NOTCH activity in the MG.

ROBO1 was recently shown to inhibit NOTCH activity in alveolar progenitor cells and promote their differentiation from the basal compartment, through paracrine stimulation via JAG1 (Cazares et al., 2021). To investigate whether ROBO2 inhibits alveolar differentiation through regulation of JAG1, we isolated stromal, basal and luminal subpopulations from PD10 MGs of *WT* and *Robo2 KO* mice and analyzed *Jag1* expression by RT-qPCR. We find that *Jag1* expression is highest in the basal subpopulation (Figure 2.7a), and that loss of *Robo2* results in decreased expression of *Jag1* in this subpopulation (Figure 2.7b). Furthermore, we cultured 3D organoids from *WT* and *Robo2 KO* primary MG epithelial cells and treated them with an activating JAG1 peptide throughout the process of growth and differentiation. We find by WB that treatment with JAG1 peptide results in decreased expression of the milk protein CSN2 in *WT* cells at DIP5, consistent with the recent observation that JAG1/Notch signaling promotes alveolar progenitor renewal at the expense of differentiation (Cazares et al., 2021). Additionally, we find the loss of *Robo2* results in increased expression of CSN2 at DIP5, and treatment of *Robo2 KO* organoids with the JAG1 peptide rescues this effect (Figure 2.7c,d). Together, these data suggest ROBO2 inhibits alveolar differentiation through the induction of *Jag1* expression in the basal compartment. This may occur by ROBO2 inhibiting ROBO1, thereby activating β-catenin, which directly binds the promoter of *Jag1* to induce its expression, in the basal compartment.

Interestingly, in addition to its canonical role in mediating transcription, the NOTCH1 ICD has also been shown to bind all of the DDR kinases and negatively regulate ATM activity (M. Adamowicz, d'Adda di Fagagna, & Vermezovic, 2018; Marek Adamowicz, Vermezovic, & Fagagna, 2016; Vermezovic et al., 2015). To investigate the relationship between NOTCH1 ICD and ATR, and whether NOTCH1 ICD may negatively regulate ATR activity as well, we evaluated the nuclear localization of NOTCH1 and pATR in 3D *WT* organoids throughout the differentiation process by IHC staining. We observe an initial peak of nuclear pATR in luminal cells on the first day of differentiation (DIP1), after which the levels of nuclear NOTCH1 and pATR in CK8+ alveolar luminal cells become inversely correlated as differentiation progresses (Figure 2.7e). Additionally, we observe an inverse relationship in their localization within the nucleus, with nuclear areas of low pATR presence having more NOTCH1 than areas of high pATR presence (Figure 2.7f). Taken together, the negative relationships observed between NOTCH1 and pATR across differentiation and within the nucleus suggest NOTCH1 ICD may be functioning to inhibit the ATR-mediated DDR to replication stress. Considering our previous studies on the role of ROBO1 in regulating alveologenesis, we propose a model in which ROBO2 directly binds and inhibits ROBO1 in *trans*, promoting JAG1 expression in basal cells and the juxtacrine induction of Notch activity in luminal alveolar progenitor cells. This, in turn, results in the inhibition of alveolar differentiation through canonical Notch signaling, as well as the inhibition of alveolar endoreplication through NOTCH1 ICD-mediated suppression of the DDR.

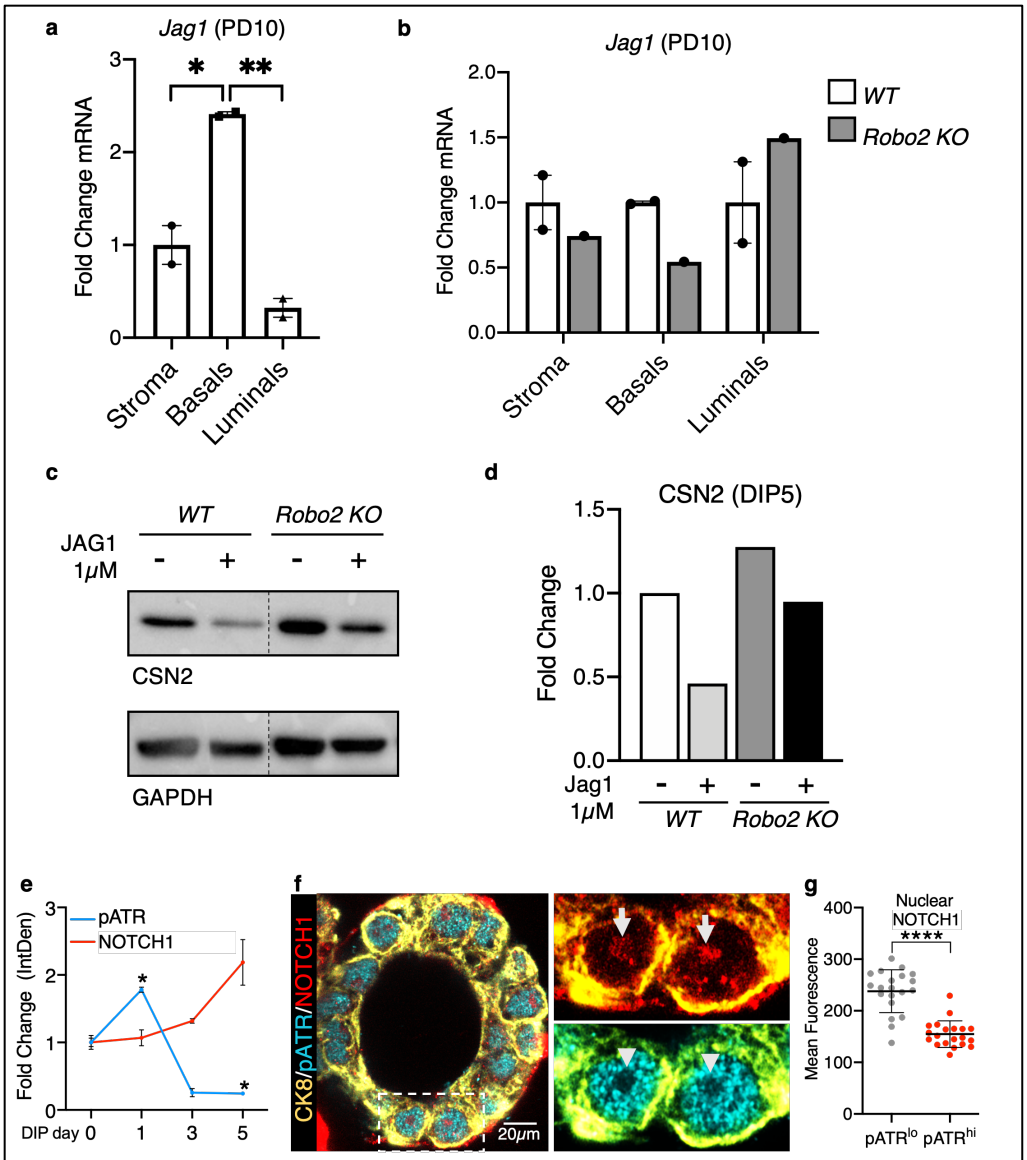

Figure 2.7: ROBO2 regulates NOTCH activity in the MG. a) Quantification of *Jag1* expression in FACS-isolated stromal, basal and luminal subpopulations from PD10 *WT* MGs, as detected by RT-qPCR. Data shown as the mean ± S.E.M, normalized to the stromal subpopulation; n=2 biological replicates; two-tailed unpaired Student's t-test. **b)** Quantification of *Jag1* expression in FACS-isolated stromal, basal and luminal subpopulations from PD10 *WT* and *Robo2 KO* MGs, as detected by RT-qPCR. Data shown as the mean ± S.E.M, normalized to *WT* for each subpopulation; n=2 biological replicates for *WT*, n=1 biological replicates for *Robo2 KO*; two-tailed unpaired Student's t-test. **c,d) (c)** Western Blot and **(d)** quantification of CSN2 expression in DIP5 *WT* and *Robo2 KO* organoids treated with JAG1 peptide. **e)** Quantification of nuclear pATR and NOTCH1 integrated-density in CK8+ luminal cells of organoids throughout differentiation, as detected by IHC. Data shown as the mean ± S.E.M; n=1 biological replicates; two-tailed unpaired Student's t-test. **f)** IHC staining of CK8 (yellow), pATR (blue)and NOTCH1 (red) in a DIP1 organoid. White square shows magnified area on right. Arrows show NOTCH1 foci, arrowheads show $pATR^{lo}$ area. **g)** Quantification of NOTCH1 mean fluorescence in $pATR^{lo}$ and $pATR^{hi}$ nuclear regions of CK8+ cells in DIP1 organoids, as detected by IHC. Data shown as the mean ± S.E.M; n=1 biological replicates; two-tailed unpaired Student's t-test. p-value: *<0.05, **<0.01, ****<0.0001

Discussion

Robo2 is dynamically expressed in all MG subpopulation during alveologenesis.

Our lab has previously characterized the expression of *Robo2* in the nulliparous MG, as well as identified a phenotype produced by the loss of *Robo2* in the nulliparous epithelium (Harburg et al., 2014; Strickland et al., 2006). The expression of *Robo2* during pregnancy and lactation, however, remained unclear. Additionally, compiled datasets of scRNA-seq reads from across development suggested there is little to no expression of *Robo2* throughout the lineage trajectories of the MG, and did not identify a subpopulation in which it is enriched (Figure 2.1a, b)(Saeki et al., 2021; Speir et al., 2021). Here, however, we show by RT-qPCR that *Robo2* is expressed in all MG subpopulations during pregnancy and early lactation, and that this expression is dynamic throughout these processes. This characterization of *Robo2* expression may provide valuable insights into the potential functions ROBO2 has in each subpopulation, as ROBO proteins are known to often function in a cell type-specific manner.

ROBO2 functions to inhibit alveolar endoreplication and differentiation.

While this study is still underway and currently incomplete, preliminary results suggest that ROBO2 functions from the luminal compartment to inhibit alveologenesis and milk production through the regulation of *Jag1* expression in the basal compartment. Moreover, we show that ROBO2 also functions to inhibit alveolar

endoreplication, a process deeply intertwined with alveolar differentiation (refer to Chapter 1). Lastly, the preliminary results of this study also suggest that the regulation of these processes by ROBO2 may occur through modulation of Notch signaling. ROBO1 was recently shown to promote alveolar differentiation from the basal compartment through the suppression of β-catenin-mediated *Jag1* expression (Cazares et al., 2021; H. Macias et al., 2011). Our data suggest that ROBO2 may create an opposing effect from the luminal compartment to promote basal cell *Jag1* expression and inhibit alveolar differentiation, potentially through direct interaction and inhibition of ROBO1 (Barak et al., 2019). Considering the previous observation that ROBO2 expressed on the surface of basal progenitor cells can inhibit the nuclear localization of β-catenin, these data provoke the question as to whether ROBO2 functions in a cell type-specific to regulate the fate of both basal and alveolar progenitor cells (Harburg et al., 2014). Furthermore, our data also bring to question whether ROBO2 inhibition of NOTCH activity also directly mediates the effect of ROBO2 on alveolar endoreplication, by reducing the level of nuclear NOTCH1 ICD and, in turn, inhibiting ATR activation. If so, this study could lead to the identification of a novel molecular mechanism by which NOTCH1 maintains the alveolar progenitor population: by inhibiting terminal differentiation through the suppression of DDR-induced endoreplication. The proposed functions of ROBO2 in inhibiting alveolar differentiation and endoreplication are consistent with the expression pattern of *Robo2* observed in luminal cells (Figure 2.1e). In this context, *Robo2* expression peaks during the hyperproliferation of early pregnancy, then is downregulated during late pregnancy to allow for differentiation and DDR-mediated endoreplication. *Robo2*

is then upregulated again during lactation to potentially preserve remaining alveolar progenitor cells for subsequent pregnancies and suppress the DDR to limit the risk of milk-producing polyploid alveolar cells undergoing apoptosis during lactation. It remains possible, however, that ROBO2 inhibits alveolar endoreplication by NOTCH-independent means. This could potentially occur in a similar manner to how ROBO2 promotes senescence of basal progenitors: by inhibiting β-catenin-mediated repression of $p16^{INK4A}$ expression, thus preventing re-initiation of the cell cycle through inhibition of Cyclin D-CDK4/6 complexes (Harburg et al., 2014).

Future Directions.

As previously stated, this study is still underway and currently incomplete. Many of the trends observed in the preliminary data must still be confirmed with additional biological replicates. At this point in time, we are troubleshooting several difficulties encountered with the IHC staining of mosaic organoids. To confirm that ROBO2 is functioning to inhibit alveolar differentiation and endoreplication from the luminal compartment, we have thus also obtained a *Robo2 conditional-KO* (cKO) mouse line and have crossed it with a CK8-CreER driver line. This cKO model will allow for the specific elimination of ROBO2 activity in luminal cells and at a certain time during MG development, thus allowing us to better interrogate the functions of ROBO2 during the processes of differentiation and endoreplication. Furthermore, the diverse functions of ROBO receptors are often determined by their homophilic interactions with other ROBO receptors, as well as their heterophilic interactions with SLIT ligands. Therefore, potential interactions between ROBO2 and other ROBO

receptors and/or SLIT ligands must be investigated to determine the molecular mechanisms by which ROBO2 regulates alveolar differentiation and endoreplication.

Experimental Procedures

Mouse strains

CD-1 mice were obtained from Charles Rivers. C57BL/6-Wee1<tm1.1 mrl> were generated by Taconic. Ck8-CreER/mTmG mice were generously provided by Dr. Diwakar R Pattabiraman. These animals were a cross of Tg(Krt8-cre/ERT2)17Blpn/J (JAX:017947) and B6.129(Cg)-*Gt(ROSA)26Sor*$^{tm4(ACTB-tdTomato,\ -EGFP)Luo}$/J (JAX: 007676). Genotyping was performed by extracting DNA from ear snips and performing an end-point PCR for the given transgene using the primers CreER: 5'-CAGATGGCGCGGCAACACC-3' and 5'-GCGCGGTCTGGCAGTAAAAAC-3'; mTmG: 5'-AGG GAG CTG CAG TGG AGT AG-3', 5'-TAG AGC TTG CGG AAC CCT TC-3' and 5'-CTT TAA GCC TGC CCA GAA GA-3'; *Wee1*: 5-GCTTCGGAACCTTCCTAATGC-3' and 5'-TGAAGTCTCACCCTGTCTCG-3. All animal procedures were both approved by and conducted in accordance with the guidelines set by the University of California, Santa Cruz (UCSC) Institutional Animal Care and Use Committee (IACUC).

Animal studies

Nulliparous analysis was performed using adult (10-12-week-old) female mice. For timed pregnancies and lactation analysis, CD-1 pregnant adult females were obtained from Charles Rivers. Embryos were examined at the time of mammary gland harvesting to confirm pregnancy state. For lactation analysis on the C57BL/6-Wee1<tm1.1 mrl> mice, adult females were checked for the presence of a vaginal

plug indicating that mating occurred. Plugged mice were considered to be PD0.5 on the day of the observed plug. All females used in this study were age matched.

Contralateral Intraductal Injections

Mice were anesthetized with isoflurane (VetOne, 501017) Prior to intraductal injections, hair was removed from around the nipples using Nair hair remover. Injections into the duct of the nipple were performed with 33G needles (Hamilton, 7803-05) and a volume of 40 μl per gland. Right inguinal, abdominal and thoracic glands were injected with doxorubicin (1.5 μg per gland, Cayman Chemical, 15007), nucleosides (40 μl per gland, Millipore-Sigma, ES-008-D) or Mk-1775 (50 μg per gland, Cayman Chemical, 21266), and left glands were injected with PBS or DMSO (Thermo Scientific, BP231) diluted in PBS.

Tamoxifen Injections

Tamoxifen (Sigma, T5648) was dissolved in corn oil (Sigma, C8267) at a concentration of 20 mg/ml. Mice were anesthetized with isoflurane (VetOne, 501017). Intraperitoneal injections of 75 mg/kg bodyweight were performed at PD17.5 and LD2 using insulin syringes (Fisher Scientific, 14-826-79).

Cell cultures

The HC11 cell line was obtained from American Type Culture Collection (ATCC) and routinely checked for mycoplasma (Mycoplasma PCR kit, ABM, G238).

Undifferentiated HC11 cells were cultured in growing medium (RPMI-1640; Thermo Fisher Scientific, 72400047), supplemented with 10% FBS, 5 μg/ml insulin (Millipore-Sigma, I6634), 10 ng/ml epidermal growth factor (EGF; Preprotech, AF-100-15) and 1× AntiAnti (Thermo Fisher Scientific, 15240112) at 37°C with 5% CO2. Cells were grown to confluency and maintained in growing medium for 2 days, until they became competent. Competent HC11 cells were primed for differentiation by culturing them in priming medium [RPMI-1640 supplemented with 5 μg/ml insulin, 1 μM dexamethasone (Millipore-Sigma, D4902-1G) and 1× Anti-Anti] for 24 h at 37°C with 5% CO2. To induce differentiation, primed HC11 cells were cultured in DIP Medium [RPMI-1640, supplemented with 10% FBS, 5 μg/ml insulin, 1 μM dexamethasone, 1× anti-anti and 3 μg/ml Prolactin (NHPP, oPRL-21)] at 37°C with 5% CO2.

For endoreplication studies, 80% confluent undifferentiated HC11 were treated with 30 μM blebbistatin (Millipore-Sigma, B0560), 5 μM Ro-3306 (Sigma Aldrich, SML0569), 100 nM doxorubicin (Cayman Chemical, 15007) or corresponding DMSO (Thermo Scientific, BP231) control. Drugs were maintained through the differentiation process and added with every change of media.

Undifferentiated HC11 were transfected with the Rc/CMV cyclin E plasmid (Addgene, #8963) for *CCNE1* overexpression. Briefly, 70% confluent HC11 were transfected using Lipofectamine 3000 kit (Thermo Fisher, L3000015) and OPTI-MEM (GIBCO, 11058021). 48 h after transfection, HC11 were selected using 50 μg/ml of geneticin (Thermo Fisher, 10131035). Geneticin was maintained during HC11 culture and differentiation for stable *CCNE1* expression.

BrdU incorporation analysis

Undifferentiated HC11 were treated with 10 μM BrdU (Abcam, ab142567) for 2 h at 37°C with 5% CO2. Cells were washed with 1X DPBS (GIBCO, 14190-250) and harvested using 0.05% Trypsin-EDTA (GIBCO, 25300-062). Cell suspension was washed with 1X DPBS and centrifuged at 1,000 rpm for 5 min at 4°C. Cell pellet was fixed in ice-cold 70% EtOH vortexing vigorously to avoid cell clumps. After fixation cells were washed with washing buffer [1X PBS (GIBCO, 14190136) containing 5% FBS] and centrifuged at 2,000 rpm for 5 min at 4°C. Cell pellet was treated with 500 μl of 2 M HCl for 20 min at room temperature. Cells were washed with 2 ml of 0.1 M sodium tetraborate (Sigma Aldrich, 221731) and centrifuged at 2,000 rpm for 5 min at 4°C. Cells were washed once more with 3 ml of 0.1M sodium tetraborate and one last time with 2 ml of washing buffer. Cells were incubated for 1 h at room temperature with anti-BrdU (Abcam, ab6326) or corresponding rat IgG (Thermo-Fisher, 10700) for isotype control. Cells were washed twice with 2 ml of washing buffer and incubated for 1 h at room temperature in darkness with FITC anti-Rat (Thermo Fisher, A24544). After incubation, cells were washed twice and resuspended in 500 μl of 1X PBS. Cells suspensions were filter through a 70 μm cell strainer (Falcon, 08-771-2) and analyzed using a BD LSRII cytometer. Populations were analyzed using FlowJo.

Western Blotting

Whole cell lysates were prepared using 1× NP40 lysis buffer (Thermo Fisher Scientific, FNN0021) supplemented with Pierce Protease and Phosphatase inhibitors (Thermo Fisher Scientific, A32959). Cells were washed with ice-cold PBS (GIBCO, 14190136) and lysed direct in buffer and kept at 4°C rocking at 70 rpm for 30 min. Lysed cells were collected and centrifuged at 12,000 rpm at 4°C for 15 min. Protein concentration was quantified using Qubit 4 fluorometer (Thermo Fisher, Q33238). Samples were resolved by SDS page and transferred to polyvinylidene difluoride (PVDF, Millipore-Sigma, IPVH00010) for 60 min at 250 mA. Immunoblots were blocked for 1 h at room temperature using either 5% non-fat milk or 5% BSA TBST. Primary antibodies [anti-GAPDH (SCBT, sc-365062), anti-Actin (SCBT, sc-47778), anti- Cyclin B1 (SCBT, sc-245), anti-Cyclin E1 (Millipore-Sigma, SAB4503516) and anti-CSN2 (ABclonal, A12749)] were incubated overnight at 4°C in a rocker. HRP-conjugated secondary antibodies (The Jackson Laboratory) were used for 1 h at room temperature. Immunoblots were developed using Clarity ECL (Bio-Rad), detected using a Bio-Rad ChemiDoc MP Image, and quantified using ImageJ.

Mammary gland single cell suspension

Mechanically dissociated inguinal, abdominal, and thoracic mammary fat pads were prepared into cell suspension for flow cytometry or fluorescence-activated cell sorting (FACS). The lymph node was removed from abdominal glands. Glands were chopped using a mechanical tissue chopper and digested for 1 h at 37°C in digestion media [RPM1 containing 1%FBS, collagenase IA (Sigma, C9891), hyaluronidase (Sigma, H3506) and DNase I (Worthington, LS002007)]. Tissue was washed with

washing buffer (1X PBS containing 2% FBS) and centrifuged at 1,000 rpm for 5 min at 4°C. Tissue was further digested using pre-warmed 0.25% Trypsin-EDTA (Thermo Fisher, 25200056), washed, and digested with 5mg/ml of pre-warmed dispase II (Roche, 4942078001). Red blood cells were lysed using Ammonium Chloride Solution (Stem Cell Technologies, 07850). Cells were washed, resuspended and filter through a 70 μm cell strainer (Falcon, 08-771-2) and processed for downstream applications.

Flow cytometry

For DNA content analysis of the mammary gland $CK8^+$ epithelial population, mammary gland cells suspension was obtained as described above. Cells were fixed in ice-cold 70% EtOH at a final concentration of 10^6 cells/ml. During fixation, cells were vigorously vortexed for 1 min to avoid the formation of cell aggregates. Cells were washed twice with washing buffer [1X PBS containing 5% FBS and 0.5% tween 20 (Fisher Chemical, BP337500)] and centrifuged at 2,000 rpm for 5 min at 4°C. Cell pellet was incubated for 1 h at room temperature with anti-CK8 (Developmental Studies Hybridoma Lab, TROMA-1), anti-GFP (Thermo Fisher, A01704) or corresponding rat (Thermo-Fisher, 10700) or rabbit (Thermo-Fisher, 10500C) IgG isotype controls. Cells were washed twice and incubated for 1h at room temperature in darkness with FITC anti-Rat (Thermo Fisher, A24544) or FITC anti-Rabbit (Thermo Fisher, A16030) and APC anti-Rat (Jackson ImmunoResearch, 712-136-153). Cells were washed twice and resuspended in propidium iodide solution [1X PBS containing 25 μg/ml of propidium iodide (Thermo Fisher, P3566) and 100 μg/ml

of RNase (Thermo Fisher, 12091021)]. For DNA content analysis on HC11, cells were washed with 1X DPBS (GIBCO, 14190-250) and harvested using 0.05% Trypsin-EDTA (GIBCO, 25300-062). Cell suspension was washed with 1X DPBS and centrifuged at 1,000 rpm for 5 min at 4°C. Cell pellet was fixed in ice-cold 70% EtOH and then vortexed vigorously to avoid cell aggregates. After fixation, cells were washed with washing buffer [1X PBS (GIBCO, 14190136) supplemented with 5% FBS] and centrifuged at 2,000 rpm for 5 min at 4°C. The pellet was resuspended in propidium iodide solution. Cell suspensions were filtered through a 70 μm cell strainer (Falcon, 08-771-2) and analyzed using a BD LSRII cytometer or a BD FACS Aria II Cell Sorter. Populations were analyzed using FlowJo.

Visualization of cells sorted based on DNA content.

Mammary gland $CK8^+$ epithelial cells or HC11 were sorted based on DNA content using BD FACS Aria II Cell Sorter. After sorting, cells were stained in suspension using Phalloidin-iFluor 488 Reagent (Abcam, ab176753) for 30 min at room temperature in darkness. Cells were spined down onto microscopy slides (Fisher, 12-550-15) using Cytospin 2 (Shandon, 599X52) at 500 rpm for 3 min. Cells were mounted using fluoromount-G (Southern Biotech, 0100-01) and visualized using Zeiss Axio Imager Microscope.

Immunofluorescence on HC11 cells

HC11 cells were fixed using ice-cold MeOH for 10 min. After washing with 1X PBS, cells were incubated for 1 h at room temperature with primary antibodies [anti-γH2AX

(SCBT, sc-517348), anti-pATR (Genetex, GTX128145), anti-PLIN2 (generously provided by Jim McManaman)] in a humid incubation chamber. After incubation, cells were washed three times using 1X PBS and incubated for 1h at room temperature in darkness using corresponding Alexa Fluor AffiniPure secondary antibodies (Jackson ImmunoResearch) and Phalloidin-iFluor 488 Reagent (Abcam, ab176753) when indicated. Cells were washed three times using 1X PBS and incubated with Hoechst 33342 (AnaSpec, AS-83218) for 10 min. Cells were mounted using fluoromount-G (Southern Biotech, 0100-01) and visualized using Zeiss Axio Imager Microscope. Integrated density of PLIN2, nuclear γH2AX and nuclear pATR was quantify using ImageJ.

Immunofluorescence of paraffin-embedded tissue

Mammary gland tissue was fixed in 10% neutral buffered formalin (EMD Millipore, MR0458682) at 4°C overnight. Fixation was quenched using 0.2% glycine (Fisher Scientific, BP381) in PBS, for 1h at room temperature. Tissue was dehydrated by incubating with 70% EtOH (Decon Labs, V1001) overnight, 95% EtOH for 1h, 100% EtOH for 1h (x3) and xylenes (Fisher Scientific, X3P) for 1h (x3). Dehydrated tissue was soaked in paraffin (VWR, 15159-409) overnight and embedded. Paraffin-embedded tissue was sectioned at a thickness of 5 μm and mounted on Superfrost Plus Microscope Slides (Fisher, 12-550-15). Sectioned tissue was hydrated by incubating with xylenes for 5 min (x3), 100% ethanol for 2 min (x2), 95% ethanol for 1 min, 70% ethanol for 1 min, 50% ethanol for 1 min, and diH2O for 5 min. Antigen retrieval was performed using antigen unmasking solution (VectorLabs, H3300-250)

in a conventional lab microwave. Sections were incubated with blocking buffer containing 10% donkey serum (Equitech-Bio, SD30), 1% BSA (VWR, 97061-422) and 0.3% triton (Millipore Sigma, X100) in PBS overnight at 4C. Incubation with primary antibodies [anti-CK8 (Developmental Studies Hybridoma Lab, TROMA-1) and anti-mouse milk proteins (Accurate Chemical and Scientific, YNRMTM)] was performed overnight at 4°C. Sections were washed with 0.3% triton in PBS for 30 min (x3) at room temperature. Incubation with secondary antibodies [(donkey anti-Rat 647 (Thermo-Invitrogen; A48272) and donkey anti-Rabbit 488 (Thermo-Invitrogen; A32790)] was performed for 2 h at room temperature. Sections were washed with 0.3% triton in PBS for 30 min (x3) at room temperature and mounted using flouromount-G (Southern Biotech, 0100-01). Image acquisition was performed using Zeiss Axio Imager Microscope. Macros were generated to quantify lumen milk integrated density per alveolus using Image J.

Immunofluorescence and optical clearing of cryosections

Mammary gland tissue was fixed in 10% neutral buffered formalin (EMD Millipore, MR0458682) at 4°C overnight. Fixation was quenched using 0.2% glycine (Fisher Scientific, BP381) in PBS, for 1h at room temperature. Tissue was incubated with 30% sucrose (Fisher Scientific, BP220-212) in PBS at 4°C for 48h and sectioned at a thickness of 100 μm. Sections were washed with PBS for 10min (x2) at room temperature. Sections were incubated with CUBIC-L(Tainaka et al., 2018) at 37C overnight, and washed with 0.3% triton in PBS for 30min (x3). Sections were incubated with blocking buffer containing 10% donkey serum (Equitech-Bio, SD30),

1% BSA (VWR, 97061-422) and 0.3% triton (Millipore Sigma, X100) in PBS overnight at 4°C. Incubation with primary antibodies [anti-γH2AX (Cell Signaling, 2577S), anti-pATR (Genetex, GTX128145), anti-CK8 (Developmental Studies Hybridoma Lab, TROMA-1)] was performed overnight at 4°C. Sections were washed with 0.3% triton in PBS for 1h (x3) at room temperature. Incubation with secondary antibodies [donkey anti-Rat 488 (Thermo-Invitrogen; A32795) and donkey anti-Rabbit 647 (Thermo-Invitrogen; A48269)], propidium iodide (Thermo Fisher, P3566) and RNase (Thermo Fisher, 12091021) was performed for 6h at room temperature. Sections were washed with 0.3% triton in PBS for 1 h (x3) at room temperature and mounted on poly-L-lysine (Sigma, P8920) coated chamber slides (Ibidi, 80827). Tissues sections were incubated with CUBIC-R(Tainaka et al., 2018) at room temperature until cleared (approximately 48h), and imaged using a ZEISS LSM 880 microscope with Airyscan. Integrated density of nuclear γH2AX and pATR was quantified using ImageJ.

3D DNA content *in situ*

Mammary gland tissue was fixed in 10% neutral buffered formalin (EMD Millipore, MR0458682) at 4°C overnight. Fixation was quenched using 0.2% glycine (Fisher Scientific, BP381) in PBS, for 1h at room temperature. Tissue was incubated with 30% sucrose (Fisher Scientific, BP220-212) in PBS at 4°C for 48h and sectioned at a thickness of 200 μm. Sections were washed with PBS for 10 min (x2) at room temperature. Sections were incubated with blocking buffer containing 10% donkey serum (Equitech-Bio, SD30), 1% BSA (VWR, 97061-422) and 0.3% triton (Millipore

Sigma, X100) in PBS overnight at 4°C. Incubation with primary antibody anti-E-cadherin (Thermo Fisher, 13-1900) was performed overnight at 4°C. Sections were washed with 0.3% triton in PBS for 1 h (x3) at room temperature. Incubation with secondary antibody donkey anti-Rat 488 (Thermo-Invitrogen; A32795), Phalloidin-647 (Invitrogen, A30107) and Hoechst 33342 (AnaSpec, AS-83218) was performed overnight at 4°C. Sections were washed with 0.3% triton in PBS for 1h (x3) at room temperature and mounted on poly-L-lysine (Sigma, P8920) coated chamber slides (Ibidi, 80827). Tissue sections were incubated 80% glycerol (Sigma, G9012) in H2O at room temperature for 72h, and imaged using a ZEISS LSM 880 microscope with Airyscan. Segmentation of nuclei and quantification of DNA integrated density in 3D was performed using Cell Profiler. Incomplete nuclei were excluded from analysis. Stromal cells were used as a reference for diploid (2C) DNA content.

RNA extraction and RT-qPCR

For RNA isolation from FACS purified populations, mammary gland cell suspensions were blocked using Mouse BD Fc Block™ (BD Biosciences) for 10 min. Cells were subsequently resuspended on 1X PBS at a density of 10^7 cells/ml and stained with the following antibodies for 30 min on ice: anti-CD24 PE (Stem Cell Technologies, 60099PE.1), anti-CD29 PE-Cy7 (BioLegend, 102222), anti-CD45-APC (BioLegend,105826), Ter119-APC (BD Biosciences, 561033), CD31-ACP (BD Biosciences, 551262). Propidium iodide at a final concentration of 0.5 μg/ml was used for the discrimination of dead cells. Stromal, basal and luminal mammary populations were sorted using a BD FACS Aria II Cell Sorter. Cells were

subsequently lysed in TRIzol reagent (ThermoFisher, 15596018) and phase separated according to the manufacturer's protocol with an additional overnight RNA precipitation step in ethanol (H. Macias et al., 2011). The RNA was further purified with TURBO DNase (Ambion, AM1906) treatment. For HC11 and whole-gland tissue RNA isolation the NucleoSpin RNA extraction kit (Macherey-Nagel, 740955.50) was utilized according to the manufacturer's instructions. Total RNA quality was analyzed by agarose gel electrophoresis and quantified using an ND-1000 spectrophotometer (NanoDrop). cDNA was prepared from 500-1000 ng of total RNA using iScript cDNA synthesis kit (Bio-Rad, 1708841). Quantitative RT-qPCR was performed in triplicates using SsoAdvanced Universal SYBR Green Supermix, (Bio-Rad, 1725272). The reactions were run in a Bio-Rad CFX'Connect Real-Time System and CFX Manager software (Bio-Rad) as follows: 95°C for 2 min followed by 40 cycles of 95°C for 15 s, 60°C for 30 s and 72°C for 45 s. Results were normalized to *Gapdh*. Primers used in this study are: *Csn2*: 5'- CCTCTGAGACTGATAGTATT-3' and 5'-TGGATGCTGGAGTGAACTTTA-3'; *Gapdh*: 5'- CATGGCCTTCCGTGTTCCTA-3' and 5'- CCTGCTTCACCACCTTCTTGAT-3'; *Cdkn1a:* 5'-ATCCAGACATTCAGAGCCACAG-3' and 5'-ACGAAGTCAAAGTTCCACCGT-3'; *Wee1*: 5'- TTGGCTGGCTCTGTTGATGA-3' and 5'-CAGCTAAACTCCCACCATTACAG-3'; *Cdkn1b*: 5'-AACGTGCGAGTGTCTAACGG-3' and 5'- CCCTCTAGGGGTTTGTGATTCT-3'; *Elf5*: 5'-TGACCCCCTGATGCCTTGGA-3' and 5'-TGGAGGCTTGTTCGGCTGTG-3'.

Contralateral Transplantation

Foxn1^{nu} athymic nude mice (JAX #002019) were cleared of their endogenous inguinal MG epithelium prior to 3 weeks of age via cauterization of the nipple. MG epithelium tissue fragments were harvested from *WT* and *Robo2 KO* nulliparous adult mice and contralaterally transplanted into the inguinal fat-pads of 3 week old athymic nude mice. Transplanted tissue was allowed to form outgrowths during pubertal development, and timed breeding of mice was performed after they reached 8 weeks of age.

3D Organoid Culture

MG tissue was harvested, chopped and placed in low-adhesion dishes with digestion media: DMEM/F12 (Thermo-Fisher 11039047) with 1X Anti-Anti, 4 mg/mL Class 3 Collagenase (Worthington Biochem. LS004206), 4 mg/mL Class 3 Dispase (Roche 4942078001), 50 mg/mL Geneticin (Thermo-Fisher 10131035) and 5% FBS. Chopped tissue was incubated in digestion media 16h at 37°C and 5% CO_2. Digested epithelial tissue fragments were washed with DPBS, pelleted at 600rcf for 10min, and the supernatant was aspirated; this was repeated 3-5 times or until no more red blood cells were visible on the top of the pellet. Fragments were then plated in a dish with maintenance media: DMEM/F12 with 1X Anti-Anti, 5 μg/mL insulin, 10 ng/mL EGF and 5% FBS. Fragments were incubated for 24-48hr at 37°C and 5% CO_2. Resulting 2D cell culture was washed with DPBS and incubated with 0.05% trypsin-EDTA. After 3-6min, detached basal epithelial cells were collected in a tube containing DPBS with 10% FBS. The dish was rinsed with DPBS and fresh 0.05% trypsin-EDTA was added again. After 7-15min, detached luminal epithelial

cells were collected in a tube containing DPBS with 10% FBS. Basal and luminal epithelial subpopulations were counted and pelleted, and the supernatant was aspirated. Basal epithelial cells were resuspended in 10% Matrigel (Corning CB40230C) at 250 cells/μL, and luminal epithelial cells were resuspended in 10% Matrigel at 750 cells/μL. Wells of a 24- or 48-well plate were coated with 50% Matrigel and incubated at 37°C for 30min until solidified. Cell resuspensions were then added to the wells in a 1:1 ratio and incubated at 37°C for 30min until solidified. 3D embedded cells were incubated with growth media: DMEM/F12 with 1X N-2 (Thermo-Fisher 17502048), 1X B27 (Thermo-Fisher 12587010), 100 ng/mL Nrg1 (R&D 5898-NR-050), 42.5 ng/mL R-spondin (PeproTech 120-38), 1nM Rho inhibitor Y-27632 (Tocris 1254) and 10 ng/mL EGF. Cells were incubated for 5 days at at 37°C and 5% CO_2, changing media every 2-3 days. The resulting organoids were then cultured for 1-5 days with alveologenesis media: DMEM/F12 with 1X N-2, 1X B27, 100 ng/mL Nrg1, 42.5 ng/mL R-spondin, 1nM Rho inhibitor Y-27632, 1 μg/mL prolactin, 5 μg/mL dexamethasone and 5 μg/mL insulin. After differentiation, the alveologenesis media was aspirated and the Matrigel was dissolved with Cell Recovery Solution (Fisher CB-40253). The organoids were then washed with DPBS and pelleted.

Immunofluorescence of organoids

Organoids were resuspended in 4% PFA and incubated on ice for 45min. Fixed organoids were washed with PBS, pelleted, and the supernatant was removed. The organoids were then resuspended in PBS with 0.2% glycine and incubated for 20min

at room temperature to quench fixation. Organoids were placed in a 24- or 48-well low-adhesion plate and incubated with blocking buffer containing 10% donkey serum (Equitech-Bio, SD30), 1% BSA (VWR, 97061-422) and 0.3% triton (Millipore Sigma, X100) in PBS overnight at 4C. Organoids were incubated with primary antibodies anti-CK8 (Developmental Studies Hybridoma Lab, TROMA-1), anti-pATR (Genetex, GTX128145) and anti-NOTCH1 (SCBT sc-373891) overnight at 4°C. Organoids were washed with 0.3% triton in PBS for 1hr (x3) at room temperature. Organoids were then incubated with secondary antibodies donkey anti-Rat 647 (Thermo-Invitrogen; A48272), donkey anti-Mouse 594 donkey (Thermo-Fisher A32744), anti-Rabbit 488 (Thermo-Invitrogen; A32790) and Hoechst overnight at 4°C. Organoids were washed with 0.3% triton in PBS for 1hr (x3), and transferred to a poly-L-lysine coated coverslip bottom chamber slide for imaging.

Statistical analyses

No statistical method was used to predetermine sample size. Statistical analysis was performed using Prism9 software. Sample size, biological replicates, statistical test, and statistical significance are denoted in the figure legends. For the statistical analysis of the experiments involving contralateral intraductal injections, paired statistical tests were performed.

Bibliography

Abukhdeir, A. M., & Park, B. H. (2008). p21 and p27: roles in carcinogenesis and drug resistance. *Expert Reviews in Molecular Medicine, 10*. doi:10.1017/s1462399408000744

Acosta, J. C., Banito, A., Wuestefeld, T., Georgilis, A., Janich, P., Morton, J. P., . . . Gil, J. (2013). A complex secretory program orchestrated by the inflammasome controls paracrine senescence. *Nature Cell Biology, 15*(8), 978-990. doi:10.1038/ncb2784

Adamowicz, M., d'Adda di Fagagna, F., & Vermezovic, J. (2018). NOTCH1 modulates activity of DNA-PKcs. *Mutat Res, 808*, 20-27. doi:10.1016/j.mrfmmm.2018.01.003

Adamowicz, M., Vermezovic, J., & Fagagna, D., D'Adda, Fabrizio. (2016). NOTCH1 Inhibits Activation of ATM by Impairing the Formation of an ATM-FOXO3a-KAT5/Tip60 Complex. *Cell Reports, 16*(8), 2068-2076. doi:10.1016/j.celrep.2016.07.038

Aleksandrova, N., Gutsche, I., Kandiah, E., Avilov, S. V., Petoukhov, M. V., Seiradake, E., & Mccarthy, A. A. (2018). Robo1 Forms a Compact Dimer-of-Dimers Assembly. *Structure, 26*(2), 320-328.e324. doi:10.1016/j.str.2017.12.003

Amani, J., Gorjizadeh, N., Younesi, S., Najafi, M., Ashrafi, A. M., Irian, S., & Azizian, K. (2021). Cyclin-dependent kinase inhibitors (CDKIs) and the DNA damage response: The link between signaling pathways and cancer. *DNA Repair (Amst), 102*, 103103. doi:10.1016/j.dnarep.2021.103103

Ansell, J. D., Barlow, P. W., & McLaren, A. (1974). Binucleate and polyploid cells in the decidua of the mouse. *J Embryol Exp Morphol, 31*(1), 223-227.

Ba-Charvet, K. T. N., Brose, K., Ma, L., Wang, K. H., Marillat, V., Sotelo, C., . . . Chédotal, A. (2001). Diversity and Specificity of Actions of Slit2 Proteolytic Fragments in Axon Guidance. *The Journal of Neuroscience, 21*(12), 4281-4289. doi:10.1523/jneurosci.21-12-04281.2001

Baker, D. J., Wijshake, T., Tchkonia, T., Lebrasseur, N. K., Childs, B. G., Van De Sluis, B., . . . Van Deursen, J. M. (2011). Clearance of p16Ink4a-positive senescent cells delays ageing-associated disorders. *Nature, 479*(7372), 232-236. doi:10.1038/nature10600

Ballard, M. S., & Hinck, L. (2012). A Roundabout Way to Cancer. In *Advances in Cancer Research* (pp. 187-235): Elsevier.

Ballard, S., Mimmi, Zhu, A., Iwai, N., Stensrud, M., Mapps, A., Postiglione, P., Maira, . . . Hinck, L. (2015). Mammary Stem Cell Self-Renewal Is Regulated by Slit2/Robo1 Signaling through SNAI1 and mINSC. *Cell Reports, 13*(2), 290-301. doi:10.1016/j.celrep.2015.09.006

Banerjee, M. R., & Wagner, J. E. (1972). Gene amplification in mammary gland at differentiation. *Biochem Biophys Res Commun, 49*(2), 480-487. doi:10.1016/0006-291x(72)90436-6

Banerjee, M. R., Wagner, J. E., & Kinder, D. L. (1971). DNA synthesis in the absence of cell reproduction during functional differentiation of mouse mammary gland. *Life Sci II, 10*(15), 867-877.

Barak, R., Lahmi, R., Gevorkyan-Airapetov, L., Levy, E., Tzur, A., & Opatowsky, Y. (2014). Crystal structure of the extracellular juxtamembrane region of Robo1. *J Struct Biol, 186*(2), 283-291. doi:10.1016/j.jsb.2014.02.019

Barak, R., Yom-Tov, G., Guez-Haddad, J., Gasri-Plotnitsky, L., Maimon, R., Cohen-Berkman, M., . . . Opatowsky, Y. (2019). Structural Principles in Robo Activation and Auto-inhibition. *Cell, 177*(2), 272-285.e216. doi:10.1016/j.cell.2019.02.004

Barnum, K. J., & O'Connell, M. J. (2014). Cell Cycle Regulation by Checkpoints. In *Methods in Molecular Biology* (pp. 29-40): Springer New York.

Besson, A., Dowdy, S. F., & Roberts, J. M. (2008). CDK Inhibitors: Cell Cycle Regulators and Beyond. *Developmental Cell, 14*(2), 159-169. doi:10.1016/j.devcel.2008.01.013

Besson, A., Gurian-West, M., Chen, X., Kelly-Spratt, K. S., Kemp, C. J., & Roberts, J. M. (2006). A pathway in quiescent cells that controls p27^{Kip1} stability, subcellular localization, and tumor suppression. *Genes & Development, 20*(1), 47-64. doi:10.1101/gad.1384406

Bester, A. C., Roniger, M., Oren, Y. S., Im, M. M., Sarni, D., Chaoat, M., . . . Kerem, B. (2011). Nucleotide deficiency promotes genomic instability in early stages of cancer development. *Cell, 145*(3), 435-446. doi:10.1016/j.cell.2011.03.044

Bisiak, F., & Mccarthy, A. A. (2019). Structure and Function of Roundabout Receptors. In *Subcellular Biochemistry* (pp. 291-319): Springer International Publishing.

Biswas, S. K., Banerjee, S., Baker, G. W., Kuo, C.-Y., & Chowdhury, I. (2022). The Mammary Gland: Basic Structure and Molecular Signaling during Development. *International Journal of Molecular Sciences, 23*(7), 3883. doi:10.3390/ijms23073883

Biteau, B., & Jasper, H. (2014). Slit/Robo signaling regulates cell fate decisions in the intestinal stem cell lineage of Drosophila. *Cell Rep, 7*(6), 1867-1875. doi:10.1016/j.celrep.2014.05.024

Blockus, H., & Chédotal, A. (2016). Slit-Robo signaling. *Development, 143*(17), 3037-3044. doi:10.1242/dev.132829

Borrell, V., Cárdenas, A., Ciceri, G., Galcerán, J., Flames, N., Pla, R., . . . Marín, O. (2012). Slit/Robo Signaling Modulates the Proliferation of Central Nervous System Progenitors. *Neuron, 76*(2), 338-352. doi:10.1016/j.neuron.2012.08.003

Bouras, T., Pal, B., Vaillant, F., Harburg, G., Asselin-Labat, M.-L., Oakes, S. R., . . . Visvader, J. E. (2008). Notch Signaling Regulates Mammary Stem Cell Function and Luminal Cell-Fate Commitment. *Cell Stem Cell, 3*(4), 429-441. doi:10.1016/j.stem.2008.08.001

Brose, K., Bland, K. S., Wang, K. H., Arnott, D., Henzel, W., Goodman, C. S., . . . Kidd, T. (1999). Slit proteins bind Robo receptors and have an evolutionarily conserved role in repulsive axon guidance. *Cell, 96*(6), 795-806. doi:10.1016/s0092-8674(00)80590-5

Bruce, A., Alexander, J., Julian, L., David, M., Martin, R., Keith, R., & Peter, W. (2015). Molecular Biology of the Cell. In (6th ed. ed.). New York: Garland Science.

Buono, K. D., Robinson, G. W., Martin, C., Shi, S., Stanley, P., Tanigaki, K., . . . Hennighausen, L. (2006). The canonical Notch/RBP-J signaling pathway controls the balance of cell lineages in mammary epithelium during pregnancy. *Dev Biol, 293*(2), 565-580. doi:10.1016/j.ydbio.2006.02.043

Burrows, A. E., & Elledge, S. J. (2008). How ATR turns on: TopBP1 goes on ATRIP with ATR: Figure 1. *Genes & Development, 22*(11), 1416-1421. doi:10.1101/gad.1685108

Buttitta, L. A., & Edgar, B. A. (2007). Mechanisms controlling cell cycle exit upon terminal differentiation. *Current Opinion in Cell Biology, 19*(6), 697-704. doi:10.1016/j.ceb.2007.10.004

Byun, T. S., Pacek, M., Yee, M.-C., Walter, J. C., & Cimprich, K. A. (2005). Functional uncoupling of MCM helicase and DNA polymerase activities activates the ATR-dependent checkpoint. *Genes & Development, 19*(9), 1040-1052. doi:10.1101/gad.1301205

Cao, L., Chen, F., Yang, X., Xu, W., Xie, J., & Yu, L. (2014). Phylogenetic analysis of CDK and cyclin proteins in premetazoan lineages. *BMC Evolutionary Biology, 14*(1), 10. doi:10.1186/1471-2148-14-10

Cazares, O., Chatterjee, S., Lee, P., Strietzel, C., Bubolz, J. W., Harburg, G., . . . Hinck, L. (2021). Alveolar progenitor differentiation and lactation depends on paracrine inhibition of Notch via ROBO1/CTNNB1/JAG1. *Development, 148*(21). doi:10.1242/dev.199940

Centonze, A., Lin, S., Tika, E., Sifrim, A., Fioramonti, M., Malfait, M., . . . Blanpain, C. (2020). Heterotypic cell–cell communication regulates glandular stem cell multipotency. *Nature, 584*(7822), 608-613. doi:10.1038/s41586-020-2632-y

Chakrabarti, R., Wei, Y., Romano, R.-A., Decoste, C., Kang, Y., & Sinha, S. (2012). Elf5 Regulates Mammary Gland Stem/Progenitor Cell Fate by Influencing Notch Signaling. *Stem Cells, 30*(7), 1496-1508. doi:10.1002/stem.1112

Chen, T., & Dent, S. Y. R. (2014). Chromatin modifiers and remodellers: regulators of cellular differentiation. *Nature Reviews Genetics, 15*(2), 93-106. doi:10.1038/nrg3607

Chevalier, C., Nafati, M., Mathieu-Rivet, E., Bourdon, M., Frangne, N., Cheniclet, C., . . . Hernould, M. (2011). Elucidating the functional role of endoreduplication in tomato fruit development. *Ann Bot, 107*(7), 1159-1169. doi:10.1093/aob/mcq257

Chowdhury, R., Sinha, B., Sankar, M. J., Taneja, S., Bhandari, N., Rollins, N., . . . Martines, J. (2015). Breastfeeding and maternal health outcomes: a systematic review and meta-analysis. *Acta Paediatrica, 104*(467), 96-113. doi:10.1111/apa.13102

Chédotal, A. Slits and Their Receptors. In *Advances in Experimental Medicine and Biology* (pp. 65-80): Springer New York.

Ciccia, A., & Elledge, S. J. (2010). The DNA Damage Response: Making It Safe to Play with Knives. *Molecular Cell, 40*(2), 179-204. doi:10.1016/j.molcel.2010.09.019

Clay, D. E., & Fox, D. T. (2021). DNA Damage Responses during the Cell Cycle: Insights from Model Organisms and Beyond. *Genes, 12*(12), 1882. doi:10.3390/genes12121882

Coleman, H. A., Labrador, J.-P., Chance, R. K., & Bashaw, G. J. (2010). The Adam family metalloprotease Kuzbanian regulates the cleavage of the roundabout receptor to control axon repulsion at the midline. *Development, 137*(14), 2417-2426. doi:10.1242/dev.047993

Coppé, J.-P., Patil, C. K., Rodier, F., Sun, Y., Muñoz, D. P., Goldstein, J., . . . Campisi, J. (2008). Senescence-Associated Secretory Phenotypes Reveal Cell-Nonautonomous Functions of Oncogenic RAS and the p53 Tumor Suppressor. *PLoS Biology, 6*(12), e301. doi:10.1371/journal.pbio.0060301

Cordero, A., Pellegrini, P., Sanz-Moreno, A., Trinidad, E. M., Serra-Musach, J., Deshpande, C., . . . González-Suárez, E. (2016). Rankl Impairs Lactogenic Differentiation Through Inhibition of the Prolactin/Stat5 Pathway at Midgestation. *Stem Cells, 34*(4), 1027-1039. doi:10.1002/stem.2271

Coverley, D., Pelizon, C., Trewick, S., & Laskey, R. A. (2000). Chromatin-bound Cdc6 persists in S and G2 phases in human cells, while soluble Cdc6 is destroyed in a cyclin A-cdk2 dependent process. *Journal of Cell Science, 113*(11), 1929-1938. doi:10.1242/jcs.113.11.1929

Cánepa, E. T., Scassa, M. E., Ceruti, J. M., Marazita, M. C., Carcagno, A. L., Sirkin, P. F., & Ogara, M. F. (2007). INK4 proteins, a family of mammalian CDK inhibitors with novel biological functions. *IUBMB Life, 59*(7), 419-426. doi:10.1080/15216540701488358

De La Serna, I. L., Ohkawa, Y., & Imbalzano, A. N. (2006). Chromatin remodelling in mammalian differentiation: lessons from ATP-dependent remodellers. *Nature Reviews Genetics, 7*(6), 461-473. doi:10.1038/nrg1882

de Pedro, I., Alonso-Lecue, P., Sanz-Gómez, N., Freije, A., & Gandarillas, A. (2018). Sublethal UV irradiation induces squamous differentiation via a p53-independent, DNA damage-mitosis checkpoint. *Cell Death Dis, 9*(11), 1094. doi:10.1038/s41419-018-1130-8

Delloye-Bourgeois, C., Jacquier, A., Charoy, C., Reynaud, F., Nawabi, H., Thoinet, K., . . . Castellani, V. (2015). PlexinA1 is a new Slit receptor and mediates axon guidance function of Slit C-terminal fragments. *Nature Neuroscience, 18*(1), 36-45. doi:10.1038/nn.3893

Dickson, B. J., & Gilestro, G. F. (2006). Regulation of Commissural Axon Pathfinding by Slit and its Robo Receptors. *Annual Review of Cell and Developmental Biology, 22*(1), 651-675. doi:10.1146/annurev.cellbio.21.090704.151234

Ding, L., Cao, J., Lin, W., Chen, H., Xiong, X., Ao, H., . . . Cui, Q. (2020). The Roles of Cyclin-Dependent Kinases in Cell-Cycle Progression and Therapeutic Strategies in Human Breast Cancer. *International Journal of Molecular Sciences, 21*(6), 1960. doi:10.3390/ijms21061960

Diril, M. K., Ratnacaram, C. K., Padmakumar, V. C., Du, T., Wasser, M., Coppola, V., . . . Kaldis, P. (2012). Cyclin-dependent kinase 1 (Cdk1) is essential for cell division and suppression of DNA re-replication but not for liver regeneration. *Proc Natl Acad Sci U S A, 109*(10), 3826-3831. doi:10.1073/pnas.1115201109

Do, K., Doroshow, J. H., & Kummar, S. (2013). Wee1 kinase as a target for cancer therapy. *Cell Cycle, 12*(19), 3348-3353. doi:10.4161/cc.26062

Domyan, E. T., Branchfield, K., Gibson, D. A., Naiche, L. A., Lewandoski, M., Tessier-Lavigne, M., . . . Sun, X. (2013). Roundabout receptors are critical for foregut separation from the body wall. *Dev Cell, 24*(1), 52-63. doi:10.1016/j.devcel.2012.11.018

Dontu, G., Jackson, K. W., Mcnicholas, E., Kawamura, M. J., Abdallah, W. M., & Wicha, M. S. (2004). Role of Notch signaling in cell-fate determination of human mammary stem/progenitor cells. *Breast Cancer Research, 6*(6). doi:10.1186/bcr920

Dunaway, C. M., Hwang, Y., Lindsley, C. W., Cook, R. S., Wu, J. Y., Boothby, M., . . . Brantley-Sieders, D. M. (2011). Cooperative Signaling between Slit2 and Ephrin-A1 Regulates a Balance between Angiogenesis and Angiostasis. *Molecular and Cellular Biology, 31*(3), 404-416. doi:10.1128/mcb.00667-10

el-Deiry, W. S., Tokino, T., Velculescu, V. E., Levy, D. B., Parsons, R., Trent, J. M., . . . Vogelstein, B. (1993). WAF1, a potential mediator of p53 tumor suppression. *Cell, 75*(4), 817-825. doi:10.1016/0092-8674(93)90500-p

Elbæk, C. R., Petrosius, V., & Sørensen, C. S. (2020). WEE1 kinase limits CDK activities to safeguard DNA replication and mitotic entry. *Mutat Res, 819-820*, 111694. doi:10.1016/j.mrfmmm.2020.111694

Enomoto, S., Mitsui, K., Kawamura, T., Iwanari, H., Daigo, K., Horiuchi, K., . . . Hamakubo, T. (2016). Suppression of Slit2/Robo1 mediated HUVEC migration by Robo4. *Biochem Biophys Res Commun, 469*(4), 797-802. doi:10.1016/j.bbrc.2015.12.075

Evans, T. A., & Bashaw, G. J. (2010). Functional Diversity of Robo Receptor Immunoglobulin Domains Promotes Distinct Axon Guidance Decisions. *Current Biology, 20*(6), 567-572. doi:10.1016/j.cub.2010.02.021

Evans, T. A., Santiago, C., Arbeille, E., & Bashaw, G. J. (2015). Robo2 acts in trans to inhibit Slit-Robo1 repulsion in pre-crossing commissural axons. *eLife, 4*. doi:10.7554/elife.08407

Fagundes, R., & Teixeira, L. K. (2021). Cyclin E/CDK2: DNA Replication, Replication Stress and Genomic Instability. *Front Cell Dev Biol, 9*, 774845. doi:10.3389/fcell.2021.774845

Fernandez-Capetillo, O., Lee, A., Nussenzweig, M., & Nussenzweig, A. (2004). H2AX: the histone guardian of the genome. *DNA Repair (Amst), 3*(8-9), 959-967. doi:10.1016/j.dnarep.2004.03.024

Fischer, M., & Müller, G. A. (2017). Cell cycle transcription control: DREAM/MuvB and RB-E2F complexes. *Critical Reviews in Biochemistry and Molecular Biology, 52*(6), 638-662. doi:10.1080/10409238.2017.1360836

Freije, A., Ceballos, L., Coisy, M., Barnes, L., Rosa, M., De Diego, E., . . . Gandarillas, A. (2012). Cyclin E drives human keratinocyte growth into differentiation. *Oncogene, 31*(50), 5180-5192. doi:10.1038/onc.2012.22

Freije, A., Molinuevo, R., Ceballos, L., Cagigas, M., Alonso-Lecue, P., Rodriguez, R., . . . Gandarillas, A. (2014). Inactivation of p53 in Human Keratinocytes Leads to Squamous Differentiation and Shedding via Replication Stress and Mitotic Slippage. *Cell Rep, 9*(4), 1349-1360. doi:10.1016/j.celrep.2014.10.012

Fujimitsu, K., Grimaldi, M., & Yamano, H. (2016). Cyclin-dependent kinase 1–dependent activation of APC/C ubiquitin ligase. *Science, 352*(6289), 1121-1124. doi:10.1126/science.aad3925

Fujiwara, T., Bandi, M., Nitta, M., Ivanova, E. V., Bronson, R. T., & Pellman, D. (2005). Cytokinesis failure generating tetraploids promotes tumorigenesis in p53-null cells. *Nature, 437*(7061), 1043-1047. doi:10.1038/nature04217

Fukuhara, N., Howitt, J. A., Hussain, S. A., & Hohenester, E. (2008). Structural and functional analysis of slit and heparin binding to immunoglobulin-like domains 1 and 2 of Drosophila Robo. *J Biol Chem, 283*(23), 16226-16234. doi:10.1074/jbc.M800688200

Gallahan, D., & Callahan, R. (1987). Mammary tumorigenesis in feral mice: identification of a new int locus in mouse mammary tumor virus (Czech II)-induced mammary tumors. *Journal of Virology, 61*(1), 66-74. doi:10.1128/jvi.61.1.66-74.1987

Gallahan, D., & Callahan, R. (1997). The mouse mammary tumor associated gene INT3 is a unique member of the NOTCH gene family (NOTCH4). *Oncogene, 14*(16), 1883-1890. doi:10.1038/sj.onc.1201035

Gallahan, D., Jhappan, C., Robinson, G., Hennighausen, L., Sharp, R., Kordon, E., . . . Smith, G. H. (1996). Expression of a truncated Int3 gene in developing secretory mammary epithelium specifically retards lobular differentiation resulting in tumorigenesis. *Cancer Res, 56*(8), 1775-1785.

Gandarillas, A., Davies, D., & Blanchard, J.-M. (2000). Normal and c-Myc-promoted human keratinocyte differentiation both occur via a novel cell cycle involving cellular growth and endoreplication. *Oncogene, 19*(29), 3278-3289. doi:10.1038/sj.onc.1203630

Gara, R. K., Kumari, S., Ganju, A., Yallapu, M. M., Jaggi, M., & Chauhan, S. C. (2015). Slit/Robo pathway: a promising therapeutic target for cancer. *Drug Discovery Today, 20*(1), 156-164. doi:10.1016/j.drudis.2014.09.008

Gardino, A. K., & Yaffe, M. B. (2011). 14-3-3 proteins as signaling integration points for cell cycle control and apoptosis. *Semin Cell Dev Biol, 22*(7), 688-695. doi:10.1016/j.semcdb.2011.09.008

Gardner, R. L., & Davies, T. J. (1993). Lack of coupling between onset of giant transformation and genome endoreduplication in the mural trophectoderm of the mouse blastocyst. *J Exp Zool, 265*(1), 54-60. doi:10.1002/jez.1402650108

Gartel, A. L., & Tyner, A. L. (1999). Transcriptional regulation of the p21((WAF1/CIP1)) gene. *Exp Cell Res, 246*(2), 280-289. doi:10.1006/excr.1998.4319

Glücksmann, A. (1951). CELL DEATHS IN NORMAL VERTEBRATE ONTOGENY. *Biological Reviews, 26*(1), 59-86. doi:10.1111/j.1469-185x.1951.tb00774.x

Gong, D., & Ferrell, J. E. (2010). The Roles of Cyclin A2, B1, and B2 in Early and Late Mitotic Events. *Molecular Biology of the Cell, 21*(18), 3149-3161. doi:10.1091/mbc.e10-05-0393

Gonzalez, N., Gevaudant, F., Hernould, M., Chevalier, C., & Mouras, A. (2007). The cell cycle-associated protein kinase WEE1 regulates cell size in relation to endoreduplication in developing tomato fruit. *Plant Journal, 51*(4), 642-655. doi:10.1111/j.1365-313X.2007.03167.x

González-Rosa, J. M., Sharpe, M., Field, D., Soonpaa, M. H., Field, L. J., Burns, C. E., & Burns, C. G. (2018). Myocardial Polyploidization Creates a Barrier to Heart Regeneration in Zebrafish. *Dev Cell, 44*(4), 433-446.e437. doi:10.1016/j.devcel.2018.01.021

Gordon, W. R., Arnett, K. L., & Blacklow, S. C. (2008). The molecular logic of Notch signaling – a structural and biochemical perspective. *Journal of Cell Science, 121*(19), 3109-3119. doi:10.1242/jcs.035683

Grieshammer, U., Ma, L., Plump, A. S., Wang, F., Tessier-Lavigne, M., & Martin, G. R. (2004). SLIT2-Mediated ROBO2 Signaling Restricts Kidney Induction to a Single Site. *Developmental Cell, 6*(5), 709-717. doi:10.1016/s1534-5807(04)00108-x

Halliwell, J. A., Frith, T. J. R., Laing, O., Price, C. J., Bower, O. J., Stavish, D., . . . Andrews, P. W. (2020). Nucleosides Rescue Replication-Mediated Genome Instability of Human Pluripotent Stem Cells. *Stem Cell Reports, 14*(6), 1009-1017. doi:10.1016/j.stemcr.2020.04.004

Harburg, G., Compton, J., Liu, W., Iwai, N., Zada, S., Marlow, R., . . . Hinck, L. (2014). SLIT/ROBO2 signaling promotes mammary stem cell senescence by inhibiting Wnt signaling. *Stem Cell Reports, 3*(3), 385-393. doi:10.1016/j.stemcr.2014.07.007

Harris, J., Stanford, P. M., Sutherland, K., Oakes, S. R., Naylor, M. J., Robertson, F. G., . . . Ormandy, C. J. (2006). Socs2 and Elf5 Mediate Prolactin-Induced Mammary Gland Development. *Molecular Endocrinology, 20*(5), 1177-1187. doi:10.1210/me.2005-0473

Hemberger, M., Hanna, C. W., & Dean, W. (2020). Mechanisms of early placental development in mouse and humans. *Nat Rev Genet, 21*(1), 27-43. doi:10.1038/s41576-019-0169-4

Herrtwich, L., Nanda, I., Evangelou, K., Nikolova, T., Horn, V., Sagar, . . . Triantafyllopoulou, A. (2016). DNA Damage Signaling Instructs Polyploid Macrophage Fate in Granulomas. *Cell, 167*(5), 1264-1280.e1218. doi:10.1016/j.cell.2016.09.054

Hivert, B., Liu, Z., Chuang, C. Y., Doherty, P., & Sundaresan, V. (2002). Robo1 and Robo2 are homophilic binding molecules that promote axonal growth. *Mol Cell Neurosci, 21*(4), 534-545. doi:10.1006/mcne.2002.1193

Ho, T. L. F., Guilbaud, G., Blow, J. J., Sale, J. E., & Watson, C. J. (2016). The KRAB Zinc Finger Protein Roma/Zfp157 Is a Critical Regulator of Cell-Cycle Progression and Genomic Stability. *Cell Rep, 15*(4), 724-734. doi:10.1016/j.celrep.2016.03.078

Howard, L. J., Reichert, M. C., & Evans, T. A. (2021). The Slit-binding Ig1 domain is required for multiple axon guidance activities of Drosophila Robo2. *genesis, 59*(9). doi:10.1002/dvg.23443

Howitt, J. A., Clout, N. J., & Hohenester, E. (2004). Binding site for Robo receptors revealed by dissection of the leucine-rich repeat region of Slit. *The EMBO Journal, 23*(22), 4406-4412. doi:10.1038/sj.emboj.7600446

Hu, C., Diévart, A., Lupien, M., Calvo, E., Tremblay, G., & Jolicoeur, P. (2006). Overexpression of Activated Murine Notch1 and Notch3 in Transgenic Mice Blocks Mammary Gland Development and Induces Mammary Tumors. *The American Journal of Pathology, 168*(3), 973-990. doi:10.2353/ajpath.2006.050416

Hussain, S.-A., Piper, M., Fukuhara, N., Strochlic, L., Cho, G., Howitt, J. A., . . . Hohenester, E. (2006). A Molecular Mechanism for the Heparan Sulfate Dependence of Slit-Robo Signaling. *Journal of Biological Chemistry, 281*(51), 39693-39698. doi:10.1074/jbc.m609384200

Hégarat, N., Crncec, A., Suarez Peredo Rodriguez, M. F., Echegaray Iturra, F., Gu, Y., Busby, O., . . . Hochegger, H. (2020). Cyclin A triggers Mitosis either via the Greatwall kinase pathway or Cyclin B. *The EMBO Journal, 39*(11). doi:10.15252/embj.2020104419

Inomata, K., Aoto, T., Binh, N. T., Okamoto, N., Tanimura, S., Wakayama, T., . . . Nishimura, E. K. (2009). Genotoxic Stress Abrogates Renewal of Melanocyte Stem Cells by Triggering Their Differentiation. *Cell, 137*(6), 1088-1099. doi:10.1016/j.cell.2009.03.037

Jacobsen, M. D., Weil, M., & Raff, M. C. (1996). Role of Ced-3/ICE-family proteases in staurosporine-induced programmed cell death. *Journal of Cell Biology, 133*(5), 1041-1051. doi:10.1083/jcb.133.5.1041

Jeffrey, P. D., Tong, L., & Pavletich, N. P. (2000). Structural basis of inhibition of CDK–cyclin complexes by INK4 inhibitors. *Genes & Development, 14*(24), 3115-3125. doi:10.1101/gad.851100

Jhappan, C., Gallahan, D., Stahle, C., Chu, E., Smith, G. H., Merlino, G., & Callahan, R. (1992). Expression of an activated Notch-related int-3 transgene interferes with cell differentiation and induces neoplastic transformation in mammary and salivary glands. *Genes & Development, 6*(3), 345-355. doi:10.1101/gad.6.3.345

Jiang, Z., Liang, G., Xiao, Y., Qin, T., Chen, X., Wu, E., . . . Wang, Z. (2019). Targeting the SLIT/ROBO pathway in tumor progression: molecular mechanisms and therapeutic perspectives. *Therapeutic Advances in Medical Oncology, 11*, 175883591985523. doi:10.1177/1758835919855238

Joaquin, A., & Fernandez-Capetillo, O. (2012). Signalling DNA Damage. In *Protein Phosphorylation in Human Health*: InTech.

Jones, R. M., Mortusewicz, O., Afzal, I., Lorvellec, M., Garcia, P., Helleday, T., & Petermann, E. (2013). Increased replication initiation and conflicts with transcription underlie Cyclin E-induced replication stress. *Oncogene, 32*(32), 3744-3753. doi:10.1038/onc.2012.387

Kerr, J. F. R., Wyllie, A. H., & Currie, A. R. (1972). Apoptosis: A Basic Biological Phenomenon with Wideranging Implications in Tissue Kinetics. *British Journal of Cancer, 26*(4), 239-257. doi:10.1038/bjc.1972.33

Kiaris, H., Politi, K., Grimm, L. M., Szabolcs, M., Fisher, P., Efstratiadis, A., & Artavanis-Tsakonas, S. (2004). Modulation of Notch Signaling Elicits Signature Tumors and Inhibits Hras1-Induced Oncogenesis in the Mouse

Mammary Epithelium. *The American Journal of Pathology, 165*(2), 695-705. doi:10.1016/s0002-9440(10)63333-0

Kidd, T., Bland, K. S., & Goodman, C. S. (1999). Slit is the midline repellent for the robo receptor in Drosophila. *Cell, 96*(6), 785-794. doi:10.1016/s0092-8674(00)80589-9

Kidd, T., Brose, K., Mitchell, K. J., Fetter, R. D., Tessier-Lavigne, M., Goodman, C. S., & Tear, G. (1998). Roundabout Controls Axon Crossing of the CNS Midline and Defines a Novel Subfamily of Evolutionarily Conserved Guidance Receptors. *Cell, 92*(2), 205-215. doi:10.1016/s0092-8674(00)80915-0

Kirk, D., & Clingan, D. A. (1980). Normal human endometrium in cell culture. III. Mechanism(s) of epithelial polyploidization. *Cell Biol Int Rep, 4*(1), 83-92. doi:10.1016/0309-1651(80)90013-2

Klein, E. A., & Assoian, R. K. (2008). Transcriptional regulation of the cyclin D1 gene at a glance. *Journal of Cell Science, 121*(23), 3853-3857. doi:10.1242/jcs.039131

Kopan, R. (2012). Notch Signaling. *Cold Spring Harbor Perspectives in Biology, 4*(10), a011213-a011213. doi:10.1101/cshperspect.a011213

Krebs, L. T., Xue, Y., Norton, C. R., Shutter, J. R., Maguire, M., Sundberg, J. P., . . . Gridley, T. (2000). Notch signaling is essential for vascular morphogenesis in mice. *Genes & Development, 14*(11), 1343-1352. doi:10.1101/gad.14.11.1343

Kreuzaler, P. A., Staniszewska, A. D., Li, W., Omidvar, N., Kedjouar, B., Turkson, J., . . . Watson, C. J. (2011). Stat3 controls lysosomal-mediated cell death in vivo. *Nature Cell Biology, 13*(3), 303-309. doi:10.1038/ncb2171

Krtolica, A., Parrinello, S., Lockett, S., Desprez, P.-Y., & Campisi, J. (2001). Senescent fibroblasts promote epithelial cell growth and tumorigenesis: A link between cancer and aging. *Proceedings of the National Academy of Sciences, 98*(21), 12072-12077. doi:10.1073/pnas.211053698

Laberge, R.-M., Awad, P., Campisi, J., & Desprez, P.-Y. (2012). Epithelial-Mesenchymal Transition Induced by Senescent Fibroblasts. *Cancer Microenvironment, 5*(1), 39-44. doi:10.1007/s12307-011-0069-4

Lafkas, D., Rodilla, V., Huyghe, M., Mourao, L., Kiaris, H., & Fre, S. (2013). Notch3 marks clonogenic mammary luminal progenitor cells in vivo. *Journal of Cell Biology, 203*(1), 47-56. doi:10.1083/jcb.201307046

Lazzeri, E., Angelotti, M. L., Peired, A., Conte, C., Marschner, J. A., Maggi, L., . . . Romagnani, P. (2018). Endocycle-related tubular cell hypertrophy and progenitor proliferation recover renal function after acute kidney injury. *Nat Commun, 9*(1), 1344. doi:10.1038/s41467-018-03753-4

Lee, H. J., Gallego-Ortega, D., Ledger, A., Schramek, D., Joshi, P., Szwarc, M. M., . . . Ormandy, C. J. (2013). Progesterone drives mammary secretory differentiation via RankL-mediated induction of Elf5 in luminal progenitor cells. *Development, 140*(7), 1397-1401. doi:10.1242/dev.088948

Lee, M. H., Reynisdóttir, I., & Massagué, J. (1995). Cloning of p57KIP2, a cyclin-dependent kinase inhibitor with unique domain structure and tissue distribution. *Genes & Development, 9*(6), 639-649. doi:10.1101/gad.9.6.639

Leone, M., Musa, G., & Engel, F. B. (2018). Cardiomyocyte binucleation is associated with aberrant mitotic microtubule distribution, mislocalization of RhoA and IQGAP3, as well as defective actomyosin ring anchorage and cleavage furrow ingression. *Cardiovascular Research, 114*(8), 1115-1131. doi:10.1093/cvr/cvy056

Li, M., & Zhang, P. (2009). The function of APC/CCdh1 in cell cycle and beyond. *Cell Division, 4*(1), 2. doi:10.1186/1747-1028-4-2

Li, S., Huang, L., Sun, Y., Bai, Y., Yang, F., Yu, W., . . . Li, X. (2015). Slit2 Promotes Angiogenic Activity Via the Robo1-VEGFR2-ERK1/2 Pathway in Both In Vivo and In Vitro Studies. *Investigative Opthalmology & Visual Science, 56*(9), 5210. doi:10.1167/iovs-14-16184

Li, T., Zhou, Z. W., Ju, Z., & Wang, Z. Q. (2016). DNA Damage Response in Hematopoietic Stem Cell Ageing. *Genomics Proteomics Bioinformatics, 14*(3), 147-154. doi:10.1016/j.gpb.2016.04.002

Lilja, A. M., Rodilla, V., Huyghe, M., Hannezo, E., Landragin, C., Renaud, O., . . . Fre, S. (2018). Clonal analysis of Notch1-expressing cells reveals the existence of unipotent stem cells that retain long-term plasticity in the embryonic mammary gland. *Nature Cell Biology, 20*(6), 677-687. doi:10.1038/s41556-018-0108-1

Limas, J. C., & Cook, J. G. (2019). Preparation for DNA replication: the key to a successful S phase. *FEBS Letters, 593*(20), 2853-2867. doi:10.1002/1873-3468.13619

Liu, D., & Hornsby, P. J. (2007). Senescent Human Fibroblasts Increase the Early Growth of Xenograft Tumors via Matrix Metalloproteinase Secretion. *Cancer Research, 67*(7), 3117-3126. doi:10.1158/0008-5472.can-06-3452

Liu, Z., Patel, K., Schmidt, H., Andrews, W., Pini, A., & Sundaresan, V. (2004). Extracellular Ig domains 1 and 2 of Robo are important for ligand (Slit) binding. *Mol Cell Neurosci, 26*(2), 232-240. doi:10.1016/j.mcn.2004.01.002

MacAuley, A., Cross, J. C., & Werb, Z. (1998). Reprogramming the cell cycle for endoreduplication in rodent trophoblast cells. *Mol Biol Cell, 9*(4), 795-807. doi:10.1091/mbc.9.4.795

Macias, D., Ganan, Y., Sampath, T. K., Piedra, M. E., Ros, M. A., & Hurle, J. M. (1997). Role of BMP-2 and OP-1 (BMP-7) in programmed cell death and skeletogenesis during chick limb development. *Development, 124*(6), 1109-1117. doi:10.1242/dev.124.6.1109

Macias, H., & Hinck, L. (2012). Mammary gland development. *Wiley Interdiscip Rev Dev Biol, 1*(4), 533-557. doi:10.1002/wdev.35

Macias, H., Moran, A., Samara, Y., Moreno, M., Compton, J. E., Harburg, G., . . . Hinck, L. (2011). SLIT/ROBO1 signaling suppresses mammary branching morphogenesis by limiting basal cell number. *Dev Cell, 20*(6), 827-840. doi:10.1016/j.devcel.2011.05.012

Marechal, A., & Zou, L. (2013). DNA Damage Sensing by the ATM and ATR Kinases. *Cold Spring Harbor Perspectives in Biology, 5*(9), a012716-a012716. doi:10.1101/cshperspect.a012716

Margall-Ducos, G., Celton-Morizur, S. V., Couton, D., BréGerie, O., & Desdouets, C. (2007). Liver tetraploidization is controlled by a new process of incomplete cytokinesis. *Journal of Cell Science, 120*(20), 3633-3639. doi:10.1242/jcs.016907

Marlow, R., Binnewies, M., Sorensen, L. K., Monica, S. D., Strickland, P., Forsberg, E. C., . . . Hinck, L. (2010). Vascular Robo4 restricts proangiogenic VEGF signaling in breast. *Proceedings of the National Academy of Sciences, 107*(23), 10520-10525. doi:10.1073/pnas.1001896107

Matsuoka, S., Edwards, M. C., Bai, C., Parker, S., Zhang, P., Baldini, A., . . . Elledge, S. J. (1995). p57KIP2, a structurally distinct member of the p21CIP1 Cdk inhibitor family, is a candidate tumor suppressor gene. *Genes & Development, 9*(6), 650-662. doi:10.1101/gad.9.6.650

Miermont, A., Antolović, V., Lenn, T., Nichols, J. M. E., Millward, L. J., & Chubb, J. R. (2019). The fate of cells undergoing spontaneous DNA damage during development. *Development, 146*(12). doi:10.1242/dev.174268

Mijit, M., Caracciolo, V., Melillo, A., Amicarelli, F., & Giordano, A. (2020). Role of p53 in the Regulation of Cellular Senescence. *Biomolecules, 10*(3), 420. doi:10.3390/biom10030420

Milona, A., Owen, B. M., van Mil, S., Dormann, D., Mataki, C., Boudjelal, M., . . . Williamson, C. (2010). The normal mechanisms of pregnancy-induced liver growth are not maintained in mice lacking the bile acid sensor Fxr. *Am J Physiol Gastrointest Liver Physiol, 298*(2), G151-158. doi:10.1152/ajpgi.00336.2009

Minamino, T., Orimo, M., Shimizu, I., Kunieda, T., Yokoyama, M., Ito, T., . . . Komuro, I. (2009). A crucial role for adipose tissue p53 in the regulation of insulin resistance. *Nature Medicine, 15*(9), 1082-1087. doi:10.1038/nm.2014

Miyaoka, Y., Ebato, K., Kato, H., Arakawa, S., Shimizu, S., & Miyajima, A. (2012). Hypertrophy and unconventional cell division of hepatocytes underlie liver regeneration. *Curr Biol, 22*(13), 1166-1175. doi:10.1016/j.cub.2012.05.016

Molinuevo, R., Freije, A., Contreras, L., Sanz, J. R., & Gandarillas, A. (2020). The DNA damage response links human squamous proliferation with differentiation. *Journal of Cell Biology, 219*(11). doi:10.1083/jcb.202001063

Molinuevo, R., Freije, A., de Pedro, I., Stoll, S. W., Elder, J. T., & Gandarillas, A. (2017). FOXM1 allows human keratinocytes to bypass the oncogene-induced differentiation checkpoint in response to gain of MYC or loss of p53. *Oncogene, 36*(7), 956-965. doi:10.1038/onc.2016.262

Mommersteeg, M. T., Andrews, W. D., Ypsilanti, A. R., Zelina, P., Yeh, M. L., Norden, J., . . . Parnavelas, J. G. (2013). Slit-roundabout signaling regulates the development of the cardiac systemic venous return and pericardium. *Circ Res, 112*(3), 465-475. doi:10.1161/CIRCRESAHA.112.277426

Monier, B., Gettings, M., Gay, G., Mangeat, T., Schott, S., Guarner, A., & Suzanne, M. (2015). Apico-basal forces exerted by apoptotic cells drive epithelium folding. *Nature, 518*(7538), 245-248. doi:10.1038/nature14152

Morlot, C., Thielens, N. M., Ravelli, R. B. G., Hemrika, W., Romijn, R. A., Gros, P., . . . Mccarthy, A. A. (2007). Structural insights into the Slit-Robo complex. *Proceedings of the National Academy of Sciences, 104*(38), 14923-14928. doi:10.1073/pnas.0705310104

Muñoz-Espín, D., Cañamero, M., Maraver, A., Gómez-López, G., Contreras, J., Murillo-Cuesta, S., . . . Serrano, M. (2013). Programmed Cell Senescence during Mammalian Embryonic Development. *Cell, 155*(5), 1104-1118. doi:10.1016/j.cell.2013.10.019

Nakano, K., & Vousden, K. H. (2001). PUMA, a novel proapoptotic gene, is induced by p53. *Mol Cell, 7*(3), 683-694. doi:10.1016/s1097-2765(01)00214-3

Nakao, J., Shinoda, J., Nakai, Y., Murase, S.-I., & Uyemura, K. (2002). Apoptosis Regulates the Number of Schwann Cells at the Premyelinating Stage. *Journal of Neurochemistry, 68*(5), 1853-1862. doi:10.1046/j.1471-4159.1997.68051853.x

Nakayama, K. I., Hatakeyama, S., & Nakayama, K. (2001). Regulation of the cell cycle at the G1-S transition by proteolysis of cyclin E and p27Kip1. *Biochem Biophys Res Commun, 282*(4), 853-860. doi:10.1006/bbrc.2001.4627

Nam, E. A., Zhao, R., Glick, G. G., Bansbach, C. E., Friedman, D. B., & Cortez, D. (2011). Thr-1989 phosphorylation is a marker of active ataxia telangiectasia-mutated and Rad3-related (ATR) kinase. *J Biol Chem, 286*(33), 28707-28714. doi:10.1074/jbc.M111.248914

Narita, M., Nuñez, S., Heard, E., Narita, M., Lin, A. W., Hearn, S. A., . . . Lowe, S. W. (2003). Rb-Mediated Heterochromatin Formation and Silencing of E2F Target Genes during Cellular Senescence. *Cell, 113*(6), 703-716. doi:10.1016/s0092-8674(03)00401-x

Nieminen, T., Toivanen, P. I., Laakkonen, J. P., Heikura, T., Kaikkonen, M. U., Airenne, K. J., & Ylä-Herttuala, S. (2015). Slit2 modifies VEGF-induced angiogenic responses in rabbit skeletal muscle via reduced eNOS activity. *Cardiovasc Res, 107*(2), 267-276. doi:10.1093/cvr/cvv161

Oakes, S. R., Naylor, M. J., Asselin-Labat, M.-L., Blazek, K. D., Gardiner-Garden, M., Hilton, H. N., . . . Ormandy, C. J. (2008). The Ets transcription factor Elf5 specifies mammary alveolar cell fate. *Genes & Development, 22*(5), 581-586. doi:10.1101/gad.1614608

Ordan, E., & Volk, T. (2015). A non-signaling role of Robo2 in tendons is essential for Slit processing and muscle patterning. *Development, 142*(20), 3512-3518. doi:10.1242/dev.128157

Pampfer, S., & Donnay, I. (1999). Apoptosis at the time of embryo implantation in mouse and rat. *Cell Death & Differentiation, 6*(6), 533-545. doi:10.1038/sj.cdd.4400516

Parrilla-Castellar, E. R., Arlander, S. J., & Karnitz, L. (2004). Dial 9-1-1 for DNA damage: the Rad9-Hus1-Rad1 (9-1-1) clamp complex. *DNA Repair (Amst), 3*(8-9), 1009-1014. doi:10.1016/j.dnarep.2004.03.032

Petersen, B. O. (1999). Phosphorylation of mammalian CDC6 by Cyclin A/CDK2 regulates its subcellular localization. *The EMBO Journal, 18*(2), 396-410. doi:10.1093/emboj/18.2.396

Planas-Silva, M. D., & Weinberg, R. A. (1997). Estrogen-dependent cyclin E-cdk2 activation through p21 redistribution. *Molecular and Cellular Biology, 17*(7), 4059-4069. doi:10.1128/mcb.17.7.4059

Raafat, A., Goldhar, A. S., Klauzinska, M., Xu, K., Amirjazil, I., Mccurdy, D., . . . Callahan, R. (2011). Expression of Notch receptors, ligands, and target genes during development of the mouse mammary gland. *Journal of Cellular Physiology, 226*(7), 1940-1952. doi:10.1002/jcp.22526

Rama, N., Dubrac, A., Mathivet, T., Ní Chárthaigh, R.-A., Genet, G., Cristofaro, B., . . . Chédotal, A. (2015). Slit2 signaling through Robo1 and Robo2 is required for retinal neovascularization. *Nature Medicine, 21*(5), 483-491. doi:10.1038/nm.3849

Raouf, A., Zhao, Y., To, K., Stingl, J., Delaney, A., Barbara, M., . . . Eaves, C. (2008). Transcriptome Analysis of the Normal Human Mammary Cell Commitment and Differentiation Process. *Cell Stem Cell, 3*(1), 109-118. doi:10.1016/j.stem.2008.05.018

Reboutier, D., Benaud, C., & Prigent, C. (2015). Aurora A's Functions During Mitotic Exit: The Guess Who Game. *Front Oncol, 5*, 290. doi:10.3389/fonc.2015.00290

Richert, M. M., Schwertfeger, K. L., Ryder, J. W., & Anderson, S. M. (2000). An atlas of mouse mammary gland development. *J Mammary Gland Biol Neoplasia, 5*(2), 227-241. doi:10.1023/a:1026499523505

Rios, A. C., Fu, N. Y., Jamieson, P. R., Pal, B., Whitehead, L., Nicholas, K. R., . . . Visvader, J. E. (2016). Essential role for a novel population of binucleated mammary epithelial cells in lactation. *Nat Commun, 7*, 11400. doi:10.1038/ncomms11400

Rodilla, V., Dasti, A., Huyghe, M., Lafkas, D., Laurent, C., Reyal, F., & Fre, S. (2015). Luminal Progenitors Restrict Their Lineage Potential during Mammary Gland Development. *PLOS Biology, 13*(2), e1002069. doi:10.1371/journal.pbio.1002069

Ronco, C., Martin, A. R., Demange, L., & Benhida, R. (2017). ATM, ATR, CHK1, CHK2 and WEE1 inhibitors in cancer and cancer stem cells. *MedChemComm, 8*(2), 295-319. doi:10.1039/c6md00439c

SACHS, L., & SHELESNYAK, M. C. (1955). The development and suppression of polyploidy in the developing and suppressed deciduoma in the rat. *J Endocrinol, 12*(2), 146-151. doi:10.1677/joe.0.0120146

Saeki, K., Chang, G., Kanaya, N., Wu, X., Wang, J., Bernal, L., . . . Chen, S. (2021). Mammary cell gene expression atlas links epithelial cell remodeling events to breast carcinogenesis. *Communications Biology, 4*(1). doi:10.1038/s42003-021-02201-2

Saldivar, J. C., Cortez, D., & Cimprich, K. A. (2017). The essential kinase ATR: ensuring faithful duplication of a challenging genome. *Nature Reviews Molecular Cell Biology, 18*(10), 622-636. doi:10.1038/nrm.2017.67

Sanidas, I., Morris, R., Fella, K. A., Rumde, P. H., Boukhali, M., Tai, E. C., . . . Dyson, N. J. (2019). A Code of Mono-phosphorylation Modulates the Function of RB. *Mol Cell, 73*(5), 985-1000.e1006. doi:10.1016/j.molcel.2019.01.004

Santoro, A., Vlachou, T., Carminati, M., Pelicci, P. G., & Mapelli, M. (2016). Molecular mechanisms of asymmetric divisions in mammary stem cells. *EMBO reports, 17*(12), 1700-1720. doi:10.15252/embr.201643021

Santos, M. A., Faryabi, R. B., Ergen, A. V., Day, A. M., Malhowski, A., Canela, A., . . . Nussenzweig, A. (2014). DNA-damage-induced differentiation of leukaemic cells as an anti-cancer barrier. *Nature, 514*(7520), 107-111. doi:10.1038/nature13483

Sanz-Gómez, N., Freije, A., Ceballos, L., Obeso, S., Sanz, J. R., García-Reija, F., . . . Gandarillas, A. (2018). Response of head and neck epithelial cells to a DNA damage-differentiation checkpoint involving polyploidization. *Head Neck, 40*(11), 2487-2497. doi:10.1002/hed.25376

Schade, A. E., Oser, M. G., Nicholson, H. E., & Decaprio, J. A. (2019). Cyclin D–CDK4 relieves cooperative repression of proliferation and cell cycle gene expression by DREAM and RB. *Oncogene, 38*(25), 4962-4976. doi:10.1038/s41388-019-0767-9

Schneider, L., Pellegatta, S., Favaro, R., Pisati, F., Roncaglia, P., Testa, G., . . . d'Adda di Fagagna, F. (2013). DNA damage in mammalian neural stem cells

leads to astrocytic differentiation mediated by BMP2 signaling through JAK-STAT. *Stem Cell Reports, 1*(2), 123-138. doi:10.1016/j.stemcr.2013.06.004

Schulze, A., Zerfass, K., Spitkovsky, D., Middendorp, S., Bergès, J., Helin, K., . . . Henglein, B. (1995). Cell cycle regulation of the cyclin A gene promoter is mediated by a variant E2F site. *Proceedings of the National Academy of Sciences, 92*(24), 11264-11268. doi:10.1073/pnas.92.24.11264

Seiradake, E., Von Philipsborn, A. C., Henry, M., Fritz, M., Lortat-Jacob, H., Jamin, M., . . . Mccarthy, A. A. (2009). Structure and functional relevance of the Slit2 homodimerization domain. *EMBO reports, 10*(7), 736-741. doi:10.1038/embor.2009.95

Seki, M., Watanabe, A., Enomoto, S., Kawamura, T., Ito, H., Kodama, T., . . . Aburatani, H. (2010). Human ROBO1 is cleaved by metalloproteinases and γ-secretase and migrates to the nucleus in cancer cells. *FEBS Letters, 584*(13), 2909-2915. doi:10.1016/j.febslet.2010.05.009

Senyo, S. E., Steinhauser, M. L., Pizzimenti, C. L., Yang, V. K., Cai, L., Wang, M., . . . Lee, R. T. (2013). Mammalian heart renewal by pre-existing cardiomyocytes. *Nature, 493*(7432), 433-436. doi:10.1038/nature11682

Sewell, C. A., Chang, C. Y., Chehab, M. M., & Nguyen, C. P. (2017). Domperidone for Lactation: What Health Care Providers Need to Know. *Obstetrics and Gynecology, 129*(6), 1054-1058. doi:10.1097/aog.0000000000002033

Sheldon, H., Andre, M., Legg, J. A., Heal, P., Herbert, J. M., Sainson, R., . . . Bicknell, R. (2009). Active involvement of Robo1 and Robo4 in filopodia formation and endothelial cell motility mediated via WASP and other actin nucleation-promoting factors. *The FASEB Journal, 23*(2), 513-522. doi:10.1096/fj.07-098269

Sherr, C. J., & Roberts, J. M. (1999). CDK inhibitors: positive and negative regulators of G1-phase progression. *Genes & Development, 13*(12), 1501-1512. doi:10.1101/gad.13.12.1501

Shibue, T., Suzuki, S., Okamoto, H., Yoshida, H., Ohba, Y., Takaoka, A., & Taniguchi, T. (2006). Differential contribution of Puma and Noxa in dual

regulation of p53-mediated apoptotic pathways. *The EMBO Journal, 25*(20), 4952-4962. doi:10.1038/sj.emboj.7601359

Simpson, J. H., Kidd, T., Bland, K. S., & Goodman, C. S. (2000). Short-Range and Long-Range Guidance by Slit and Its Robo Receptors. *Neuron, 28*(3), 753-766. doi:10.1016/s0896-6273(00)00151-3

Smith, G. H., Gallahan, D., Diella, F., Jhappan, C., Merlino, G., & Callahan, R. (1995). Constitutive expression of a truncated INT3 gene in mouse mammary epithelium impairs differentiation and functional development. *Cell Growth Differ, 6*(5), 563-577.

Smith, G. H., & Vonderhaar, B. K. (1981). Functional differentiation in mouse mammary gland epithelium is attained through DNA synthesis, inconsequent of mitosis. *Dev Biol, 88*(1), 167-179.

Smith, H. L., Southgate, H., Tweddle, D. A., & Curtin, N. J. (2020). DNA damage checkpoint kinases in cancer. *Expert Rev Mol Med, 22*, e2. doi:10.1017/erm.2020.3

Smith-Berdan, S., Nguyen, A., Hassanein, D., Zimmer, M., Ugarte, F., Ciriza, J., . . . Forsberg, E. C. (2011). Robo4 Cooperates with Cxcr4 to Specify Hematopoietic Stem Cell Localization to Bone Marrow Niches. *Cell Stem Cell, 8*(1), 72-83. doi:10.1016/j.stem.2010.11.030

Sone, H., & Kagawa, Y. (2005). Pancreatic beta cell senescence contributes to the pathogenesis of type 2 diabetes in high-fat diet-induced diabetic mice. *Diabetologia, 48*(1), 58-67. doi:10.1007/s00125-004-1605-2

Sornapudi, T. R., Nayak, R., Guthikonda, P. K., Pasupulati, A. K., Kethavath, S., Uppada, V., . . . Kurukuti, S. (2018). Comprehensive profiling of transcriptional networks specific for lactogenic differentiation of HC11 mammary epithelial stem-like cells. *Sci Rep, 8*(1), 11777. doi:10.1038/s41598-018-30122-4

Speidel, D. (2015). The role of DNA damage responses in p53 biology. *Archives of Toxicology, 89*(4), 501-517. doi:10.1007/s00204-015-1459-z

Speir, M. L., Bhaduri, A., Markov, N. S., Moreno, P., Nowakowski, T. J., Papatheodorou, I., . . . Haeussler, M. (2021). UCSC Cell Browser: visualize your single-cell data. *Bioinformatics, 37*(23), 4578-4580. doi:10.1093/bioinformatics/btab503

Storer, M., Mas, A., Robert-Moreno, A., Pecoraro, M., Ortells, C., M., Giacomo, D., Valeria, . . . Keyes, M., William. (2013). Senescence Is a Developmental Mechanism that Contributes to Embryonic Growth and Patterning. *Cell, 155*(5), 1119-1130. doi:10.1016/j.cell.2013.10.041

Straight, A. F., Cheung, A., Limouze, J., Chen, I., Westwood, N. J., Sellers, J. R., & Mitchison, T. J. (2003). Dissecting temporal and spatial control of cytokinesis with a myosin II Inhibitor. *Science, 299*(5613), 1743-1747. doi:10.1126/science.1081412

Strickland, P., Shin, G. C., Plump, A., Tessier-Lavigne, M., & Hinck, L. (2006). Slit2 and netrin 1 act synergistically as adhesive cues to generate tubular bi-layers during ductal morphogenesis. *Development, 133*(5), 823-832. doi:10.1242/dev.02261

Sun, Y., Dilkes, B. P., Zhang, C., Dante, R. A., Carneiro, N. P., Lowe, K. S., . . . Larkins, B. A. (1999). Characterization of maize (Zea mays L.) Wee1 and its activity in developing endosperm. *Proc Natl Acad Sci U S A, 96*(7), 4180-4185. doi:10.1073/pnas.96.7.4180

Tainaka, K., Murakami, T. C., Susaki, E. A., Shimizu, C., Saito, R., Takahashi, K., . . . Ueda, H. R. (2018). Chemical Landscape for Tissue Clearing Based on Hydrophilic Reagents. *Cell Rep, 24*(8), 2196-2210.e2199. doi:10.1016/j.celrep.2018.07.056

Tan, J., Raja, S., Davis, M. K., Tawfik, O., Dey, S. K., & Das, S. K. (2002). Evidence for coordinated interaction of cyclin D3 with p21 and cdk6 in directing the development of uterine stromal cell decidualization and polyploidy during implantation. *Mech Dev, 111*(1-2), 99-113. doi:10.1016/s0925-4773(01)00614-1

Tanaka, S., & Araki, H. (2010). Regulation of the initiation step of DNA replication by cyclin-dependent kinases. *Chromosoma, 119*(6), 565-574. doi:10.1007/s00412-010-0291-8

Tear, G., Seeger, M., & Goodman, C. S. (1993). To cross or not to cross: a genetic analysis of guidance at the midline. *Perspect Dev Neurobiol, 1*(4), 183-194.

Tong, M., Jun, T., Nie, Y., Hao, J., & Fan, D. (2019). The Role of the Slit/Robo Signaling Pathway. *Journal of Cancer, 10*(12), 2694-2705. doi:10.7150/jca.31877

Topacio, B. R., Zatulovskiy, E., Cristea, S., Xie, S., Tambo, C. S., Rubin, S. M., . . . Skotheim, J. M. (2019). Cyclin D-Cdk4,6 Drives Cell-Cycle Progression via the Retinoblastoma Protein's C-Terminal Helix. *Molecular Cell, 74*(4), 758-770.e754. doi:10.1016/j.molcel.2019.03.020

Técher, H., Koundrioukoff, S., Nicolas, A., & Debatisse, M. (2017). The impact of replication stress on replication dynamics and DNA damage in vertebrate cells. *Nature Reviews Genetics, 18*(9), 535-550. doi:10.1038/nrg.2017.46

Ullah, Z., Kohn, M. J., Yagi, R., Vassilev, L. T., & Depamphilis, M. L. (2008). Differentiation of trophoblast stem cells into giant cells is triggered by p57/Kip2 inhibition of CDK1 activity. *Genes & Development, 22*(21), 3024-3036. doi:10.1101/gad.1718108

Ullah, Z., Lee, C. Y., & Depamphilis, M. L. (2009). Cip/Kip cyclin-dependent protein kinase inhibitors and the road to polyploidy. *Cell Div, 4*, 10. doi:10.1186/1747-1028-4-10

Ullah, Z., Lee, C. Y., Lilly, M. A., & DePamphilis, M. L. (2009). Developmentally programmed endoreduplication in animals. *Cell Cycle, 8*(10), 1501-1509. doi:10.4161/cc.8.10.8325

Uyttendaele, H., Soriano, J. V., Montesano, R., & Kitajewski, J. (1998). Notch4 and Wnt-1 proteins function to regulate branching morphogenesis of mammary epithelial cells in an opposing fashion. *Dev Biol, 196*(2), 204-217. doi:10.1006/dbio.1998.8863

Van Keymeulen, A., Fioramonti, M., Centonze, A., Bouvencourt, G., Achouri, Y., & Blanpain, C. (2017). Lineage-Restricted Mammary Stem Cells Sustain the Development, Homeostasis, and Regeneration of the Estrogen Receptor Positive Lineage. *Cell Reports, 20*(7), 1525-1532. doi:10.1016/j.celrep.2017.07.066

Van Keymeulen, A., Rocha, A. S., Ousset, M., Beck, B., Bouvencourt, G., Rock, J., . . . Blanpain, C. (2011). Distinct stem cells contribute to mammary gland development and maintenance. *Nature, 479*(7372), 189-193. doi:10.1038/nature10573

Vassilopoulos, A., Tominaga, Y., Kim, H.-S., Lahusen, T., Li, B., Yu, H., . . . Deng, C.-X. (2015). WEE1 murine deficiency induces hyper-activation of APC/C and results in genomic instability and carcinogenesis. *Oncogene, 34*(23), 3023-3035. doi:10.1038/onc.2014.239

Vermezovic, J., Adamowicz, M., Santarpia, L., Rustighi, A., Forcato, M., Lucano, C., . . . D'Adda Di Fagagna, F. (2015). Notch is a direct negative regulator of the DNA-damage response. *Nature Structural & Molecular Biology, 22*(5), 417-424. doi:10.1038/nsmb.3013

Victora, C. G., Bahl, R., Barros, A. J., França, G. V., Horton, S., Krasevec, J., . . . Group, L. B. S. (2016). Breastfeeding in the 21st century: epidemiology, mechanisms, and lifelong effect. *Lancet, 387*(10017), 475-490. doi:10.1016/S0140-6736(15)01024-7

Vigneron, S., Sundermann, L., Labbé, J.-C., Pintard, L., Radulescu, O., Castro, A., & Lorca, T. (2018). Cyclin A-cdk1-Dependent Phosphorylation of Bora Is the Triggering Factor Promoting Mitotic Entry. *Developmental Cell, 45*(5), 637-650.e637. doi:10.1016/j.devcel.2018.05.005

Wang, J., Sun, Q., Morita, Y., Jiang, H., Groß, A., Lechel, A., . . . Rudolph, K. L. (2014). A Differentiation Checkpoint Limits Hematopoietic Stem Cell Self-Renewal in Response to DNA Damage. *Cell, 158*(6), 1444. doi:10.1016/j.cell.2014.08.033

Ward, I. M., & Chen, J. (2001). Histone H2AX Is Phosphorylated in an ATR-dependent Manner in Response to Replicational Stress. *Journal of Biological Chemistry, 276*(51), 47759-47762. doi:10.1074/jbc.c100569200

Watson, C. J. (2022). Alveolar cells in the mammary gland: lineage commitment and cell death. *Biochem J, 479*(9), 995-1006. doi:10.1042/BCJ20210734

Welcker, M., Singer, J., Loeb, K. R., Grim, J., Bloecher, A., Gurien-West, M., . . . Roberts, J. M. (2003). Multisite Phosphorylation by Cdk2 and GSK3 Controls

Cyclin E Degradation. *Molecular Cell, 12*(2), 381-392. doi:10.1016/s1097-2765(03)00287-9

Woo, R. A., & Poon, R. Y. (2003). Cyclin-dependent kinases and S phase control in mammalian cells. *Cell Cycle, 2*(4), 316-324.

Wood, D. J., & Endicott, J. A. (2018). Structural insights into the functional diversity of the CDK–cyclin family. *Open Biology, 8*(9), 180112. doi:10.1098/rsob.180112

Wright, M., Kevin, Lyon, A., Krissy, Leung, H., Leahy, J., Daniel, Ma, L., & Ginty, D., David. (2012). Dystroglycan Organizes Axon Guidance Cue Localization and Axonal Pathfinding. *Neuron, 76*(5), 931-944. doi:10.1016/j.neuron.2012.10.009

Wuidart, A., Ousset, M., Rulands, S., Simons, B. D., Van Keymeulen, A., & Blanpain, C. (2016). Quantitative lineage tracing strategies to resolve multipotency in tissue-specific stem cells. *Genes & Development, 30*(11), 1261-1277. doi:10.1101/gad.280057.116

Xu, X., Chen, E., Mo, L., Zhang, L., Shao, F., Miao, K., . . . Deng, C. X. (2019). BRCA1 represses DNA replication initiation through antagonizing estrogen signaling and maintains genome stability in parallel with WEE1-MCM2 signaling during pregnancy. *Hum Mol Genet, 28*(5), 842-857. doi:10.1093/hmg/ddy398

Yalcin-Ozuysal, Ö., Fiche, M., Guitierrez, M., Wagner, K.-U., Raffoul, W., & Brisken, C. (2010). Antagonistic roles of Notch and p63 in controlling mammary epithelial cell fates. *Cell Death & Differentiation, 17*(10), 1600-1612. doi:10.1038/cdd.2010.37

Yan, Y., Frisén, J., Lee, M. H., Massagué, J., & Barbacid, M. (1997). Ablation of the CDK inhibitor p57Kip2 results in increased apoptosis and delayed differentiation during mouse development. *Genes & Development, 11*(8), 973-983. doi:10.1101/gad.11.8.973

Yom-Tov, G., Barak, R., Matalon, O., Barda-Saad, M., Guez-Haddad, J., & Opatowsky, Y. (2017). Robo Ig4 Is a Dimerization Domain. *Journal of Molecular Biology, 429*(23), 3606-3616. doi:10.1016/j.jmb.2017.10.002

Zabihi, M., Lotfi, R., Yousefi, A.-M., & Bashash, D. (2022). Cyclins and cyclin-dependent kinases: from biology to tumorigenesis and therapeutic opportunities. *Journal of Cancer Research and Clinical Oncology*. doi:10.1007/s00432-022-04135-6

Zack, T. I., Schumacher, S. E., Carter, S. L., Cherniack, A. D., Saksena, G., Tabak, B., . . . Beroukhim, R. (2013). Pan-cancer patterns of somatic copy number alteration. *Nature Genetics, 45*(10), 1134-1140. doi:10.1038/ng.2760

Zakrys, L., Ward, J., Richard, Pediani, D., John, Godin, G., Antoine, Graham, J., Gerard, & Milligan, G. (2014). Roundabout 1 exists predominantly as a basal dimeric complex and this is unaffected by binding of the ligand Slit2. *Biochemical Journal, 461*(1), 61-73. doi:10.1042/bj20140190

Zanet, J., Freije, A., Ruiz, M., Coulon, V., Sanz, J. R., Chiesa, J., & Gandarillas, A. (2010). A mitosis block links active cell cycle with human epidermal differentiation and results in endoreplication. *PLoS One, 5*(12), e15701. doi:10.1371/journal.pone.0015701

Zelina, P., Blockus, H., Zagar, Y., Péres, A., Friocourt, F., Wu, Z., . . . Chédotal, A. (2014). Signaling Switch of the Axon Guidance Receptor Robo3 during Vertebrate Evolution. *Neuron, 84*(6), 1258-1272. doi:10.1016/j.neuron.2014.11.004

Zeman, M. K., & Cimprich, K. A. (2014). Causes and consequences of replication stress. *Nat Cell Biol, 16*(1), 2-9. doi:10.1038/ncb2897

Zerfass-Thome, K., Schulze, A., Zwerschke, W., Vogt, B., Helin, K., Bartek, J., . . . Jansen-Dürr, P. (1997). p27KIP1 blocks cyclin E-dependent transactivation of cyclin A gene expression. *Molecular and Cellular Biology, 17*(1), 407-415. doi:10.1128/mcb.17.1.407

Zhang, B., Dietrich, U. M., Geng, J. G., Bicknell, R., Esko, J. D., & Wang, L. (2009). Repulsive axon guidance molecule Slit3 is a novel angiogenic factor. *Blood, 114*(19), 4300-4309. doi:10.1182/blood-2008-12-193326

Zhang, Y., Li, F., Song, Y., Sheng, X., Ren, F., Xiong, K., . . . Yu, Z. (2016). Numb and Numbl act to determine mammary myoepithelial cell fate, maintain

epithelial identity, and support lactogenesis. *FASEB J, 30*(10), 3474-3488. doi:10.1096/fj.201600387R

Zhang, Y., Wang, Z., & Ravid, K. (1996). The Cell Cycle in Polyploid Megakaryocytes Is Associated with Reduced Activity of Cyclin B1-dependent Cdc2 Kinase. *Journal of Biological Chemistry, 271*(8), 4266-4272. doi:10.1074/jbc.271.8.4266

Zhou, B., Lin, W., Long, Y., Yang, Y., Zhang, H., Wu, K., & Chu, Q. (2022). Notch signaling pathway: architecture, disease, and therapeutics. *Signal Transduction and Targeted Therapy, 7*(1). doi:10.1038/s41392-022-00934-y

Zou, L., & Elledge, S. J. (2003). Sensing DNA damage through ATRIP recognition of RPA-ssDNA complexes. *Science, 300*(5625), 1542-1548. doi:10.1126/science.1083430

Øvrebø, J. I., & Edgar, B. A. (2018). Polyploidy in tissue homeostasis and regeneration. *Development, 145*(14). doi:10.1242/dev.156034

Šale, S., Lafkas, D., & Artavanis-Tsakonas, S. (2013). Notch2 genetic fate mapping reveals two previously unrecognized mammary epithelial lineages. *Nature Cell Biology, 15*(5), 451-460. doi:10.1038/ncb2725